Pre-Clinical Research and Development of Novel FKBP12 Antagonists for Enhanced Wound Healing and Regenerative Therapy

By

Brandon J. Peiffer

A dissertation submitted to Johns Hopkins University in conformity with the requirements for the degree of Doctor of Philosophy.

Baltimore, MD

February, 2019

ABSTRACT

The combination of AMD3100 and low-dose FK506 has been shown to accelerate wound healing in vivo. Though AMD3100 is known to work by releasing hematopoietic stem cells into circulation, the mechanism of FK506 in this setting has remained unknown. In this study, we investigated the activities of FK506 in human cells and a diabetic-rat wound model using a non-immunosuppressive FK506 analog named FKVP. While FKVP was incapable of inhibiting calcineurin, wound healing enhancement with AMD3100 was unaffected. Further study showed that both FK506 and FKVP activate BMP signaling in multiple cell types through FKBP12 antagonism. Furthermore, selective inhibition of BMP signaling abolished stem cell recruitment and wound healing enhancement by combination treatment. These results shed new light on the mechanism of action of FK506 in BMP-mediated acceleration of wound healing, and raised the possibility that less toxic non-immunosuppressive FKBP ligands such as FKVP can replace FK506 as novel leads for wound healing. Moreover, new synthetic techniques and *in vitro* screening systems have translated into a methodology for the production and identification of additional non-immunosuppressive analogs to be tested *in vivo*. Further study shows that FKBP12 protein degradation can be chemically-induced using either a specialized FK506 analog or SNAP protein substrate. This technique generated our most potent BMP-activator, as well as a new method for identifying protein-protein interactions in live cells.

Thesis Advisor: Jun O. Liu, Ph.D. (reader)

Thesis Committee: Caren Freel Meyers, Ph.D. (reader), Zhaoli Sun, M.D., Ph.D. (reader), Gregg Semenza, M.D., Ph.D.

PREFACE

I need to thank so many people for their support and guidance during my educational campaign, starting with my parents. Their love and encouragement took me through several challenging points in my life, even though I didn't always make it easy. I also need to thank my wife for moving to a new state and standing by me through all 4 and a half years of grad school. Her support is the reason for any success I may obtain now or in the future.

I have had many mentors during my time in grad school, but Dr. Jun Liu provided the majority of my training and experience. I can't thank him enough as, even in his own time of crisis, he remained available to guide me towards my research and academic goals. His mentorship style blended seamlessly with what I wanted from an advisor, and his insights have changed the way I approach new scientific problems. Additionally, Dr. Zhaoli Sun has functioned as a second mentor for my pre-clinical training. I felt so fortunate to have the project I received, as working with Dr. Sun gave me a new outlook on the translational capacity of bench research. I look forward to working with him in the future as I expand my training towards the clinic. Last, but not least, I want to thank Dr. Caren Freel-Meyers for her guidance during some of my most difficult academic milestones.

I have worked with several highly-skilled researchers during my thesis work. Although we have very different backgrounds, it was our differences that allowed us to translate several aspects of my research towards clinical application. The surgical expertise of Dr. Le Qi gave us the opportunity to test new compounds in animal models, and the chemistry expertise of Dr. Yuefan Wang gave us a new synthetic methodology for future drug development.

TABLE OF CONTENTS

LIST OF TABLES

LIST OF FIGURES

1. INTRODUCTION

Wounding due to accidents, diseases, and armed conflict is one of the most common medical problems. Cost of care for chronic, non-healing wounds associated with severe burns and diseases such as diabetes has been estimated to exceed 50 billion dollars per year (Fife et al., 2012). Chronic wounds make the human body more susceptible to infection, increasing the risk of acquiring opportunistic pathogens that can lead to sepsis. Thus, accelerating wound healing (WH) can reduce the risk of infection, improving the mortality and morbidity rates of wounded patients. However, there are limited options to shorten wound healing, calling for development of new therapies.

We have previously reported the discovery of a synergistic drug combination for the acceleration of cutaneous WH (**Fig. 1.1**, Lin et al., 2014) and the induction of long-term allograft survival through host repopulation (Okabayashi et al., 2011, Hu et al., 2016, Cameron et al., 2016). The combination of two FDA-approved drugs, Tacrolimus (FK506) and Plerixafor (AMD3100), reduced the complete healing time by 25% in mice with four circular full-thickness excisional wounds, which is unprecedented by existing therapeutic modalities. To date, there has not been an approved small-molecule treatment for wound healing. This leaves a large subset of patients that may not respond to current biologic therapies such as topical PDGF-BB (Becaplermin, brand name Regranex) or protein-imbedded matrices.

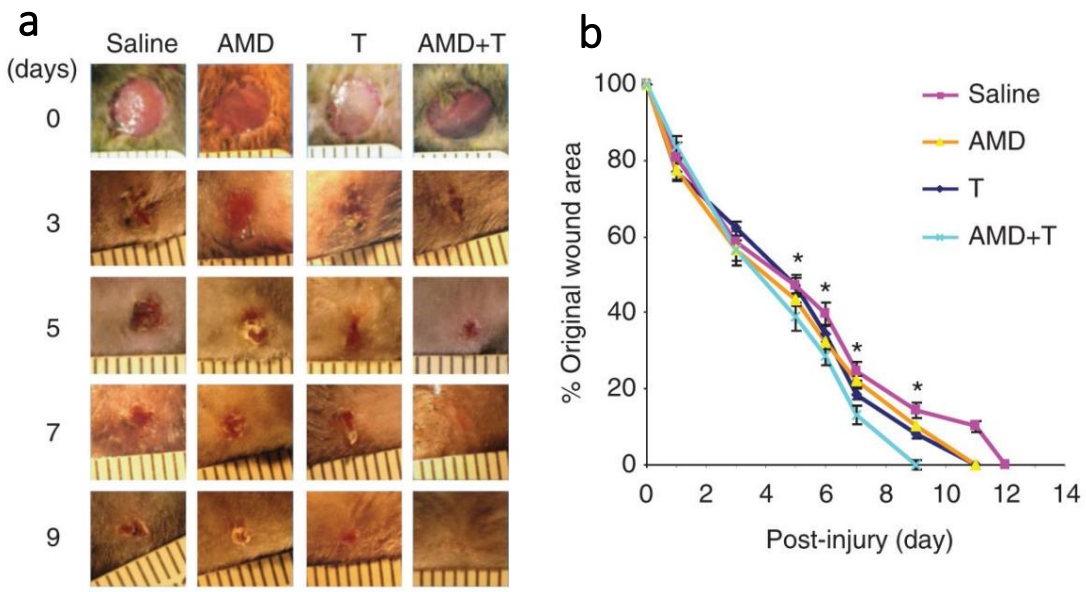

Figure 1.1: Previous work in the lab of Dr. Zhaoli Sun uncovered a combination treatment for acceleration of wound healing. In 2014, the Sun lab published an article in the Journal of Investigative Dermatology showing that concomitant AMD3100 and low-dose Tacrolimus accelerated wound healing in mice by 25% (Lin et al, 2014). (a) Early healing. Representative photographs of wounds in mice (n=6) showing striking differences beginning at day 5. (b) Quantitative analysis of wound closure in mice (n=6). *P<0.05.

Accelerated WH is accompanied by the mobilization of bone marrow (BM)-derived stem cells (CD133, CD34, and cKit) and the recruitment of CD133 stem cells into wound sites, as well as augmented stromal derived factor 1 (SDF-1), fibroblast growth factor (FGF), and vascular endothelial growth factor (VEGF) release in granulation tissues (Lin et al., 2014). The underlying molecular mechanism by which the combination of FK506 and AMD3100 (AF) accelerates WH has not been extensively studied.

AMD3100 is a selective antagonist of the chemokine receptor CXCR4 (Hatse et al., 2002) and has been used clinically to drive hematopoietic stem cells (HSCs) out of the bone marrow (BM) into the peripheral blood (Liles et al., 2003) where they can be recovered and preserved until the completion of ablative irradiation and/or chemotherapy. In addition to HSCs, the injection of AMD3100 augmented the mobilization of BM derived endothelial progenitor cells (EPCs), which are associated with more rapid neovascularization and functional recovery after myocardial infarction in mice (Jujo et al., 2010; Balaji et al., 2013). However, increased number of circulating stem cells by AMD3100 treatment alone exhibited only slightly faster healing due to reduced recruitment in wound sites (Lin et al., 2014).

In contrast to AMD3100, the precise role played by low-dose FK506 in the combination treatment (AF) has remained a mystery. FK506, a macrolide produced by the bacteria *Streptomyces tsukubaensis,* is an immunosuppressant widely used for prevention of transplant rejection as well as treatment of certain autoimmune disorders (Tanaka et al., 1987; Fung et al., 2004). The underlying mechanism for the immunosuppressive activity of FK506 has been well established. At the cellular level, FK506 inhibits the activation of T helper cells. At the pathway level, it blocks the intracellular signal transduction emanating from the T cell receptor leading to transcriptional activation of IL-2 and other cytokine genes. At the molecular level, it binds to FKBP12 and other members of the FKBP family before the binary FKBP-FK506 complex associates with and inhibits the activity of the protein phosphatase activity of calcineurin, preventing calcium-dependent dephosphorylation of the nuclear factor of

activated T-cells (NFAT) (**Figure 1.2**) (Liu et al., 1991; Griffith et al., 1995; Kissinger et al., 1995).

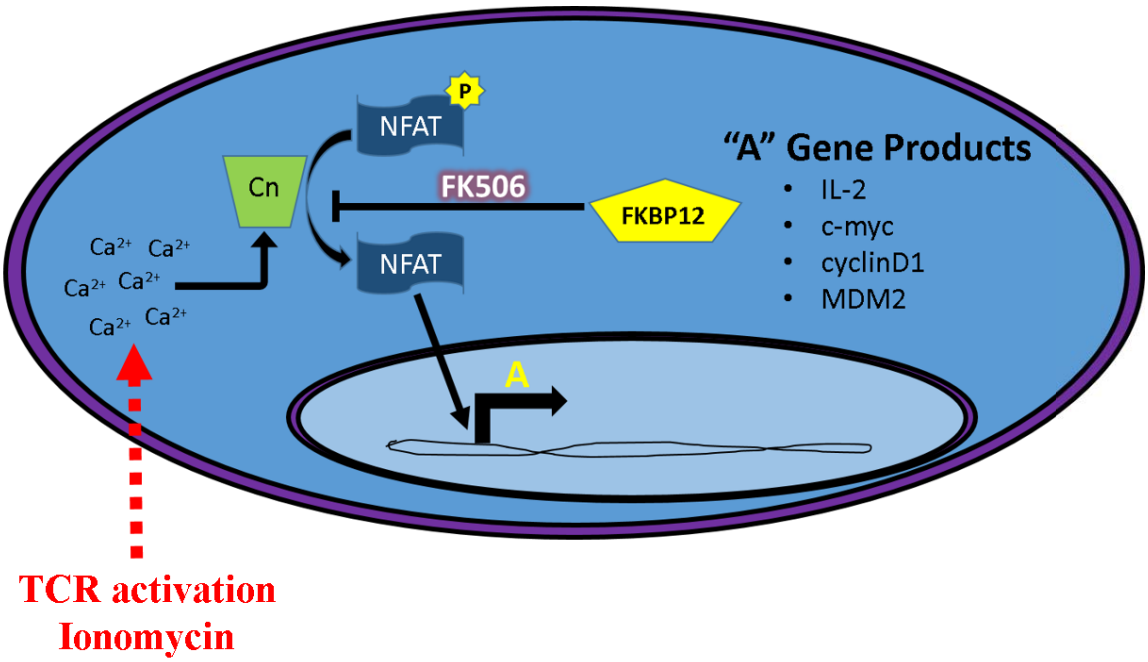

Figure 1.2: The NFAT Pathway is inhibited by FK506. Schematic depicting FKBP12's use of FK506 to inhibit calcineurin-mediated dephosphorylation of NFAT. Calcineurin is activated through both T-cell receptor (TCR) activation and calcium flux.

A possible underlying mechanism for FK506 in WH is through inhibition of calcineurin. However, it has been shown that topical FK506 has a detrimental effect on WH (Schäffer et al., 1998). Furthermore, we have shown that animals treated with low-dose FK506 (0.1 mg/kg) alone exhibited slightly faster healing compared to the saline control group, but the standard dose of FK506 (1 mg/kg) for immunosuppression delayed

healing time, leaving unanswered the question of whether calcineurin inhibition is responsible for the effect of FK506 on WH.

Further reports have shown alternate biological activities for FK506, some of which are not related to calcineurin inhibition. Of particular interest are modulation of Bone Morphogenic Protein (BMP) signaling and neuroregenerative capabilities, both of which are suggested to work through FKBP binding.

FK506 competes with FKBP12 for association with TGF-β, ryanodine, and inositol trisphosphate (IP_3) receptors. However, there is limited evidence that competition alone is enough to activate these receptors in the absence of endogenous signal. Calcium flux activity by IP_3 receptors was only shown to be enhanced in the presence of exogenous IP3 (in lipid microsomes) (Cameron, 1995). Further reports state that an FK506 analog was unable to activate a luciferase reporter driven by TGF-β receptor (in mink lung cells) activation unless exogenous TGF-β protein was added. Additionally, Spiekerkoetter et al. showed that FK506 could not activate a TGF-β luciferase reporter in C2C12 musculoskeletal cells (Spiekerkoetter et al., 2013). It should be recognized that FK506 was found to upregulate the TGF-β co-receptor endoglin through BMP activation (Albiñana et al., 2011), possibly increasing sensitivity towards endogenous TGF-β protein.

In general, the propensity of FK506 and its analogs to modulate calcium signaling through ryanodine and IP3 should be the greatest concern in cardiac/vascular muscle cell contractility. However, Spiekerkoetter et al. demonstrated that low-dose FK506 treatment did not adversely affect blood pressure in mice (over 3 week treatment period) (Spiekerkoetter et al., 2013). Recent clinical trials have also highlighted the human

tolerability of low-dose (sub-immunosuppressive) FK506 for the treatment of pulmonary arterial hypertension (Spiekerkoetter et al., 2017).

FKBP12 has been shown to inhibit BMP type 1 receptor activation (Wang et al., 1996). Importantly, this interaction could be relieved by FK506 (Spiekerkoetter et al., 2013), causing downstream signaling changes and BMP-dependent phenotypic changes in endothelial cells. BMP signaling has not yet been directly linked to any stage of wound healing, although it has been reported that epithelial cells down-regulate BMP receptors in response to injury (Lewis et al., 2014). Conversely, it has been recently reported that enhanced BMP signaling within myofibroblasts may promote scarless wound healing (Plikus et al., 2017), suggesting that regeneration of wounded tissue may be preferred to conventional wound healing processes (inflammation, proliferation, remodeling). BMPs have been demonstrated to produce a pro-inflammatory phenotype in endothelial cells, thereby increasing leukocyte adhesion and SDF-1 secretion (Csiszar et al., 2006; Young et al., 2012). Upon activation, BMP receptors phosphorylate and activate the SMAD transcription factors 1, 5, and 8. One major target gene of these SMADs is inhibitor of differentiation 1 (ID-1), which inhibits transcription of several genes related to embryogenesis and stem cell self-renewal (**Figure 1.3**).

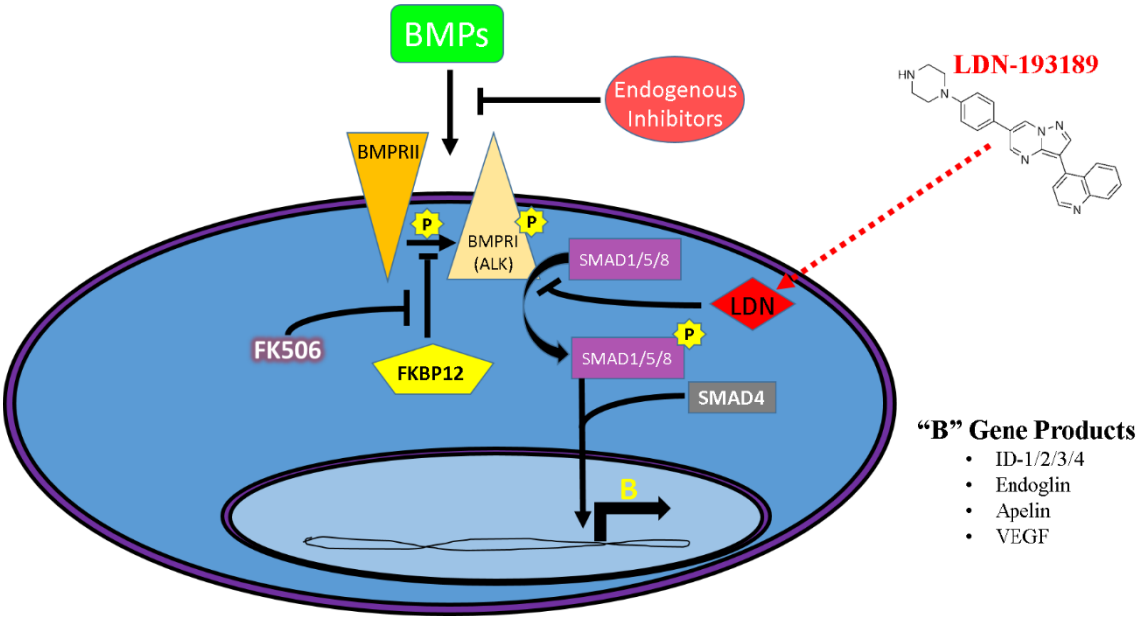

Figure 1.3: The BMP Pathway is activated by FK506. Schematic depicting FKBP12 as a modulator of BMP type 1 receptor activation. Activated receptor kinases phosphorylate SMAD1/5/8 transcription factors, causing them to translocate into the nucleus and promote expression of ID-1 and other genes. The compound LDN-193189 has been shown to inhibit receptor kinase activity, preventing downstream signaling.

Previous studies have examined some of the downstream effects of BMP receptor activation following FK506 treatment, which is accompanied by increases in SMAD1 and SMAD5 (denoted SMAD1/5) and/or SMAD8 (denoted SMAD1/5/8) phosphorylation in skeletal muscle cells (Spiekerkoetter et al., 2013) and human synovial stromal (hSSC) cells (Tateishi et al, 2007). Additionally, increases were observed in MAPKK phosphorylation and ID-1 expression, and the activity of FK506 was sufficient to rescue endothelial dysfunction in mice induced by a conditional BMP receptor type 2 (BMPR2) knockout (Spiekerkoetter et al., 2013). It has been reported that FK506

upregulated phosphorylation of SMADs downstream of the TGF-β signaling pathway (SMAD 2 and 3) in smooth muscle cells (Giordano et al Cardiovasc Res. 2008; Bennet et al. J Clin Med. 2016). However, downstream transcriptional activity was only seen in the presence of supplemented exogenous TGF-β (Spiekerkoetter et al., 2013; Wang et al., 1996). In another study, it was shown that FK506 increased expression of the TGF-β type 3 co-receptor endoglin, and stimulated both migratory and angiogenic activity of endothelial cells (Albiñana et al., 2011).

Together, these observations raised the possibility that FK506 may exert its WH effect through FKBP12 alone, independent of calcineurin inhibition. We hypothesized that non-immunosuppressive analogs of FK506 would retain activity in WH, while reducing off-target toxicity related to immunosuppression. Active compounds lacking immunosuppressive activity presents a valuable opportunity to improve the safety profile of this exciting new treatment for wound healing acceleration, especially in immunocompromised patients with chronic, non-healing wounds.

2. DISCOVERY OF FKVP BY FK506 DERIVATIZATION USING RUTHENIUM-CATALYZED CROSS METATHESIS

2.1 INTRODUCTION

FK506 also known as tacrolimus or fujimycin is a 23-member, macrolide natural product derived from the bacterium *Streptomyces tsukubaensis* (**Fig. 2.1**). Since 1994, FK506 has been widely used in the clinic for prevention of allogeneic transplant rejection (Tanaka et al., 1997; Fung et al., 2004).

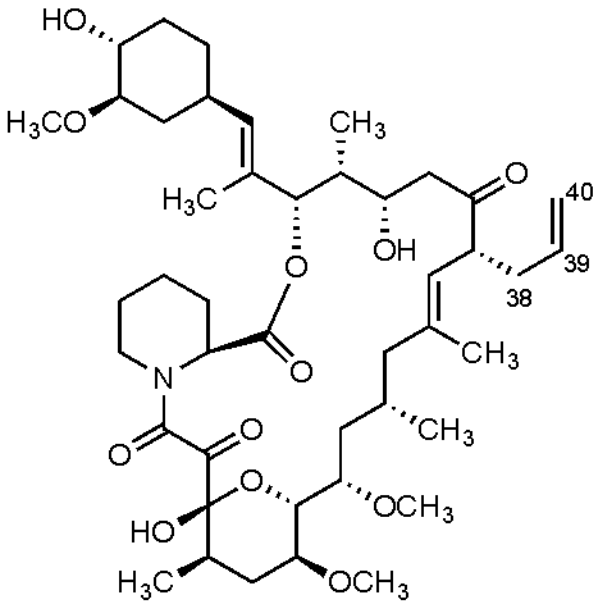

Figure 2.1: Structure of FK506.

It has been shown through crystal structure studies that FKBP12 interacts with several proteins in both an inducible (FKBP12-FK506-calcineurin) and non-inducible (FKBP12-BMPR1) fashion (Griffith et al., 1995, Kissinger et al., 1995, Chaikuad et al., 2012). FK506 has shown unique biological activities unrelated to

immunosuppression and is currently a lead pre-clinical compound for treating diseases such as pulmonary hypertension (Speierkoketter et al, 2013) and bladder cancer (Shin et al, 2014).

To generate a series of FK506 analogs devoid calcineurin inhibition, we decided to employ ruthenium-catalysed cross metathesis (CM). Previous reports have used CM to generate non-immunosuppressive FK506 analogs (Clemons et al, 2002; Marinec et al., 2009), which modifies the terminal alkene of FK506 on the C39 and C40 positions. At this position, steric bulk was shown to prevent calcineurin association and inhibition of NFAT transcriptional activity. To determine if calcineurin inhibition was required for enhanced healing by the AF combination, we designed and synthesized analogs of FK506 by using ruthenium-catalysed cross-metathesis to fuse different polar moieties to the terminal alkene as a "bump" in the effector domain of FK506 (**Figure 2.2**). We hypothesized that the addition of polar groups would not only clash with the hydrophobic binding pocket of calcineurin, but also improve solubility.

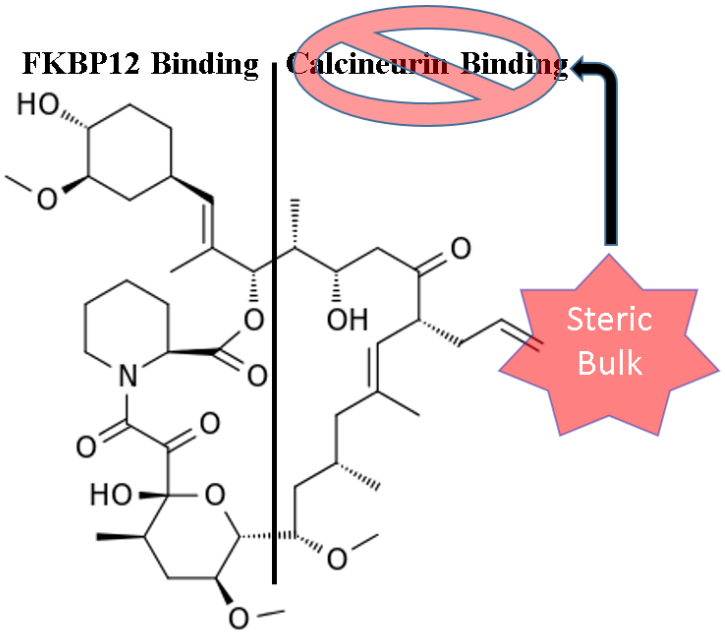

Figure 2.2: Scheme for formation of non-immunosuppressive analogs. Using chemistry to append bulky substituents at the C40 terminal alkene of FK506 has previously been shown to prevent calcineurin inhibition.

Additionally, we wanted to explore the use of free phosphoryl moiety in our study, yet vinyl-phosphonic acid did not give product in the CM reaction. Therefore, we designed a disoproxil-protected phosphonate that would lose its protecting groups after cleavage by intracellular esterases. This these groups protect the charged phosphate during both CM reaction and cell permeation.

Generated analogs were characterized by high-resolution mass spectrometry before they were screened in both NFAT reporter and wound healing assays. To assist in determining lead candidates for further study, the BMP reporter activation profile was also measured.

2.2 RESULTS

Synthesis of FK506 analogs by ruthenium-catalyzed cross metathesis

Cross metathesis reactions gave different yields based primarily on chelation ability of allylic or vinylic substrates. Nitrogen-containing moieties had the most difficulty, with boc or tosylate-salt protection needed for modest yields (**Fig. 2.3**). Conversely, yield of compound **1** did not improve with tosylate-salt protection during the CM reaction. Introduction of polar moieties greatly improved purification by increasing chromatographic separation from the parent compound (FK506). This process proved vital for isolation of compounds on a larger (20-100 mg) scale.

Addition of charged phosphonates to FK506 via CM gave no recoverable yields. In an attempt to access these interesting moieties, a protected phosphonate was designed (compound **4**) in the same prodrug-strategy employed by anti-retroviral nucleotide analogs such as tenofovir disoproxil. The disoproxil-protected FK506 analog (**3**) was generated by standard CM reaction with a vinyl phosphonate that had been substituted with two carbonate-based protecting groups (Houghton et al, 2010). These protecting groups can be cleaved by intracellular esterases, producing a charged phosphonate group at the terminal alkene (Compound **10**, **Fig. 2.4**).

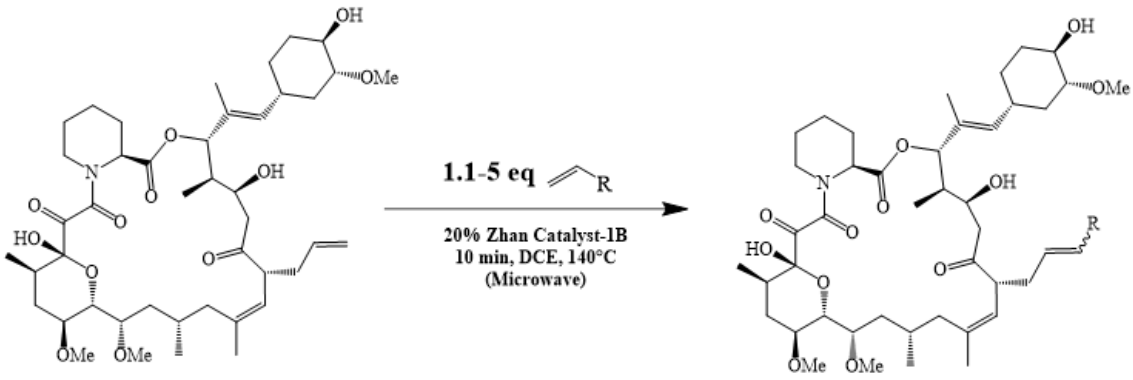

Entry	Reagent	Eq.	Product	Yield (%)
1		1.1	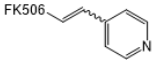	8
2	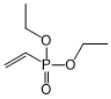	5	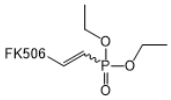	25
3	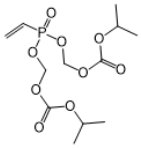	5	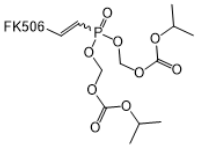	32
4	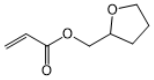	5	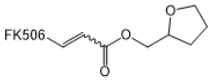	22
5	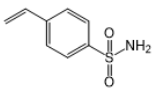	5	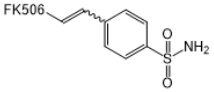	31
6	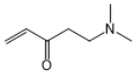	1.1	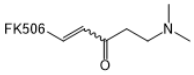	24
7	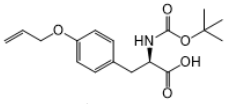	5	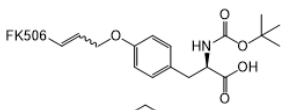	31
8	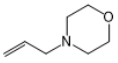	1.1	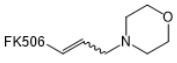	25
9	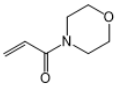	5	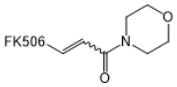	37

Figure 2.3: Synthesis of FK506 analogs by CM. High concentrations of ruthenium catalyst allowed for modest yields of most substrates. Reactions with amines required tosylate-salt or Boc protection for respectable yields. Synthesis of compound **1** did not improve with salt protection.

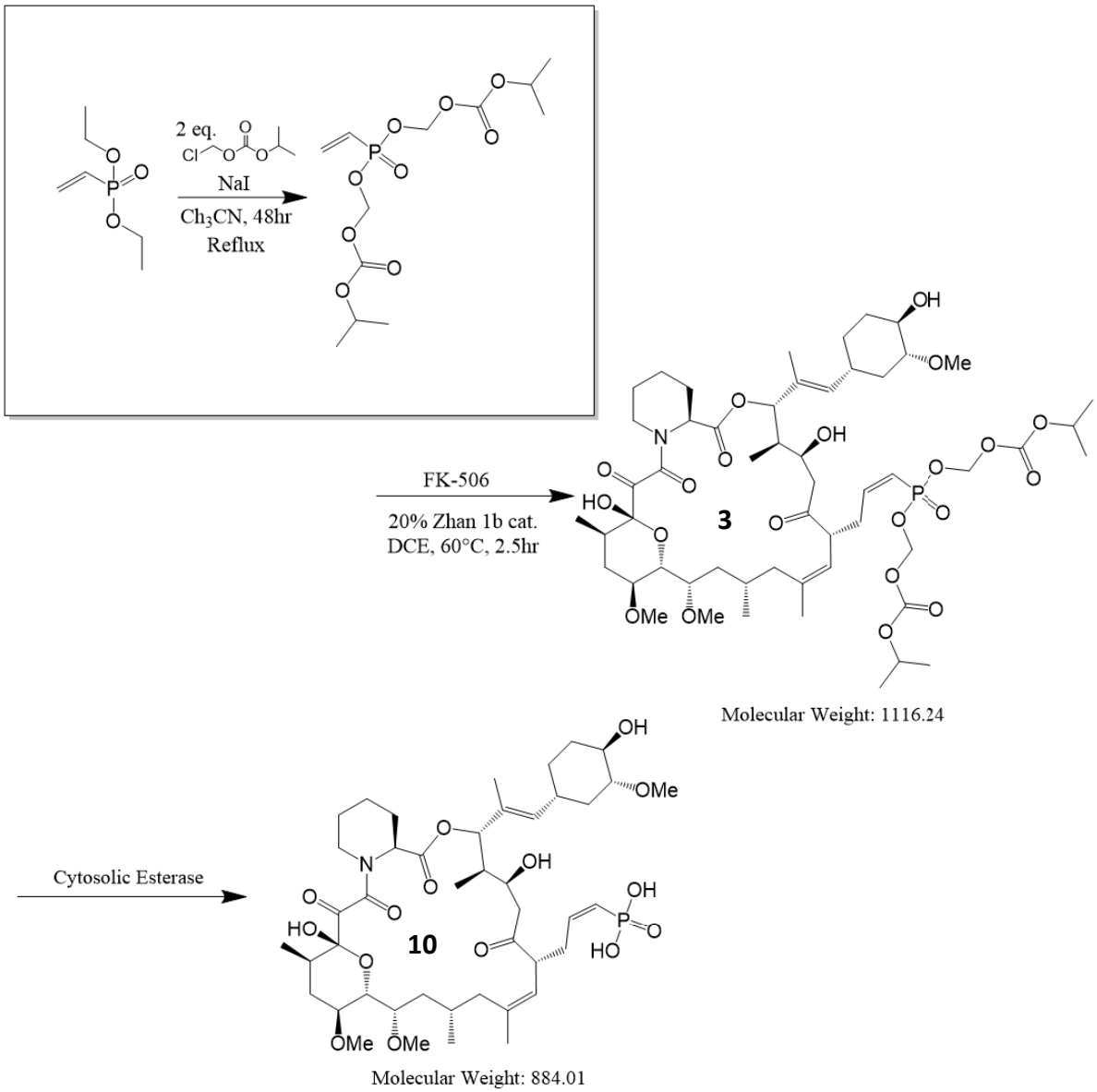

Figure 2.4: Synthesis scheme of disoproxil-protected phosphonate FK506 analog (3).

Diethyl vinyl phosphonate (substrate for compound **2**) was protected in one step, followed by CM to FK506. The esterase-cleavable groups were designed to be hydrolyzed upon cell entry, revealing a free phosphonate at the C40 position (**10**).

CM-generated FK506 analogs show variable activity in an NFAT reporter assay

In total, nine FK506 analogs were produced and purified. These compounds were initially tested for immunosuppressive activity in an NFAT reporter system (**Figure 2.5**) (Clemons et al, 2002). Calcineurin activity was measured by the ability of compounds to prevent luciferase transcription activated by PMA and ionomycin. Known immunosuppressive compounds FK506 and cyclosporine A (CsA) potently inhibited luciferase transcription relative to activated, DMSO-treated samples (**Fig. 2.6**). Additionally, the FKBP-ligand SLF showed no significant inhibition of the reporter at doses under 10 μM.

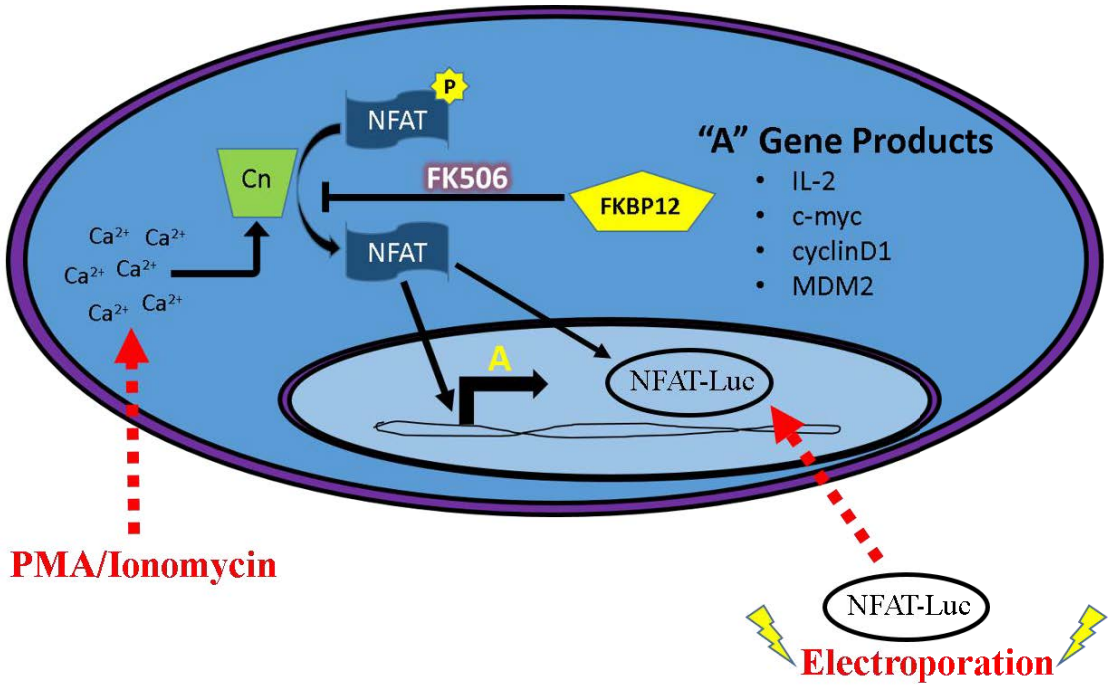

Figure 2.5: Schematic of NFAT reporter activation. PMA/Ionomycin is used to activate calcineurin dephosphorylation of NFAT. Subsequent translocation of NFAT promotes expression of the luciferase vector. FK506 and its analogs are

screened for their ability (or lack thereof) to block luciferase expression and its resulting luminescence.

Of the compounds tested, most were found to have limited or no calcineurin inhibition. Compounds **3**, **4**, and **7** showed immunosuppressive activity (**Table 2.1**), with compound **3** showing the most potent reporter inhibition. This data strongly suggests that disoproxil groups on **3** are cleaved upon cellular entry, producing a free phosphonate (**10**) that is accommodated by calcineurin during the FKBP12-calcineruin interaction. This is also supported in that compound **4** remained non-active in the assay, as the addition of ethyl groups to the phosphonate is enough to block calcineurin inhibition.

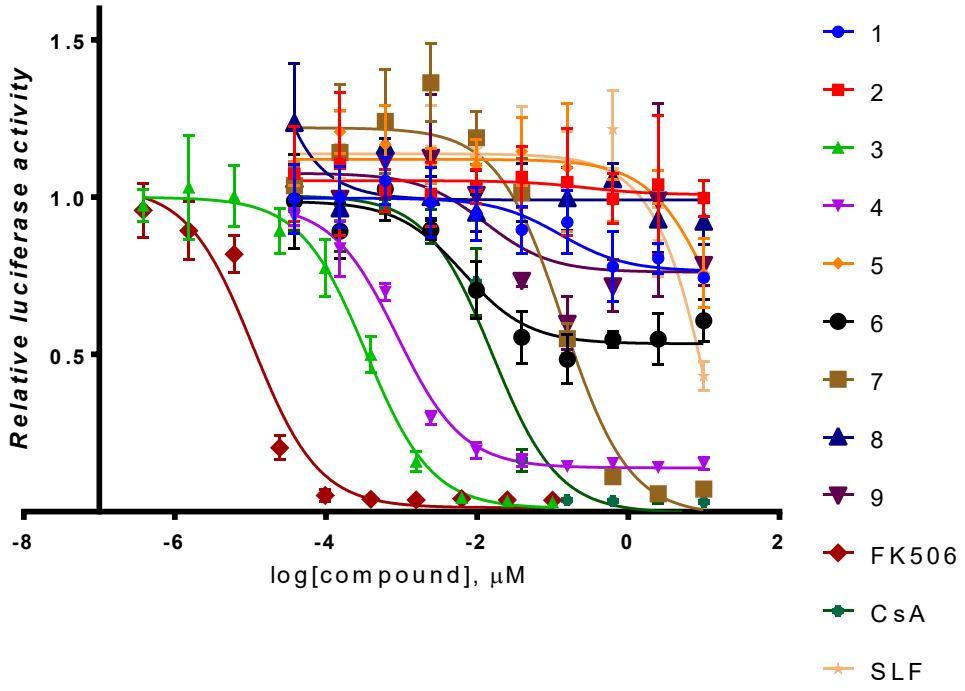

Figure 2.6: Dose response curves for FK506 and analogs in the NFAT reporter assay. Transfected Jurkat cells were activated by PMA/Ionomycin 30 min after

compound treatment. Luciferase activity was normalized to activated DMSO control samples. FK506 and CsA serve as positive controls, while SLF serves as a negative control.

Table 2.1: Calculated IC_{50} values of CM analogs in NFAT reporter assay.

COMPOUND	IC_{50} (nM)
1	N/A
2	N/A
3	0.34
4	0.876
5	N/A
6	N/A
7	137.4
8	N/A
9	N/A
FK506	0.00109
CsA	15.91
SLF	N/A

CM-generated FK506 analogs activate a BMP reporter assay

To further characterize the FK506 analogs, we employed a BMP reporter assay (Figure 2.7) (Speierkoketter et al, 2013). After testing C2C12 cells for reporter activity (as used in the publication), we found that Jurkat cells produced a better signal-to-noise ratio with far lower basal activity. Jurkat cells express all necessary components of calcineurin-NFAT, BMP, and CXCR4 signaling pathways, making these cells an appropriate model for cell-based assays.

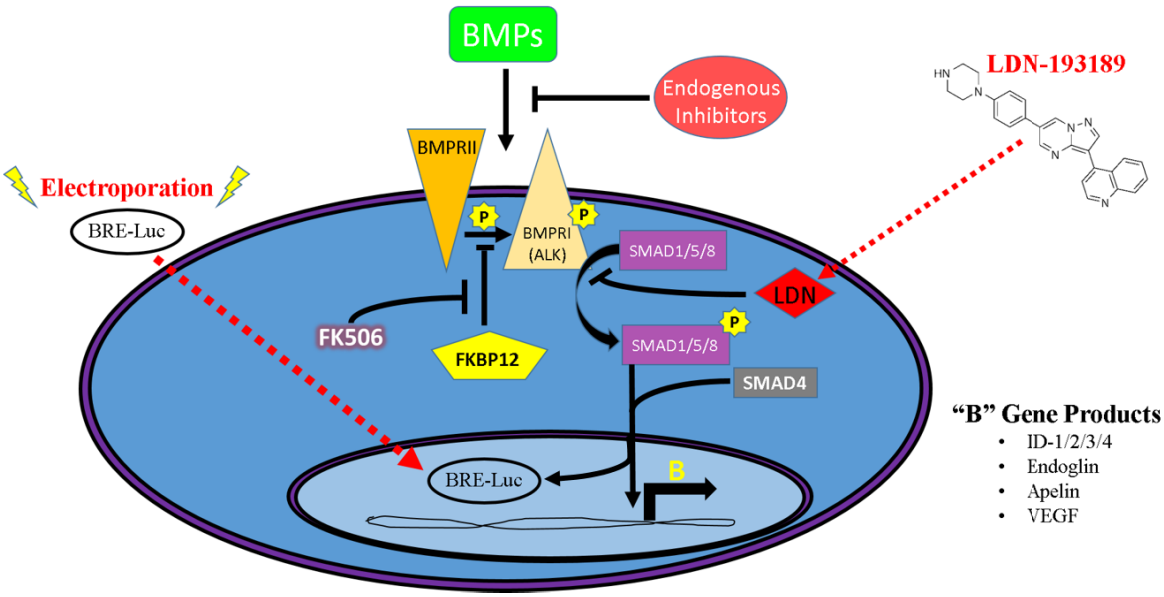

Figure 2.7: Schematic of BMP reporter activation. FK506 and its analogs are screened for their ability to activate luciferase expression and its resulting luminescence.

All analogs were found capable of activating the BMP reporter with similar potency when compared to FK506 (**Fig. 2.8**). The only exception to this trend was compound 7,

suggesting decreased cellular permeability that aligns with results from NFAT assay (**Fig. 2.6**). EC_{50} values for all compounds (except **7**) were in the low nanomolar range, with the most potent compound being analog **4** (**Table 2.2**). Interestingly, calcineurin activity did not correlate with BMP activation potential. This finding contradicts findings by Speierkoketter and colleagues, who reported that calcineurin inhibition played a role in FK506's activation of BMP signaling. This could be a result of differences in basal BMP signaling between Jurkat cells used here (low) and C2C12 mouse musculoskeletal cells (high) used in previous work (Speierkoketter et al, 2013).

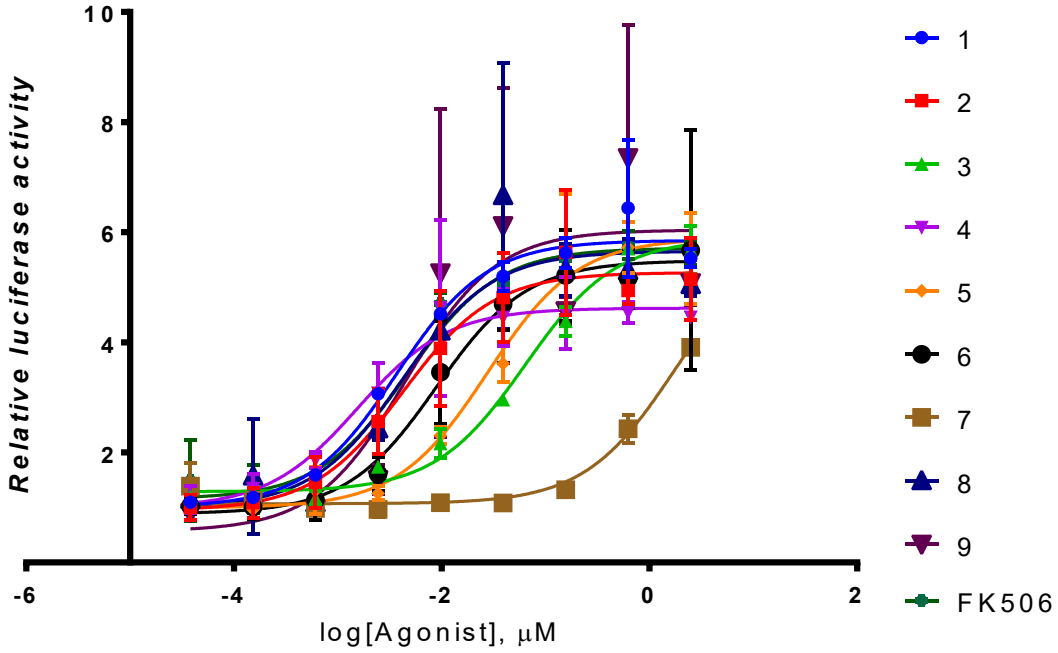

Figure 2.8: EC_{50} curves determined by relative luciferase activity in the BMP reporter assay. Transfected Jurkat cells were treated with indicated compounds for 18 hours before luciferase measurement. Luciferase activity was normalized to activated DMSO control samples. FK506 served as a positive control.

Table 2.2: Calculated EC_{50} values of CM analogs in BMP reporter assay.

COMPOUND	EC_{50} (nM)
1	3.689
2	4.262
3	63.83
4	1.557
5	27.56
6	8.896
7	N/A
8	4.183
9	4.509
FK506	4.736

FK506 analogs show WH enhancement in preliminary *in vivo* screening

To determine the ability of FK506 analogs to promote wound healing acceleration, compounds were tested in combination with AMD3100 in a wound-healing assay in SD rats. Compounds were dissolved into a formulation of 20% Cremophor in ethanol before 1:50 dilution into saline (0.1 mg/mL final concentration). Solutions were injected subcutaneously on alternating day until wound re-epithelialization. Four full-thickness excisions were created by 8 mm surgical punch, and monitored daily until complete wound re-epithelialization (**Fig. 2.9**). FK506 + AMD3100 combination treatment served as a positive control.

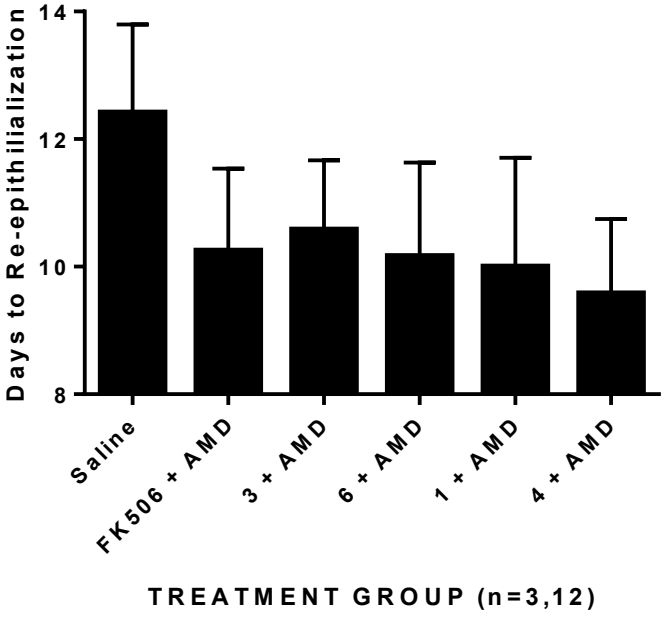

Figure 2.9: Hits from initial screening of FK506 analogs in wound healing. Three SD rats from each treatment group were given four excisional wounds, followed by concomitant treatment with AMD3100 every-other-day until wound closure (re-epithelialization). FK506 served as a positive control.

Four analogs gave significant healing acceleration when compared to saline (**Table 2.3**) that was insignificant when compared to FK506, suggesting equal WH activity. Of these hits, three analogs were found earlier to have no calcineurin inhibition (**Fig. 2.6**). Moreover, two analogs that gave fastest healing (**1** and **4**) also performed best in the BMP reporter (**Fig. 2.8**), but had opposite effects in the NFAT reporter. These results strongly suggest that wound healing acceleration by FK506 and its analogs is more dependent on BMP activation than NFAT inhibition.

Table 2.3: P-values from one-way ANOVA analysis of treatment results.

Group 1	Group 2	P
Saline	4+AMD	1.8E-05
Saline	FK506+AMD	0.00064
Saline	6+AMD	0.00082
Saline	1+AMD	0.00094
Saline	3+AMD	0.00151

2.3 MATERIALS AND METHODS

Chemicals: Research-grade FK506 (>98%) was purchased from APExBIO. Substrates and solvents were purchased form MilliporeSigma. Zhan-1b Ruthenium catalyst (CAS: 918870-76-5) was purchased from STREM Chemicals.

General Analog Synthesis: To a solution of FK506 (100 mg, 0.120 mmol) and 30mol% Zhan1b catalyst $RuCl_2[C_{21}H_{26}N_2][C_{12}H_{17}NO_3S]$, in 3mL anhydrous DCE was added 4-vinylpyridine (14.2 μL, 0.132 mmol) or other reagent (**Fig. 2.1**). The mixture was stirred for 30 s before microwave irradiation at 120 °C for 20 min. The mixture was then purified using flash chromatography, preparative-TLC, and/or reverse-phase HPLC. Both LC-MS and ^{1}H-NMR experiments were used to confirm the new compounds were >95% pure. Product was characterized using high-resolution MS or ^{1}H-NMR, then dissolved in DMSO or used in formulation for animal experiments.

For animal experiments, FKVP powder was dissolved into 80% EtOH/20% Cremophor RH60 solution at 5 mg/mL. This stock was diluted 1:50 into saline before subcutaneous injection.

Cell Culture and Transfections

Jurkat (E6.1, ATCC) cells were cultured in RPMI with 10% FBS and 1.5% PennStrep. Jurkat cells (1×10^6) were transfected with 10 μg of BRE-Luciferase (kindly provided by

Martine Roussel & Peter ten Dijke) or NFAT-Luciferase cDNA (Promega) by electroporation (BioRad, square-wave, 250V, 950μF) in 400 μL serum/antibiotic free RPMI with 0.5% DMSO. Thirty minutes after transfection, cells were transferred to complete RPMI and rested overnight. Before plating, cells were re-suspended in fresh media and diluted to 0.5x106 cells/mL. HUVEC cells were cultured in Lonza Endothelial cell Growth Medium (EGM-2) and used between passages 3 and 7. All cells were grown and assayed at 37 °C with 5% added CO_2.

BMP and NFAT Pathway Reporters

Jurkat cells used for each experiment were transfected at the same time and cultured together overnight until plating and treatment the following day.

Jurkat T cells transfected with BRE-Luc were split into a 96-well plate (80 μL/well of $0.5x10^6$ cells/mL)) and treated with previously stated compounds (20 μL of 5X stock in RPMI, 0.5% DMSO) for 18 hours. Cells were lysed and measured for luminescence using a PerkinElmer Microbeta2. Luminescence values were background subtracted (lysis buffer + substrate) and normalized to DMSO control values.

Jurkat T cells transfected with NFAT-Luc were split into a 96-well plate (80 μL/well of 0.5x106 cells/mL) and treated with indicated compounds (20 μL of 5X stock in RPMI, 0.5% DMSO) 30 min before activation with PMA/Ionomycin (40nM/1μM). After 6 hours, wells were lysed and measured for luminescence. FK506 served as positive control while DMSO and non-activated wells gave negative and background control values, respectively.

EC_{50} Determinations

Calculations were performed using GraphPad Prism 6. Curves were fit using non-linear, log(agonist) vs. response (three parameters). 95% confidence intervals of EC_{50} values are reported below.

Declaration of Ethical Animal Care and Use

Goto-Kakizaki (GK) type-2 diabetic rats obtained from Charles River (Boston, MA) were housed in a pathogen-free facility and cared for according to NIH guidelines and a protocol approved by the Johns Hopkins University Animal Care and Use Committee (ACUC). Both male and female GK rats at age of 4-5 months were used in this study.

In vivo Excisional Wound Model

Full-thickness wounds were created in the dorsal skin of rats with a sterile disposable biopsy punch (8 mm in diameter). The animals were injected subcutaneously with saline, AMD3100 (1 mg/kg) plus FK506 (0.1 mg/kg) or AMD3100 (1 mg/kg) plus FKVP (0.1 mg/kg) immediately after wounding and every other day until complete healing, defined as complete re-epithelialization of the wound area. Wounds were evaluated daily according to the method described previously (Lin et al., 2014).

Statistics

The one-way analysis of variance (ANOVA) was used to determine the statistically difference in wound healing among AF, AF+LDN, Saline and S+LDN groups or between AF, AV and Saline groups when comparing days of wound healing. Bonferroni-Holm post-hoc procedure was used for p value adjustment. $p<0.05$ is considered significantly different.

2.4 COMPOUND CHARACTERIZATION

High resolution mass spectrometry for all compounds was performed by UCIC's mass spectrometry facility. Samples were sent dissolved in DMSO.

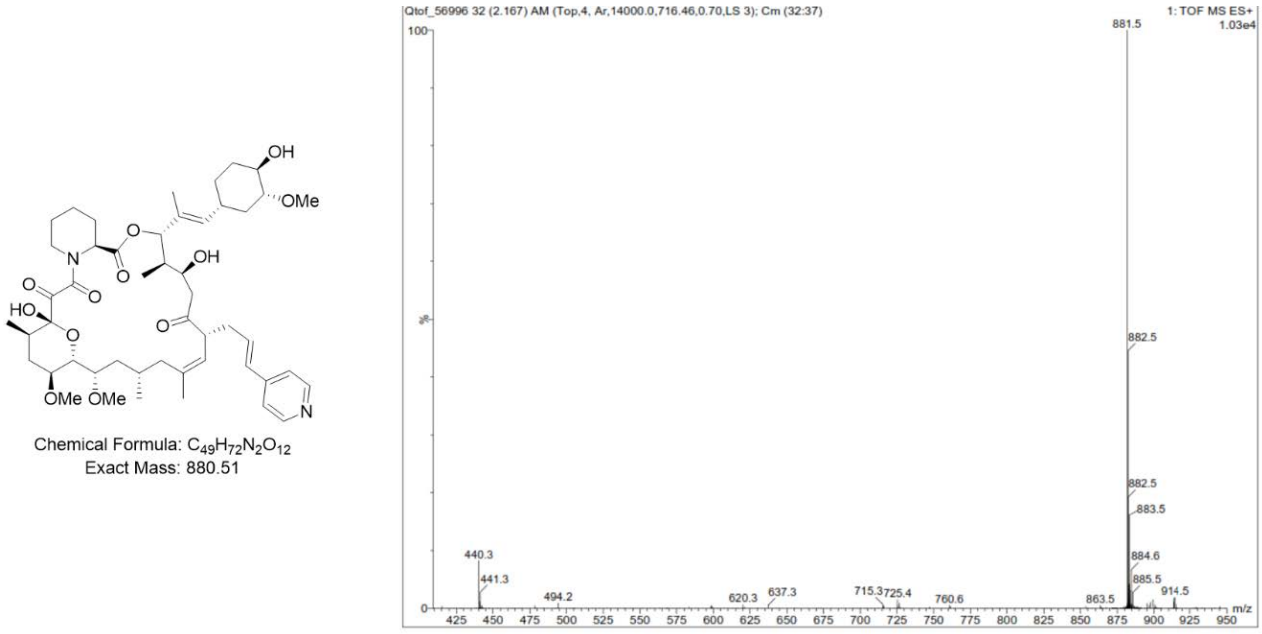

Figure 2.10: High-resolution mass-spectrometry profile of compound 1.

Calculated mass = 881.5135, Found =881.5164.

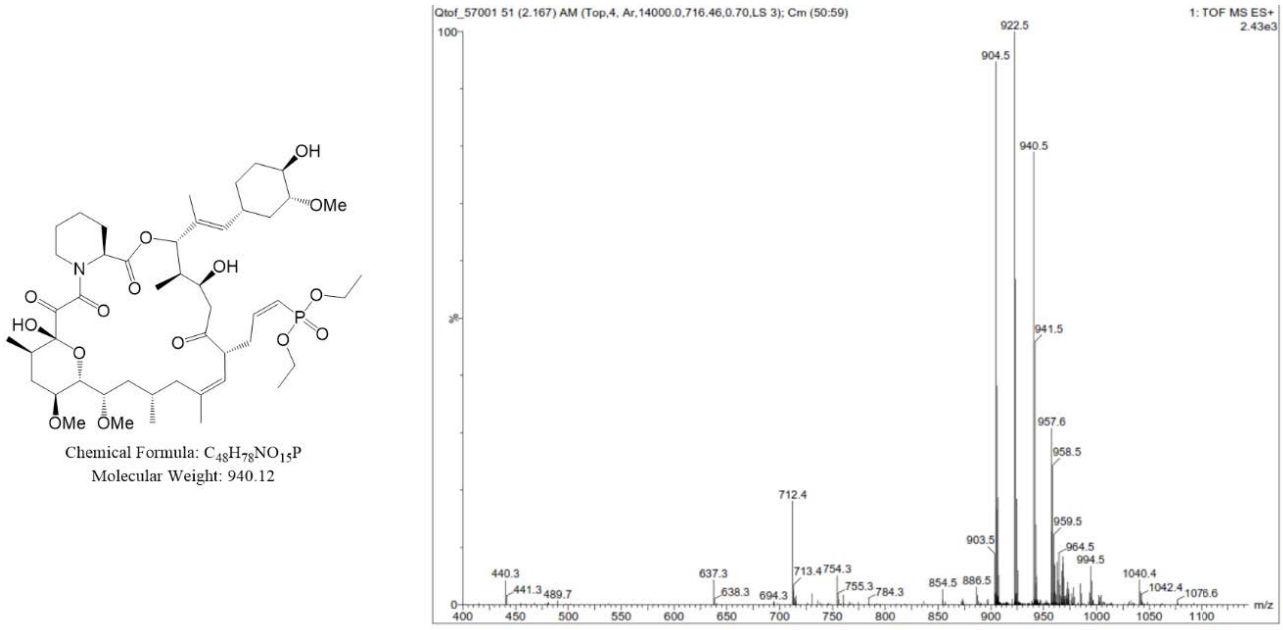

Figure 2.11: High-resolution mass-spectrometry profile of compound 2.

Calculated mass = 940.5203, Found = 940.5187.

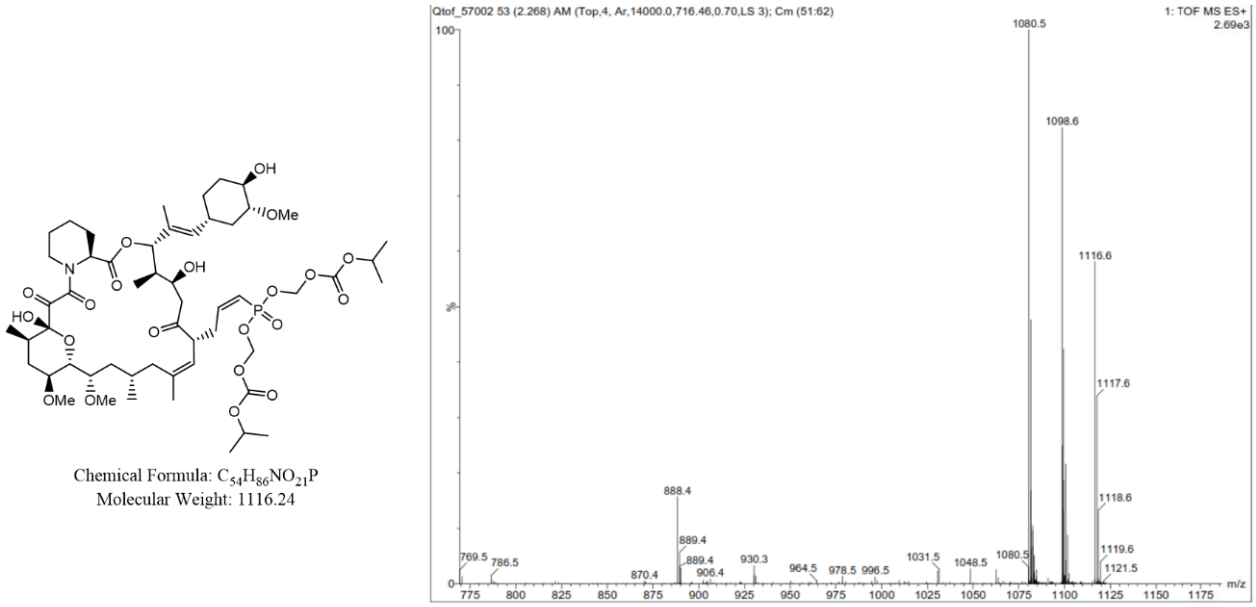

Figure 2.12: High-resolution mass-spectrometry profile of compound 3.

Calculated mass = 1116.5533, Found = 1116.5508.

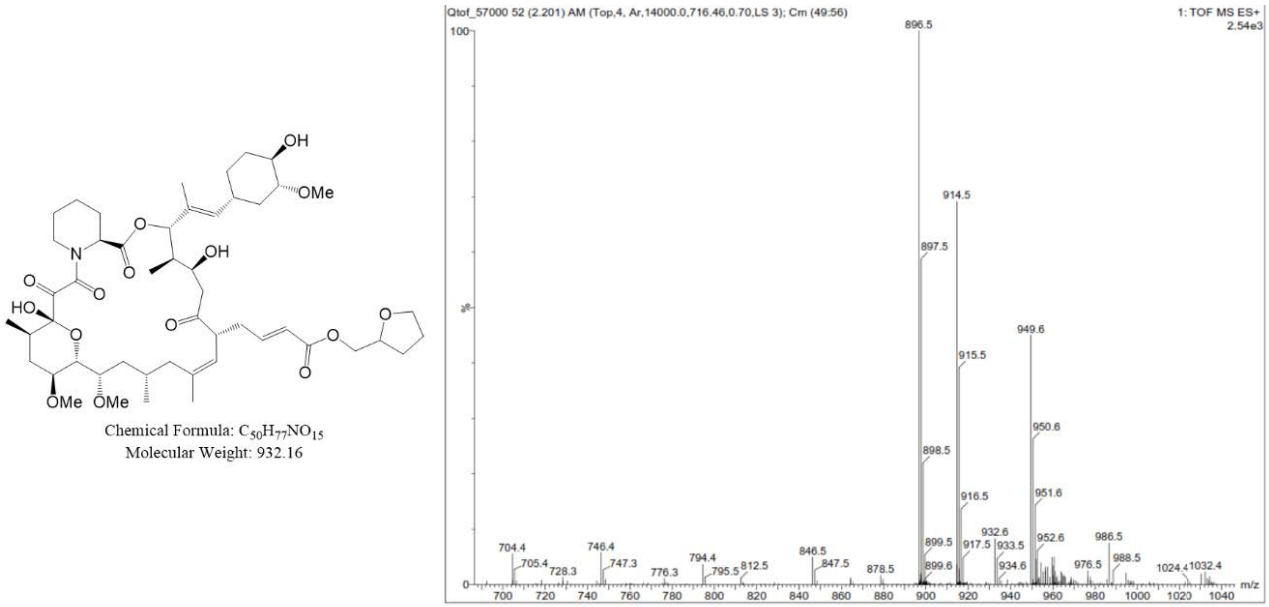

Figure 2.13: High-resolution mass-spectrometry profile of compound 4.

Calculated mass = 932.5397, Found = 932.5371.

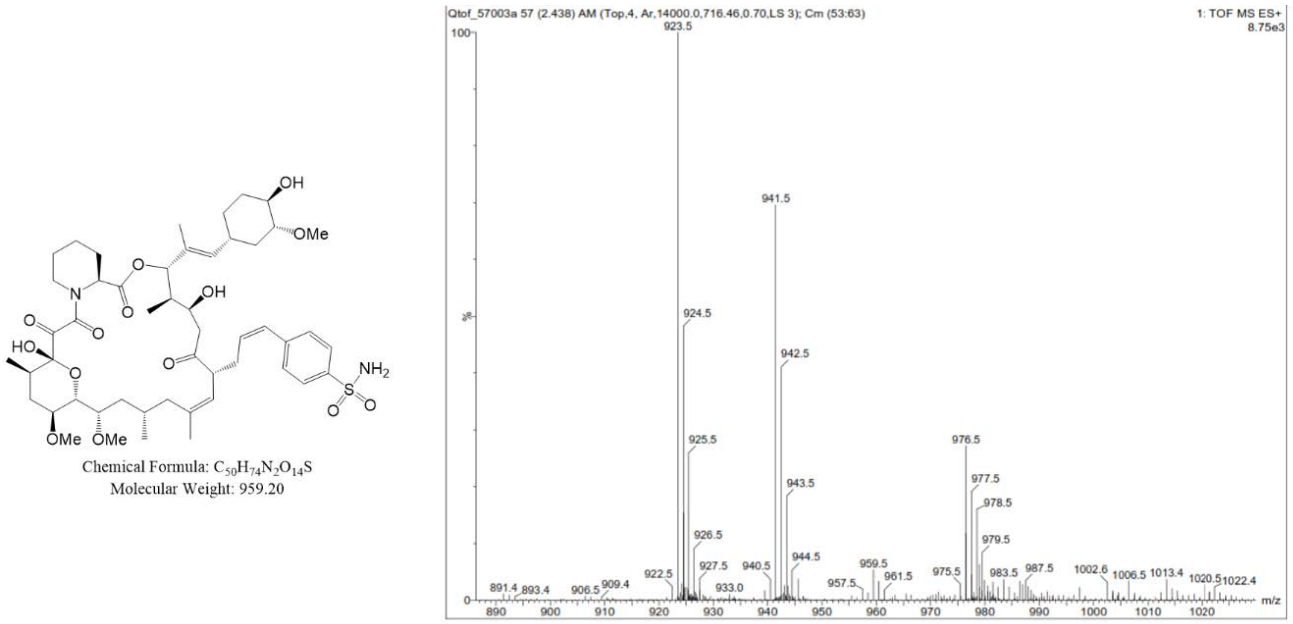

Figure 2.14: High-resolution mass-spectrometry profile of compound 5.

Calculated mass = 959.4952, Found = 959.4939.

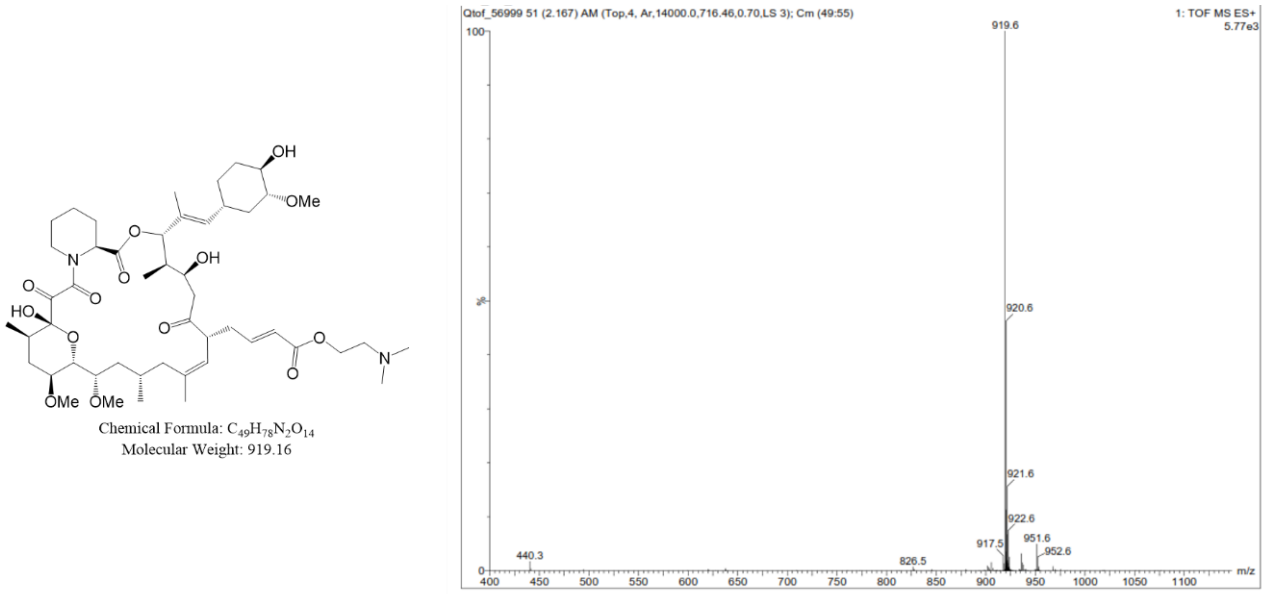

Figure 2.15: High-resolution mass-spectrometry profile of compound 6.

Calculated mass = 919.5555, Found = 919.5531.

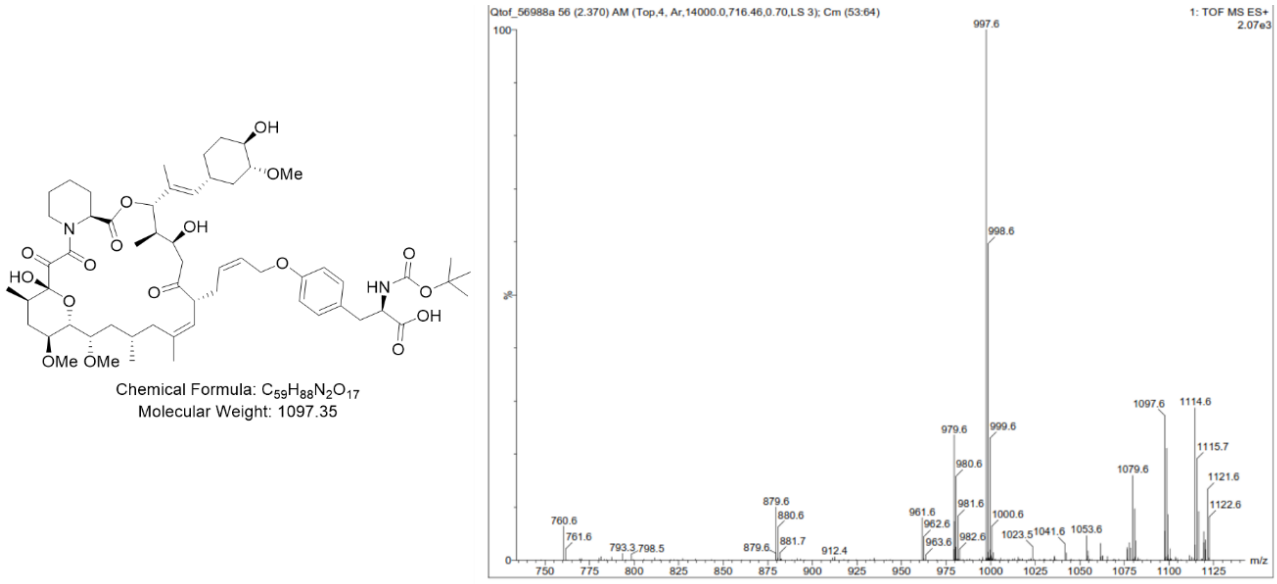

Figure 2.16: High-resolution mass-spectrometry profile of compound 7.

Calculated mass = 1097.6150, Found = 1097.6161.

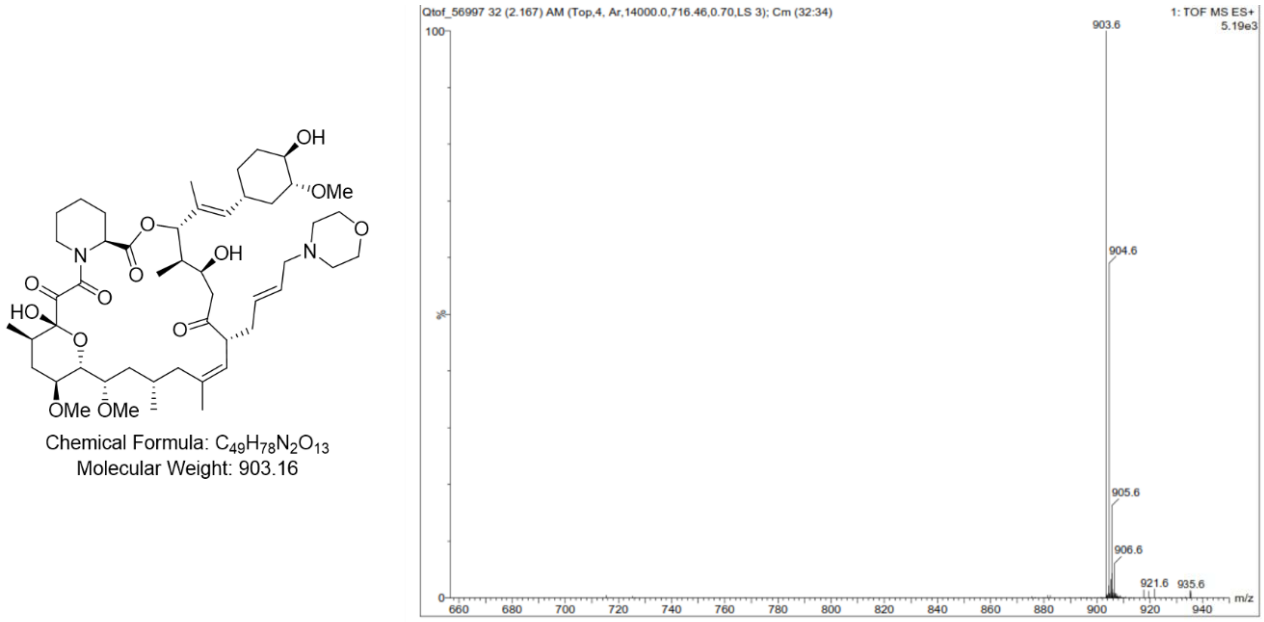

Figure 2.17: High-resolution mass-spectrometry profile of compound 8.

Calculated mass = 903.5614, Found = 903.5582.

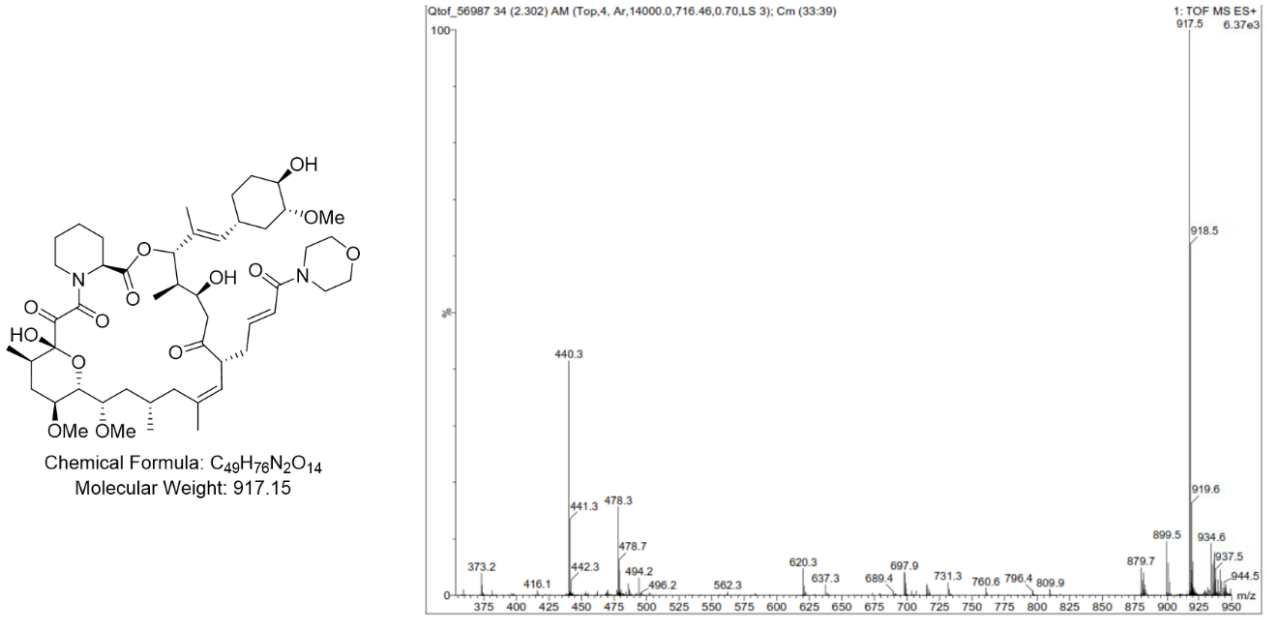

Figure 2.18: High-resolution mass-spectrometry profile of compound 9.

Calculated mass = 917.5353, Found = 917.5375.

Although integration is difficult for these large macrocycles, we can compare the spectra to that of FK506. In the 5.5-6.0 ppm range, it can be seen that a multiplet caused by the terminal alkene of FK506 is not present in compound 1 (**Fig. 2.16**). Moreover, peaks from 4-vinylpyridine are also seen in compound **1** (8.5 and 7.0ppm).

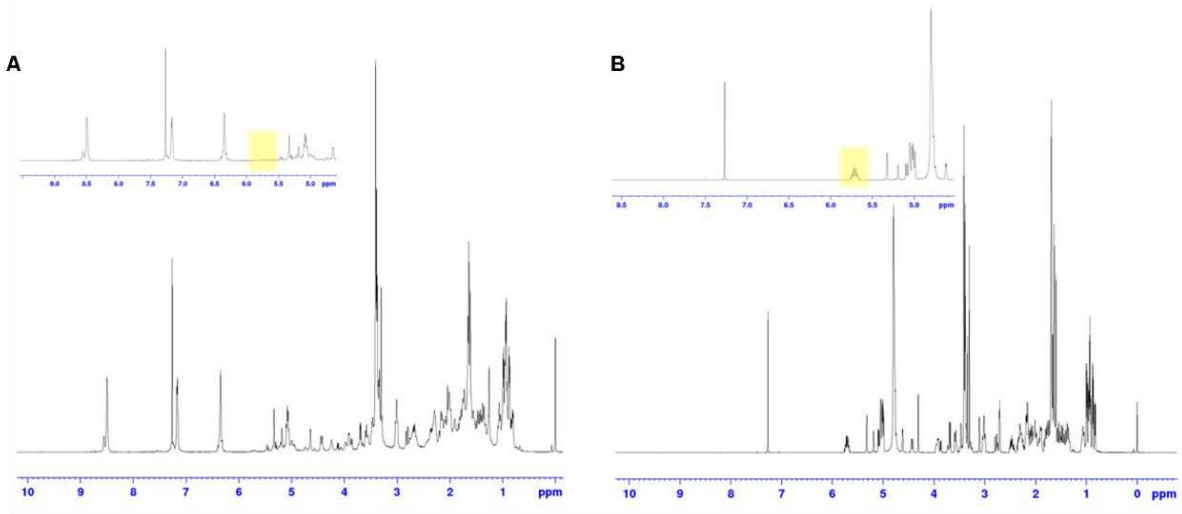

Figure 2.19: FKVP structure characterization. ^{1}H-NMR spectra of (**A**) FKVP and (**B**) FK506 ($CDCl_3$), including detail of 5.5ppm~6.0ppm showing disappearance of terminal alkene in FKVP (present in FK506, highlighted in yellow).

2.5 DISCUSSION

Our biological analysis of CM-prepared FK506 analogs suggests that FKVP (**1)** is the optimal lead compound for further study into non-immunosuppressive BMP activation and wound healing acceleration. While compound 4 showed slightly better BMP activation and WH acceleration, its retention of potent calcineurin inhibition makes it unfit for future study. Moreover, any increases in WH and BMP activity over the non-immunosuppressive analog FKVP (**1**) were insignificant. This suggests that WH acceleration is operates through FKBP12, independent of calcineurin inhibition. Interestingly, the prodrug form of phosphonate analog **3** showed the strongest calcineurin inhibition of all analogs (IC_{50}<1nM), suggesting that addition of free phosphonate (after cellular hydrolysis of carbonate groups) to the terminal alkene does not prevent calcineurin association. This also suggests that while compound 2 performed well in testing, it is a poor translational candidate for fears of phosphonate hydrolysis.

We began this project by questioning the necessity of calcineurin inhibition in wound healing acceleration by AF. Results show that out of the four hits in the wound healing screen, three are non-immunosuppressive. This indicates that the calcineurin inhibition activity of FK506 is not required for wound healing acceleration by AF. Moreover, trends in BMP activation potential and wound healing suggest a correlation that stems through FKBP binding alone.

Conversely, calcineurin has recently been reported to interact with the FKBP12-BMPR1 axis. This was evidenced by reduced activity of a linear FKBP antagonist (Shield-1) in the BMP reporter compared to FK506. Moreover, they showed a small increase in activity by a calcineurin inhibitor (cyclosporine A) that does not function

through FKBP. While we could not yet rule out the involvement of calcineurin, we show here that macrocyclic FK506 analogs activate BMP signaling at nearly the same level, regardless of calcineurin inhibition. Our findings suggest analog induced BMP activation may only be hampered by reduced cell-permeability, as the poorest performing analog had a large amino acid with a free carboxylate at the terminal alkene. This data supports the theory that FKBP binding may be the only requirement for BMP activation. Further study into the BMP pathway and its activation by FKVP may reveal important clues into the mechanism of AF-induced wound healing acceleration. Additionally, through a second round of structure-activity relationship studies based on FKVP, we may find further improvements in therapeutic potency.

3 ACTIVATION OF BMP SIGNALING SYNERGIZES WITH CXCR4 INHIBITION TO ACELLERATE WOUND HEALING*#

*This work was completed in collaboration with Dr. Le Qi.
#LQ performed animal surgery and histology, BP performed synthesis and cell-based assays

3.1 INTRODUCTION

In the previous chapter, we reported the discovery of FKVP for non-immunosuppressive wound healing acceleration. Our results suggest that the calcineurin-opposed (non-immunosuppressive) FK506 analog not only activates BMP reporter with higher potency, it also performs equally well in acceleration of wound healing. However, the question still remains as to whether or not the BMP pathway is relevant to wound healing. Studies have been inconclusive as to the precise mechanism for BMP activation by FK506, and at least one report suggests that calcineurin is required for signaling through BMP receptors (Spiekerkoetter et al., 2013).

In this chapter, we attempt to deconvolute the BMP pathway in regards to activation by FK506 and FKVP. Furthermore, we show that BMP receptor activity is intimately involved in wound healing *in vivo*, increasing mobilization and recruitment of stem cells at wounded tissues. To further display the power of this treatment, we chose clinically relevant Goto-Kakazaki (GK) rats as a model organism to demonstrate the potency of our treatment in a diseased model. GK rats spontaneously develop type-2 diabetes early in life, and suffer from many of the same complications as humans including slowed healing of wounds. A treatment for accelerated healing of diabetic wounds/ulcers in the clinic may significantly decrease co-morbidities associated with this disease, for which no small-molecule therapies currently exist. Moreover, these compounds may eventually be

used treat chronic, non-healing wounds that are sometimes present in diabetic patients with an advanced stage of disease.

3.2 RESULTS

Characterization of the non-immunosuppressive analog - FKVP

From our previous study, we identified compound **1** (FKVP) as our lead non-immunosupressive candidate for BMP and wound healing studies. We assessed the cytotoxicity of FKVP and compared it to that of FK506 in both Jurkat T (**Fig. 3.1A**) and primary HUVEC cells (**Fig. 3.1B**). Like FK506, FKVP did not affect cell viability at concentrations up to 10 μM.

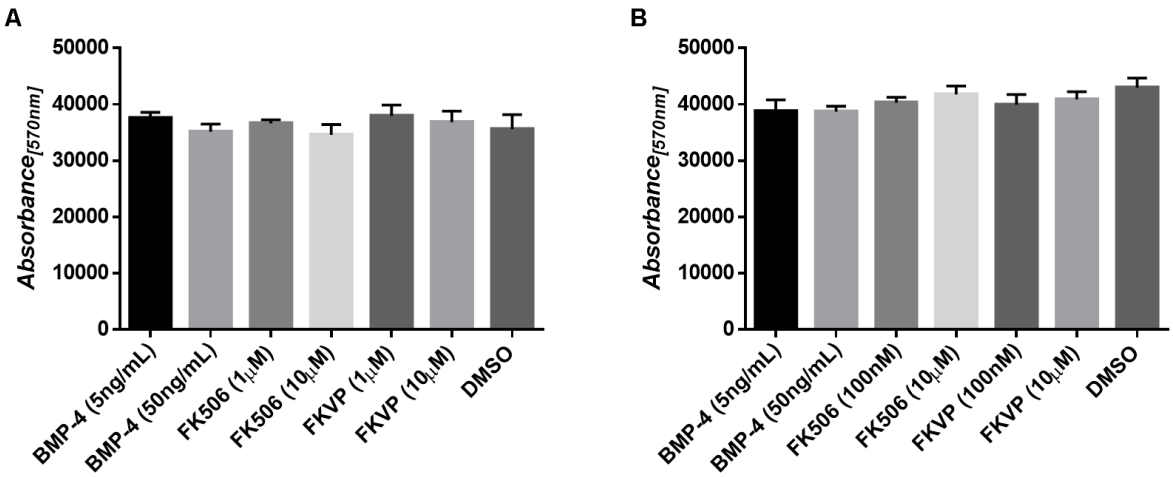

Figure 3.1: FKVP treatment of Jurkat cells does not significantly affect proliferation in several cell types. In resazurin-based (**A**) Jurkat and (**B**) HUVEC cell viability assays, FKVP treatment shows no significant changes after 3 day treatment (compared to DMSO treatment) (n=4). Error bars represent standard deviation from mean.

To confirm that FKVP retained the ability to bind FKBP, we applied it to a competition assay in combination with FK506 and rapamycin, as sequestration of free FKBP will prevent the formation of active FKBP12-FK506 or FKBP-rapamycin complexes and thus antagonizing the activity of both drugs (Rao et al., 1997, Abraham et al., 1996).

The effect of FK506 on calcineurin was determined using as a readout the phosphorylation state of NFATc2. Thus, FK506 blocked the dephosphorylation of NFATc2 in response to stimulation with PMA and ionomycin (**Fig. 3.2A**). The presence of 10 μM of FKVP reversed the inhibitory effect of FK506 on NFATc2 dephosphorylation (**Figure 1.2**), suggesting mutual antagonism between FKVP and FK506. Similarly, we examined the effect of rapamycin on mTOR activity as judged by the phosphorylation state of its substrate p70s6k. Once again, high concentration of FKVP reversed the inhibition of rapamycin on p70s6k phosphorylation (**Fig. 3.2B**). Together, these results clearly showed that FKVP is capable of antagonizing the activities of both FK506 and rapamycin through competitive binding to endogenous FKBP proteins.

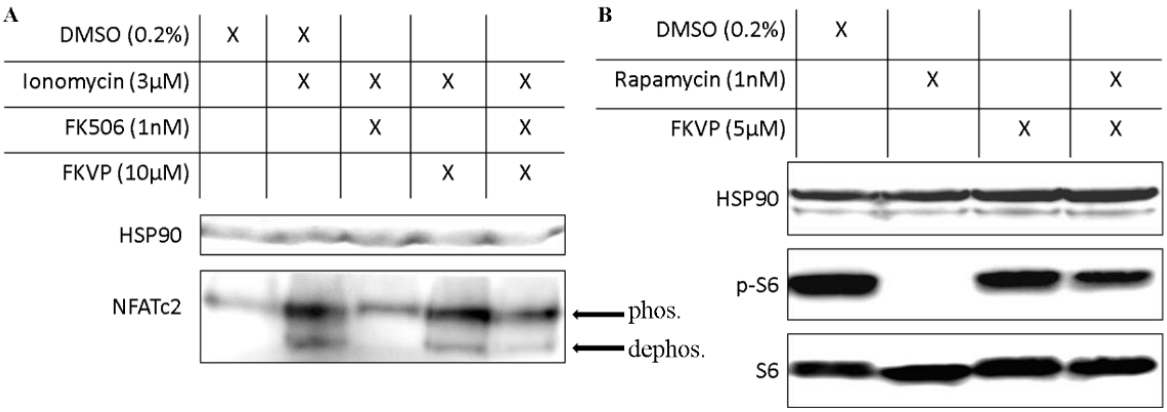

Figure 3.2: FKVP competes both FK506 and Rapamycin for FKBP12 binding Both FK506 and rapamycin require FKBP12 for activity. (A) FKVP blocks FK506 inhibition of calcineurin-mediated NFAT dephosphorylation (lower band), **(B)** as well as inhibition of mTOR-mediated S6 phosphorylation by rapamycin.

FKVP in combination with AMD3100 accelerated wound healing.

We have previously reported the synergistic activity of AMD3100 and FKVP (AV) in accelerating wound healing after full-thickness skin excision. To further confirm this finding, we performed a wound healing experiment in a rat model of type 2 diabetes. Four full-thickness wounds were generated by 8-mm diameter circular excisions on the shaved back of a diabetic GK rat and each wound site was photographed digitally at the indicated time intervals (**Fig. 3.3A**). Re-epithelialization of entire wound areas was used as a defining parameter of complete healing, and the complete healing time of four wounds in each animal were calculated in days (**Fig. 3.3B**). Wounded rats were divided randomly into three experimental groups and received subcutaneous injections of saline, AF (AMD3100 (1.0 mg/kg) plus FK506 (0.1 mg/kg)) or AV (AMD3100 plus FKVP (0.1

mg/kg)) immediately after wounding and every other day until complete healing. While the saline control group showed an average complete healing time of 26 days, the animals treated with AF exhibited significantly faster healing as wounds reached complete re-epithelialization at day 21, which is consistent with our report in non-diabetic rodent models of surgical excisional wounds (Lin et al., 2014). Importantly, ten rats receiving AV therapy displayed an AF-equivalent effect of significantly reduced time for complete healing from 26 to 20 days (**Fig. 3.3C**). These results strongly suggest that inhibition of calcineurin is not involved in the synergistic activity of AMD3100 and FK506 in accelerating wound healing.

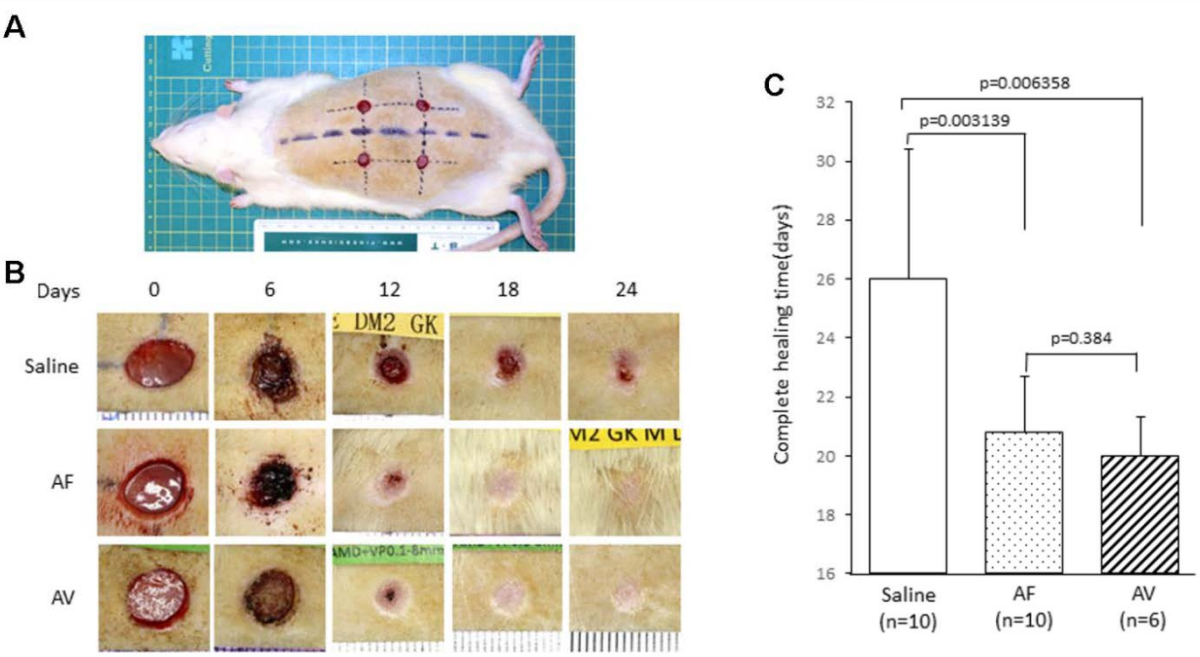

Figure 3.3: Accelerated wound healing in diabetic GK rats treated with combination of AMD3100 and FK506 or FKVP. (**A**) The wound model: four circular excisional wounds (8-mm in diameter) were created on the dorsal of GK rats. (**B**) Representative photographs of wounds in GK rats for each treatment group (AF=AMD3100+FK506,

AV=AMD3100+FKVP), at days 0, 6, 12, 18 and 24. (**C**) Quantitative analysis of complete healing time in GK rats. All data represented by mean ± SEM.

FKVP activates ID-1 reporter and SMAD1/5 phosphorylation through BMP type 1 receptor

Having ruled out calcineurin as a relevant mediator of the WH acceleration activity of FK506, we turned to FKBP12 and the BMP signaling pathway it is reported to regulate (**Figure 1.3**). We began by determining whether FK506 and FKVP are both capable of activating the BMP signaling pathway by employing a BMP-response-element (BRE) pathway reporter (luciferase under the control of the ID1 gene promoter) (**Figure 2.7**) (Spiekerkoetter et al., 2013) in Jurkat [E6.1] T cells. The Jurkat line was found to express working components of BMP signaling (BMPRs, SMAD1/5) in addition to high levels of FKBP12 and CXCR4, making it an excellent model system. To confirm reporter selectivity, rBMP-4 and rTGF-β1 were used as positive and negative controls, respectively. Treatment with both FKVP and FK506 caused dose-dependent activation of the reporter, and the increases in luciferase activity were completely blocked by the selective BMP1R inhibitor LDN-193189 (LDN) (**Fig. 3.4**). In contrast to FK506 and FKVP, cyclosporine A (CsA) did not activate the reporter (**Fig. 3.4**), consistent with the notion that calcineurin is not involved in BMPR1 kinase activation by FK506.

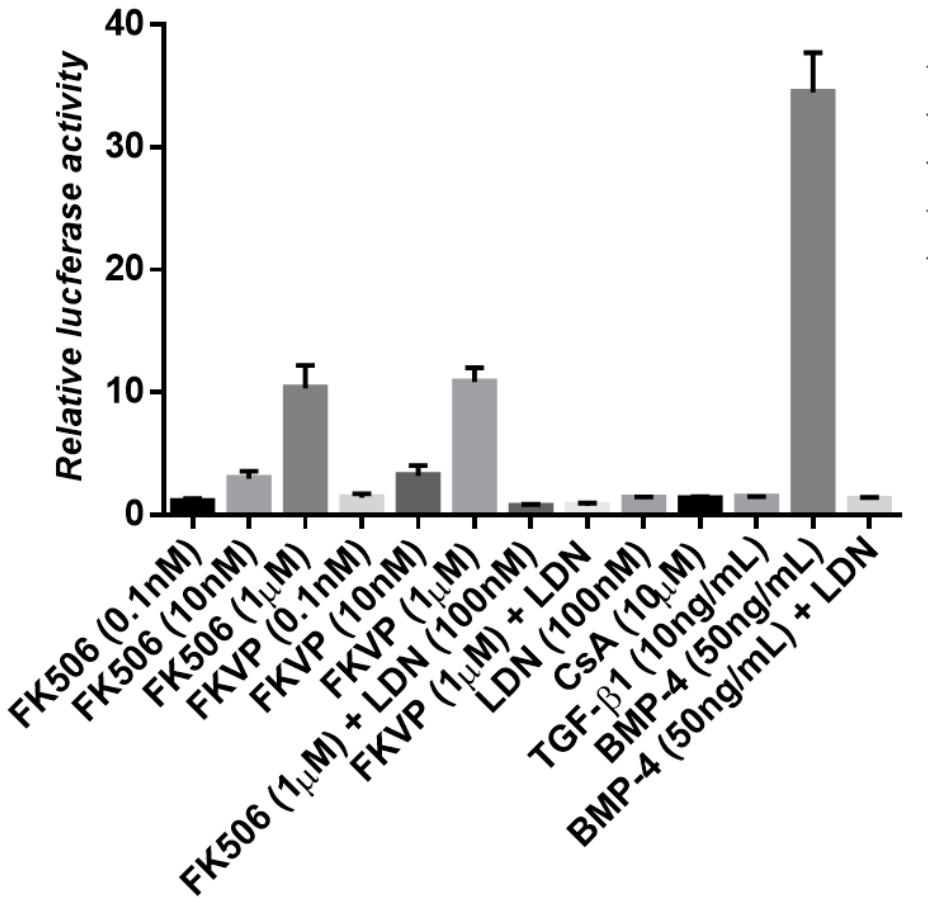

Figure 3.4: FKVP activates ID-1 reporter and pSMAD1/5 phosphorylation through BMP type 1 receptor activation. (**A**) BMP-response-element (BRE) reporter activity in Jurkat cells after treatment with increasing amounts of FK506 and FKVP. This activity is strongly inhibited by the addition of 100 nM LDN-193182. TGF-β1 serves as negative control, while BMP4 shows strong induction of luciferase expression after 18 hours. Relative luciferase activities were determined upon normalization to DMSO control values. Error bars represent standard deviation from mean.

To study downstream BMPR1 signaling events, we determined the effects of FK506 and FKVP on the phosphorylation of SMAD1/5. Both compounds induced SMAD1/5 phosphorylation in a dose-dependent manner (**Fig. 3.5A**), an effect abolished by LDN treatment (**Fig. 3.5B**).

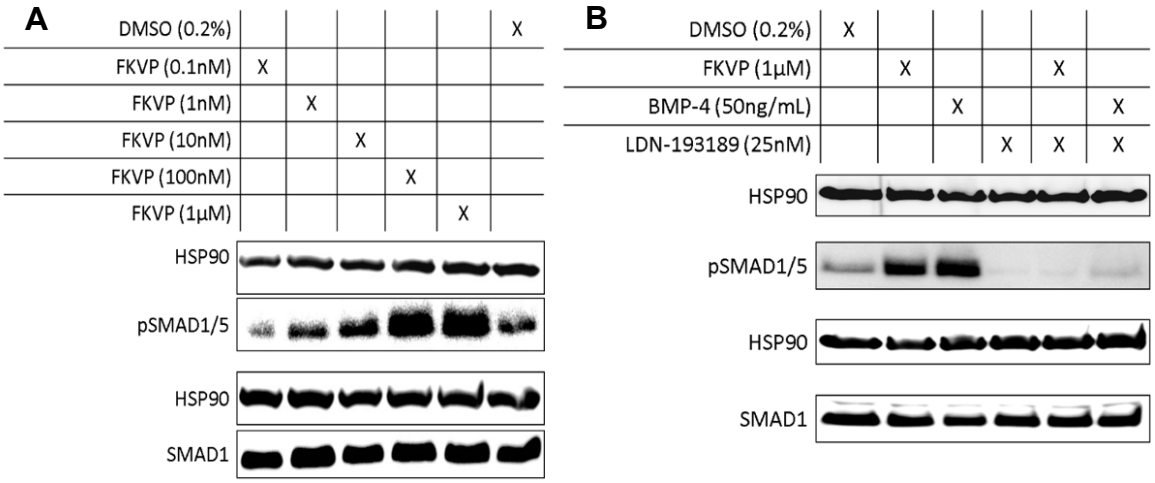

Figure 3.5: Western blotting for FKVP-induced SMAD1/5 phosphorylation in Jurkat cells. (A) Dose-dependent induction of SMAD1/5 phosphorylation by 2 hour FKVP treatment in Jurkat cells. (**B**) BMPR1-selective inhibitor LDN-193189 inhibits SMAD1/5 phosphorylation induced by FKVP or BMP-4 (positive control) treatment after 2 hours.

In contrast, there were no increases in phosphorylated SMAD2/3 under the same conditions (**Fig. 3.6**), suggesting that while FKBP12 may bind TGF-β receptors (Chen et al., 1997), its dissociation is insufficient to activate receptor kinase activity in the absence of TGF-β. This result is in agreement with previous studies showing that FK506 and non-immunosuppressive analogs are incapable of activating TGF-β pathway reporters without the addition of exogenous ligand (Spiekerkoetter et al., 2013; Wang et al., 1996).

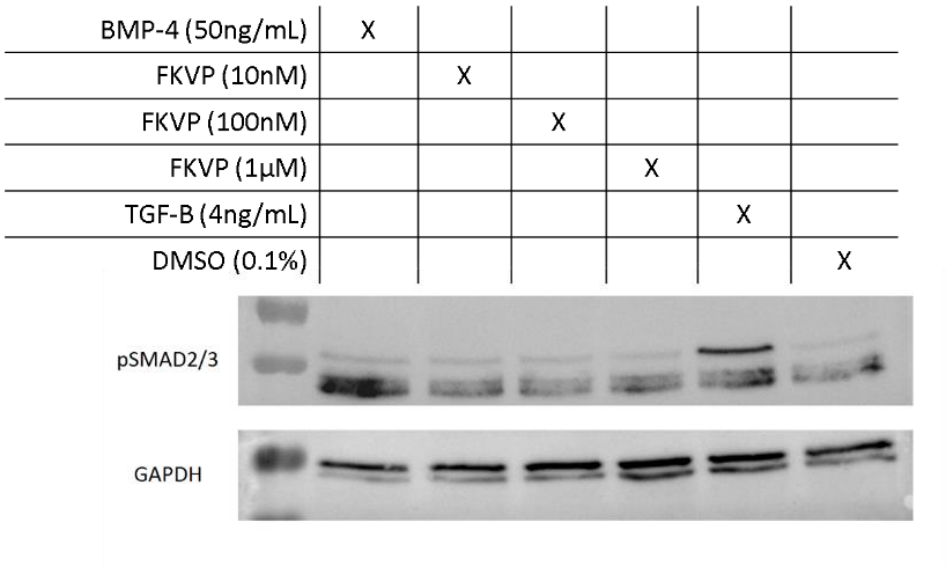

Figure 3.6: Western blotting for FKVP-induced SMAD2/3 phosphorylation in Jurkat cells. After 2 hours, FKVP does not induce SMAD2/3 phosphorylation in Jurkat cells compared to TGF-β1 (positive control).

In the BRE-luciferase reporter, AMD3100 was found to have no significant effect on ID-1 promoter stimulation alone or in combination with FKVP (**Fig. 3.7**). This suggests that the synergistic activity of these drugs does not converge at BMP signaling. A previous report has suggests that BMP-9 treatment enhances CXCR4 mRNA

expression in endothelial cells (Young et al, 2012), but it remains to be seen if small-molecule BMP activation can mimic this effect.

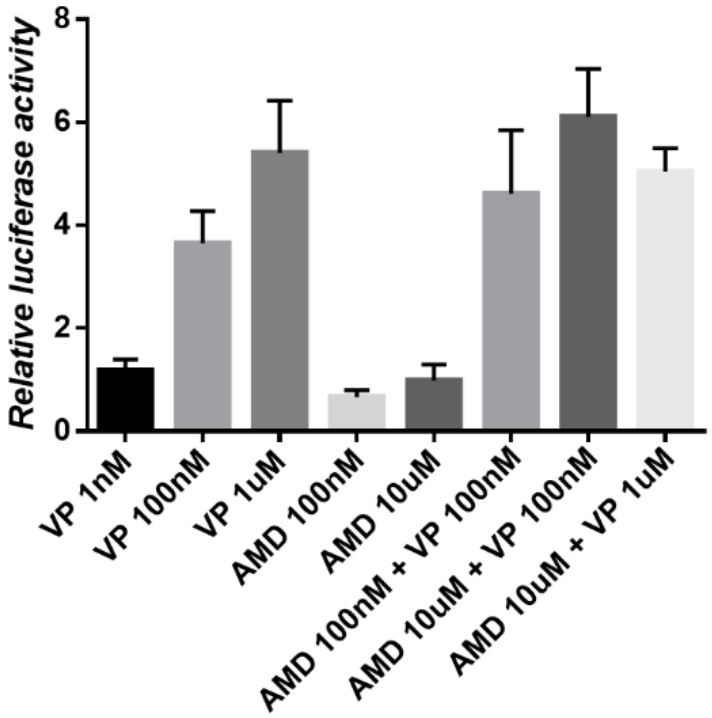

Figure 3.7: AMD-3100 does not affect BMP signaling alone, or in combination with FKVP. FKVP and AMD3100 single and combination treatments in Jurkat BMP activation luciferase assay (n=3). Relative luciferase activities were determined upon normalization to DMSO control values. Error bars represent standard deviation from mean.

The extracellular space contains several extracellular BMP inhibitors that are critical for embryogenesis and stem cell differentiation. These ubiquitous proteins bind to BMPs, preventing activation of BMPR and downstream signaling. This environment may

complicate the use of recombinant BMP protein for clinical uses. Conversely, we found that the extracellular BMP-inhibitor protein, noggin, was not effective at reducing FK506- or FKVP-mediated induction of the BMP reporter (**Fig. 3.8**). These observations suggest that endogenous BMP is not required for signaling activation by FK506 or FKVP, and that these compounds could activate BMP in tissues with under-expression of BMP protein, or overexpression of extracellular inhibitors like noggin.

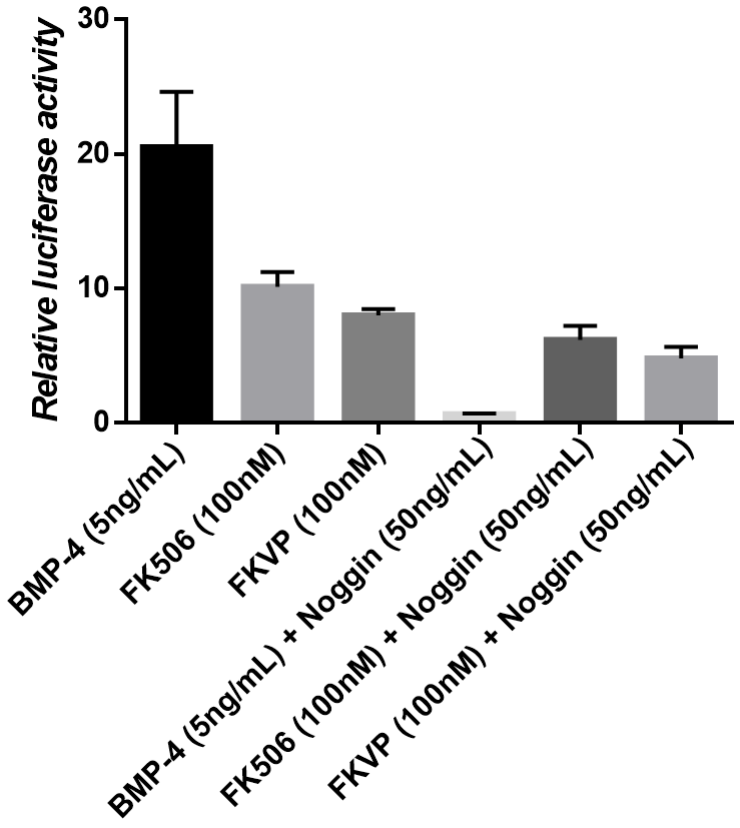

Figure 3.8: FKVP Activates BMP Signaling in the presence of the BMP inhibitor, Noggin. BMP-4, FKVP, FK506, and Noggin combination treatments in Jurkat BMP activation luciferase assay (n=3). Relative luciferase activities were determined upon normalization to DMSO control values. Error bars represent standard deviation from mean.

In addition, FKVP boosted the sensitivity of cells to BMP-4 stimulation in an additive fashion, suggesting that inhibition of FKBP12 binding promotes receptor activation by endogenous ligand (**Fig. 3.9**). While this is also observed in the case of TGF-β signaling (Wang et al, 1997), only BMP receptors have been found to be activated by FKBP12 inhibition in the absence of exogenous ligand (**Figure 3.8**). The reasoning for this may stem from the subtle differences in activation of the two receptor types (Mueller et al., 2015).

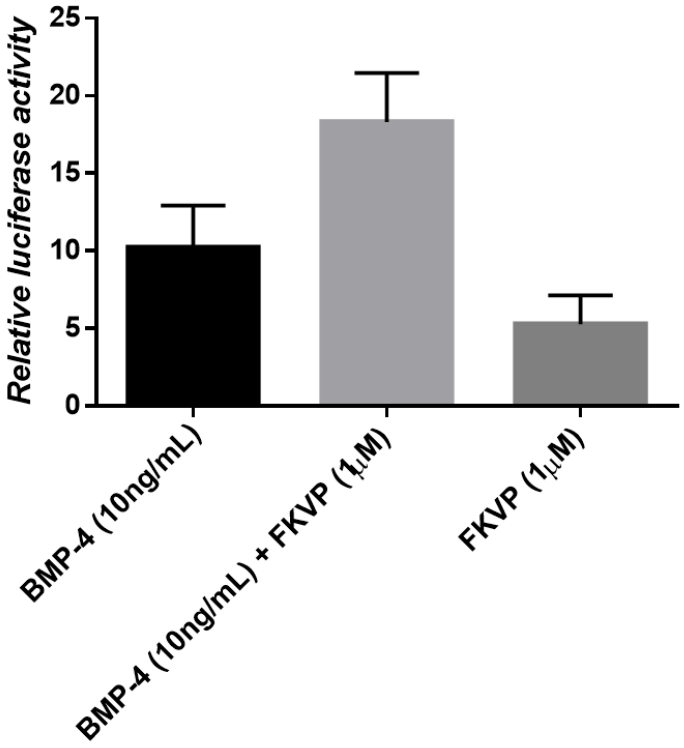

Figure 3.9: FKVP increases sensitivity of cells to BMP-4 stimulation. BMP-4, FKVP, and combination treatments in Jurkat BMP activation luciferase assay (n=3). Relative luciferase activities were determined upon normalization to DMSO control values. Error bars represent standard deviation from mean.

In addition to Jurkat, SMAD1/5 phosphorylation was significantly increased in HUVEC cells after FKVP treatment (**Fig. 3.10**), providing evidence that more than one cell type is sensitive to BMP activation by FKVP. A transient increase in erk (**Fig. 3.10b**) phosphorylation was found to occur as SMAD1/5 phosphorylation reached 50 percent.

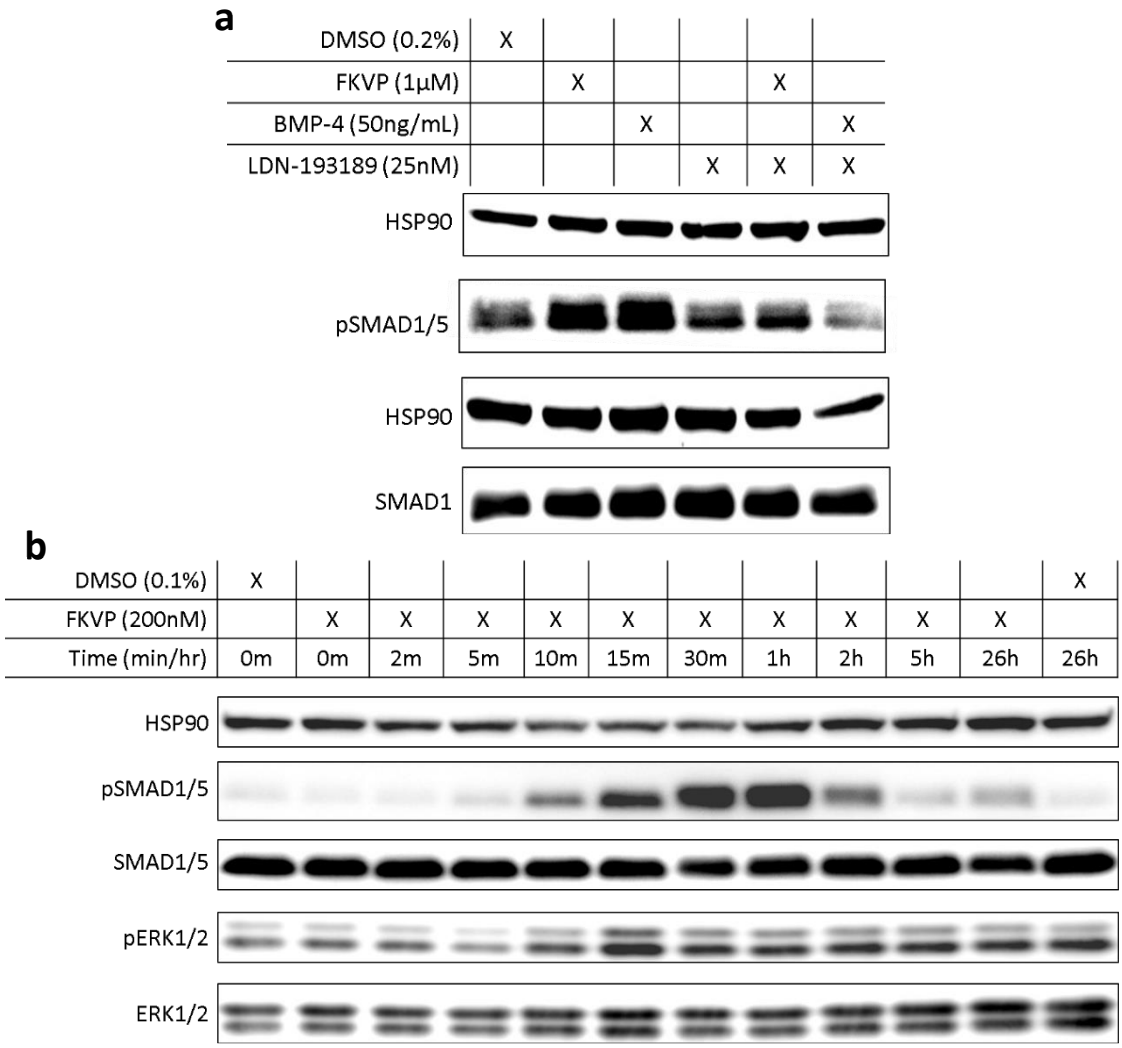

Figure 3.10: FKVP activates SMAD1/5 and ERK1/2 phosphorylation in HUVEC. **(A)** Western blot of SMAD1/5 phosphorylation after 2 hour treatment with BMP-4, FKVP, or LDN combination treatments in HUVEC cells. **(B)** Time-course western blot of HUVEC cells treated with 200 nM FKVP and blotted for both erk and SMAD1/5 phosphorylation.

A dominant downstream target of BMP pathway activation is ID protein expression. This class of proteins uses a pseudo-domain to bind and inhibit transcription factors involved in several cellular processes. We found that FKVP strongly activated ID1 expression in HUVEC cells as early as 1 hour after treatment. This increase coincides with the maximum state of SMAD1/5 phosphorylation (1 hour) after compound treatment (**Figure 3.10b**).

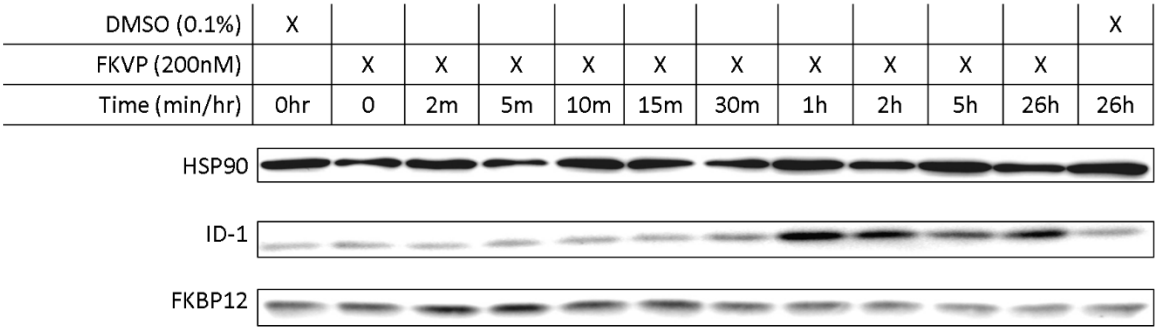

Figure 3.11: FKVP activates ID-1 expression in HUVEC. Time-course western blot of HUVEC cells treated with 200 nM FKVP and blotted for ID-1 expression. FKBP12 and HSP90 serve as loading controls.

Beyond canonical signaling, BMP receptor activation has been shown to crosstalk with other signaling pathways using BMP type 2 receptors. FKVP treatment was found to mimic these effects in a time-dependent manner. Specifically, a potent but transient increase in akt phosphorylation occurs just as SMAD1/5 phosphorylation begins to increase (**Fig. 3.12**). Furthermore, a modest increase in JNK phosphorylation was seen during the timeframe of peak SMAD1/5 phosphorylation (**Fig. 3.13**). This presents a

complex model of BMP activation by FKVP, as previous reports state that only BMPR1 is inhibited by FKBP12 (Wang et al, 1997). If BMPR2 is indeed activated by FKVP, it is most likely a result of association with an uninhibited BMPR1.

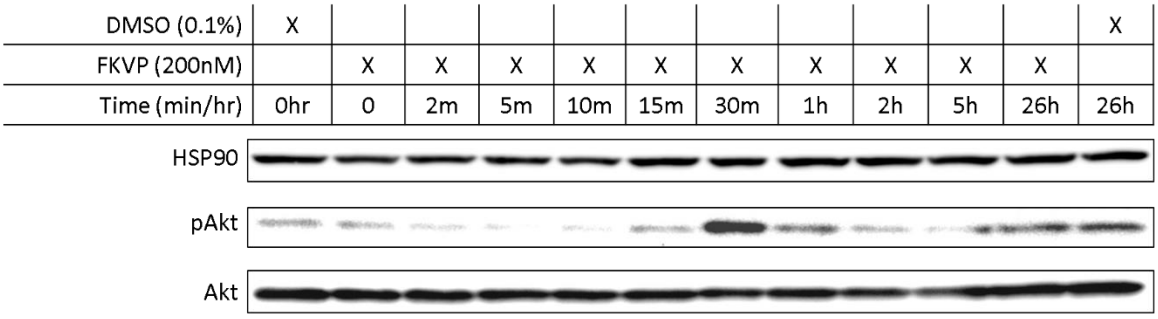

Figure 3.12: FKVP activates transient Akt phosphorylation in HUVEC. Time-course western blot of HUVEC cells treated with 200nM FKVP and blotted for phospho-Akt. Total Akt and HSP90 serve as loading controls.

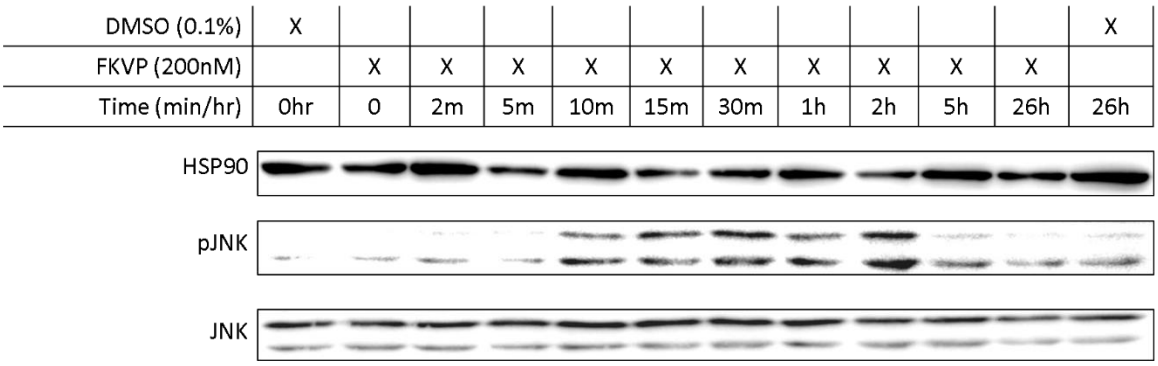

Figure 3.13: FKVP activates JNK phosphorylation in HUVEC. Time-course western blot of HUVEC cells treated with 200nM FKVP and blotted for phospho-JNK. Total JNK and HSP90 serve as loading controls.

To further challenge the ability of FKVP to activate TGF-B signaling, we probed for time dependent SMAD2/3 phosphorylation in HUVEC cells after compound treatment. Western blotting revealed a modest increase in SMAD2/3 phosphorylation that persisted through 26 hours, though this effect is not as prominent as seen in SMAD1/5 phosphorylation (**Fig. 3.10b**). Conversely, it can be suggested that DMSO treated cells also showed a time dependent increase. This may be a result of autocrine TGF-β signaling that occurs as cells divide and become more numerous within culture. HUVEC cells most likely produce more TGF-β protein than Jurkat cells, allowing FKBP12 antagonism to promote kinase activity in the presence of ligand.

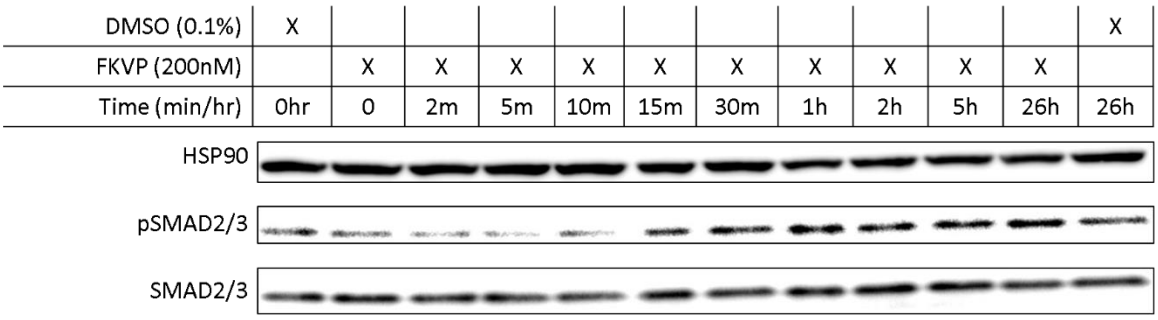

Figure 3.14: FKVP weakly increases SMAD2/3 phosphorylation in HUVEC. Time-course western blot of HUVEC cells treated with 200nM FKVP and blotted for phospho-SMAD2/3. Total SMAD2/3 and HSP90 serve as loading controls.

Together, these results indicated that both FK506 and FKVP are capable of activating BMPR1 kinase signaling, raising the possibility that this activation plays a key role in the healing acceleration activity of FK506 in the AF combination therapy.

FKBP12 alone is required for FKVP-induced SMAD1/5 phosphorylation.

FKBP12 is a member of the FKBP superfamily of proteins. In previous work, FKBP12 has been shown to be associated with the BMPR1 activin-like kinase 2 (ALK2). However, attempts to knock down several FKBPs failed to reveal a specific effect on BMPR1 signaling (Spiekerkoetter et al., 2013), likely due to the relative stability and high abundance of FKBPs. To address this problem, we generated CRISPR-Cas9 knockouts of three cytosolic FKBPs, FKBP12, FKBP51, and FKBP52 (**Fig. 3.15**).

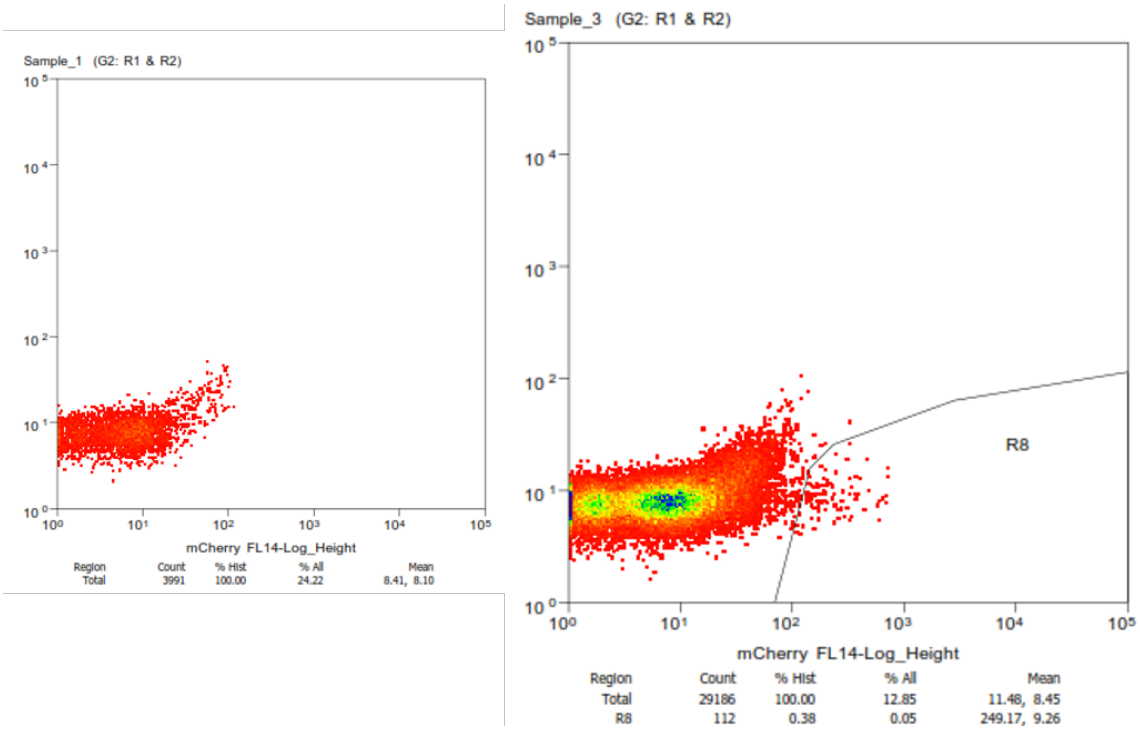

Figure 3.15: Representative plot of Jurkat FKBP-knockout cell sorting. Transfected Jurkat cells were single-cell sorted by m-cherry fluorescence (650nm laser) and PI staining into 96-well plates. Left panel indicates negative control cells, while right panel shows gating of m-cherry positive cells.

All three FKBP proteins have been reported to bind FK506 (Kozany et al., 2009). In the BRE-luciferase reporter assay, it was found that only FKBP12 knockout cells lost sensitivity to FK506 and FKVP (**Fig. 3.16**). While BMP activation looks to be reduced by FKBP12 knockout, the total value was actually higher. This is because FKBP12 knockout produces induces a BMP activated cell type with increased basal (DMSO) reporter activity.

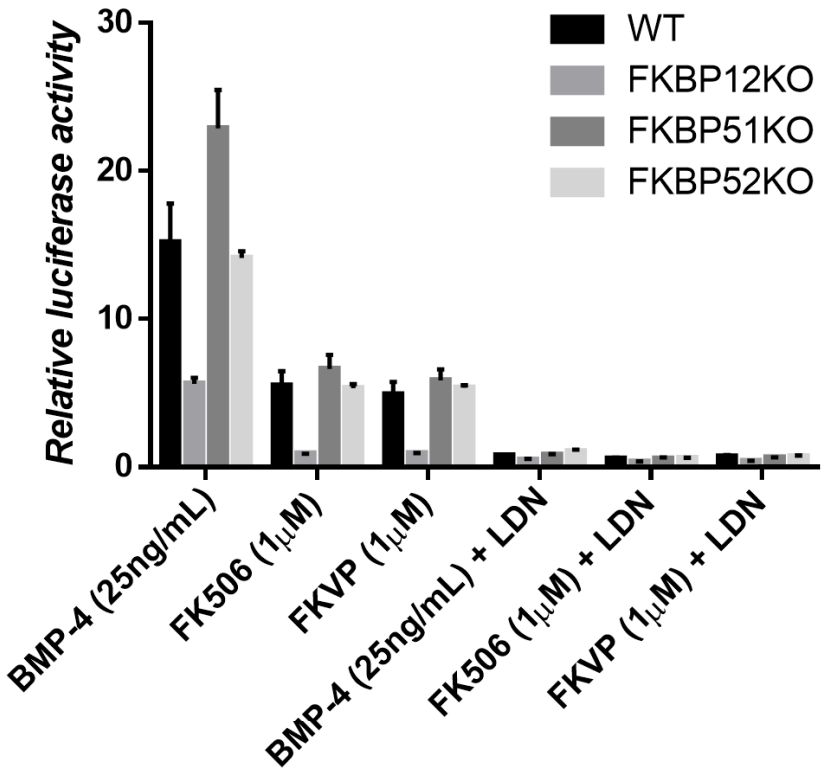

Figure 3.16: FKBP12 alone is required for FK506 and FKVP-induced SMAD1/5 phosphorylation. Activation of BMP pathway reporter by FKVP and FK506 in different FKBP isoform knockout cells and inhibition of the reporter gene activation by LDN (n = 3). Relative luciferase activities were determined upon normalization to DMSO control values. Error bars represent standard deviation from mean.

In agreement with reporter assays, it can be seen that FKBP12KO cells showed constitutively elevated levels of SMAD1/5 phosphorylation and resistance to further activation by FKVP (**Fig. 3.17**).

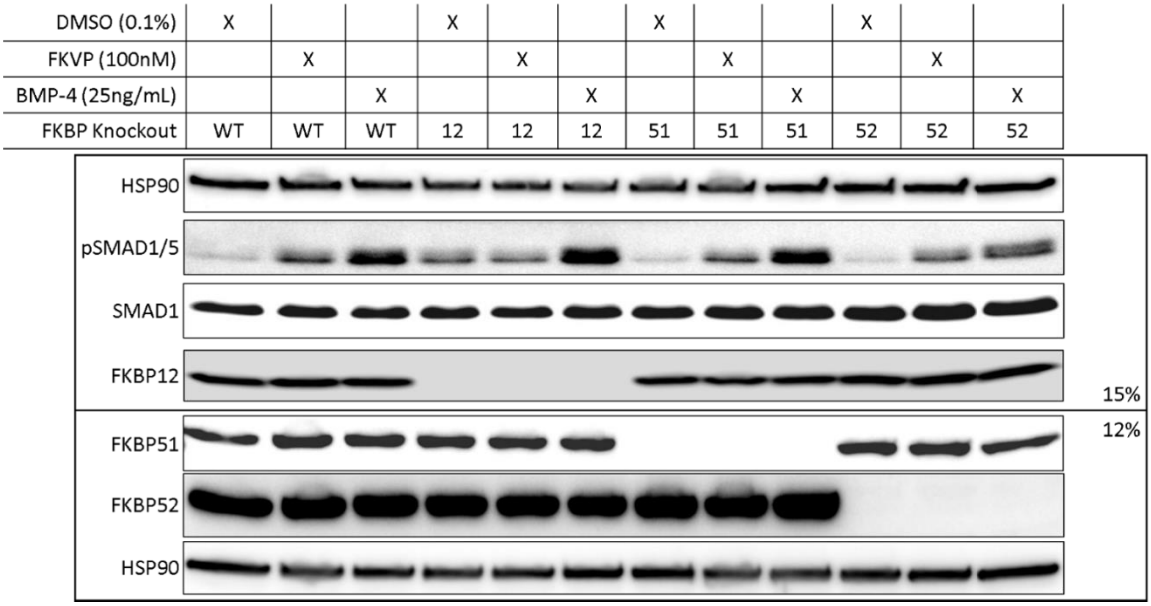

Figure 3.17: FKBP12 knockout cells show enhanced basal SMAD1/5 phosphorylation, and are insensitive to FKVP. Induction of SMAD1/5 phosphorylation by FKVP and BMP-4 in wild type and different FKBP isoform knockout cells.

To further validate FKBP12, we designed a fusion protein that could be used for further pulldown experiments. This protein was designed to include a c-terminal SNAP tag, known to covalently bind specialized probes. Using RaptorX software, we are able to model the fusion construct as evidence that the FK506 binding pocket was unobstructed. Furthermore, reconstitution of FKBP12 knockout cells with the fusion construct restored FK506/FKVP sensitivity in KO cells to that of the original parental line (**Fig. 3.18**). These results show that the designed FKBP12-SNAP protein retains the ability to bind either BMPR or FKVP/FK506.

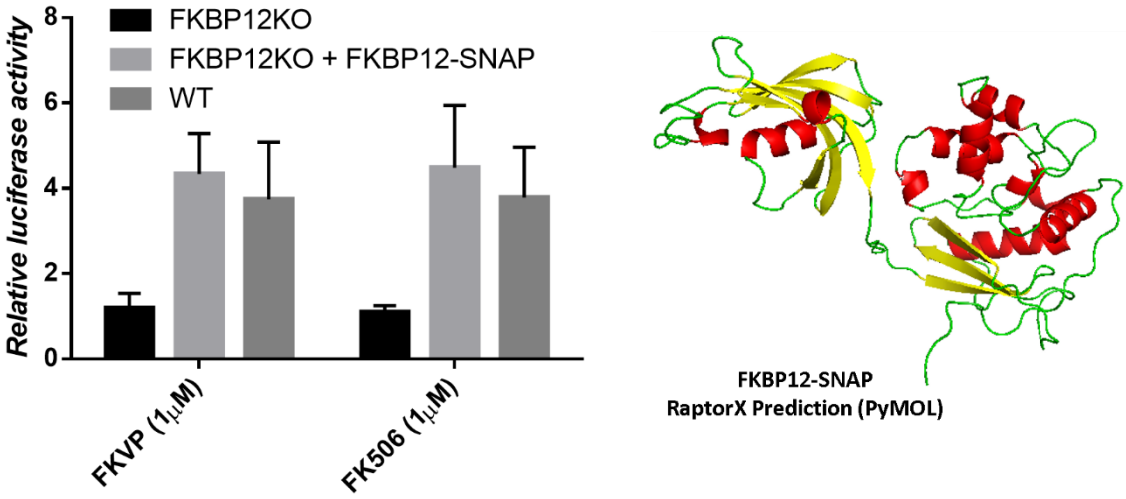

Figure 3.18: FKBP12-SNAP fusion construct restores FK506 and FKVP sensitivity in FKBP12 knockout cells. (A) BMP reporter assay in FKBP12KO cells show that expression of a novel FKBP12-SNAP fusion protein restores activation potential of FK506 and FKVP (n = 3). **(B)** RaptorX prediction of FKBP12-SNAP fusion protein.

We were able to use the aforementioned FKBP12-SNAP fusion protein to pull down calcineurin and mTOR in the presence of FK506 and rapamycin, respectively (**Fig. 3.19**). This further validates the use of FKBP12-SNAP for pulldown of BMP receptors, as it can be seen that all molecular targets of FKBP12 can be precipitated when the adaptor molecule is added. Moreover, the lack of staining in samples treated with FKVP supports the claim that FKVP does not cause FKBP12 to associate with calcineurin.

Input/Pulldown	I	I	I	I	I	I	P	P	P	P	P	P
DMSO	X						X					
FKVP (10uM)		X						X				
FK506 (10uM)			X						X			
Rapamycin (10uM)				X						X		
BMP-9 (25ng/mL)					X						X	
BMP-4 (50ng/mL)						X						X

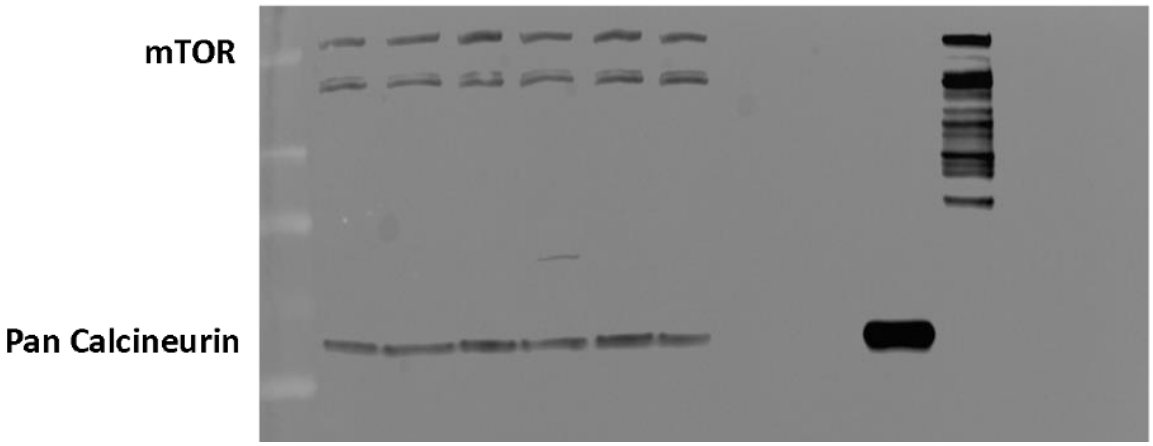

Figure 3.19: FKBP12-SNAP interacts with both mTOR and calcineurin. SNAP-tag pull-down and western blot showing that FKBP12-SNAP efficiently associates with both calcineurin and mTOR in the presence of FK506 and rapamycin, respectively. As a negative control, FKVP does not induce calcineurin association. BMP protein treatments were not probed for this experiment.

Continuing from our validation of FKBP12-SNAP in pulldown experiments, we then applied the same construct to pull down V5- or HA-tagged ALK (BMPR1) receptors from transfected HEK293T cells. From western blotting, we observed that SNAP-FKBP12 and ALK receptors did indeed interact with each other and the association was sensitive to competition by FKVP (**Fig. 3.20 - Fig 3.26**). This effect was most prominent in ALKs 1, 2, 3, and 5. The first three of these receptors (ALK 1,2,3) activate BMP signaling, while ALK 5 is the primary TGF-β type 1 receptor. These results suggest that FKVP and other FKBP12 antagonists act as *pan* BMP activators, where the receptor and level of activation are dependent on receptor expression.

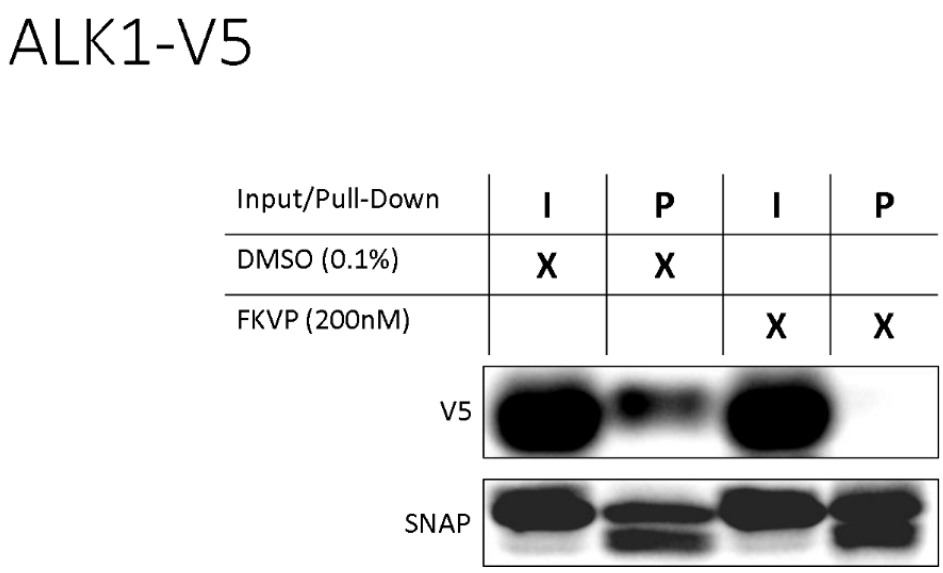

Figure 3.20: Pulldown of ALK1 receptor by FKBP12 is competed by FKVP treatment. V5-tagged ALK1 receptor and FKBP12-SNAP were co-expressed in FKBP12KO Hek293T cells, and SNAP-functionalized beads were used to precipitate associated proteins. Pulldowns were performed in the absence and presence of FKVP.

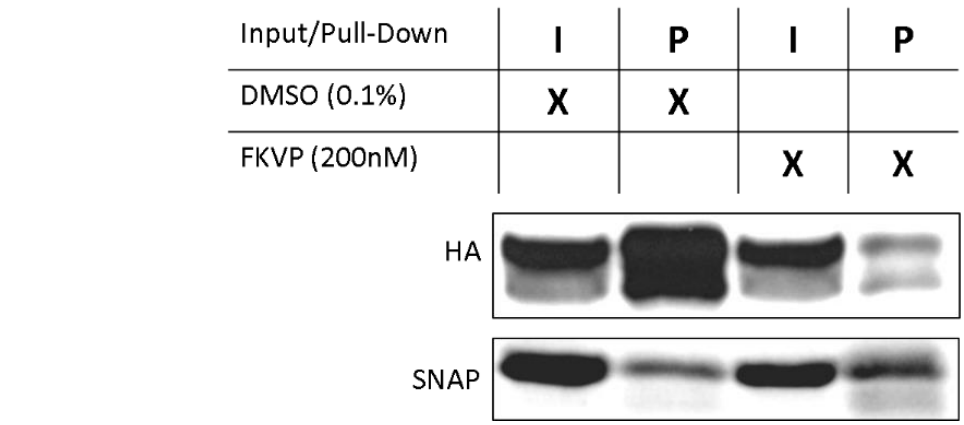

Figure 3.21: Pulldown of ALK2 receptor by FKBP12 is competed by FKVP treatment. HA-tagged ALK2 receptor and FKBP12-SNAP were co-expressed in FKBP12KO Hek293T cells, and SNAP-functionalized beads were used to precipitate associated proteins. Pulldowns were performed in the absence and presence of FKVP.

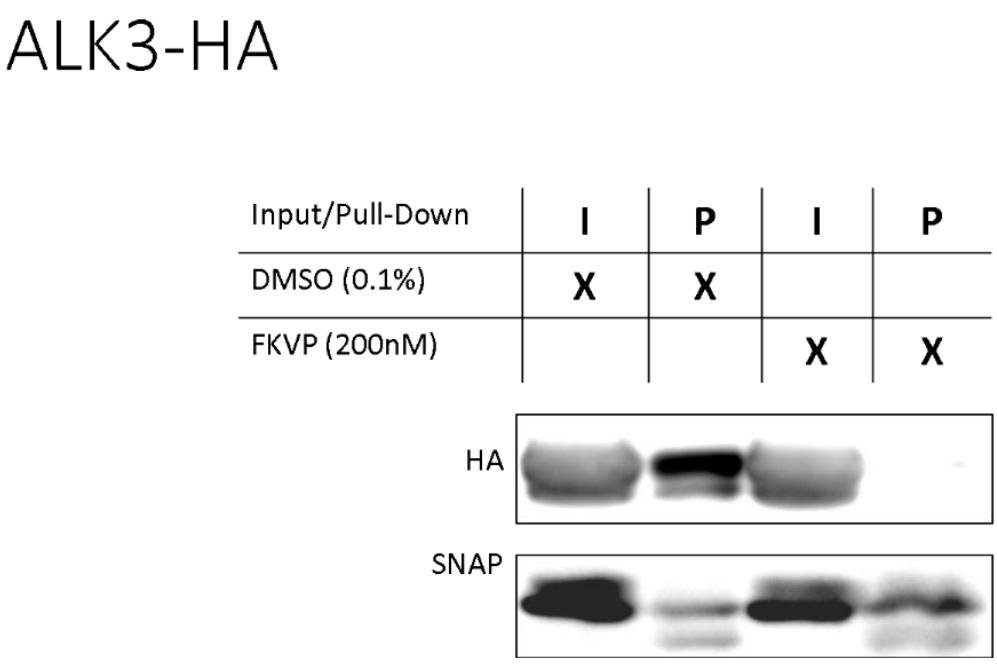

Figure 3.22: Pulldown of ALK3 receptor by FKBP12 is competed by FKVP treatment. HA-tagged ALK3 receptor and FKBP12-SNAP were co-expressed in FKBP12KO Hek293T cells, and SNAP-functionalized beads were used to precipitate associated proteins. Pulldowns were performed in the absence and presence of FKVP.

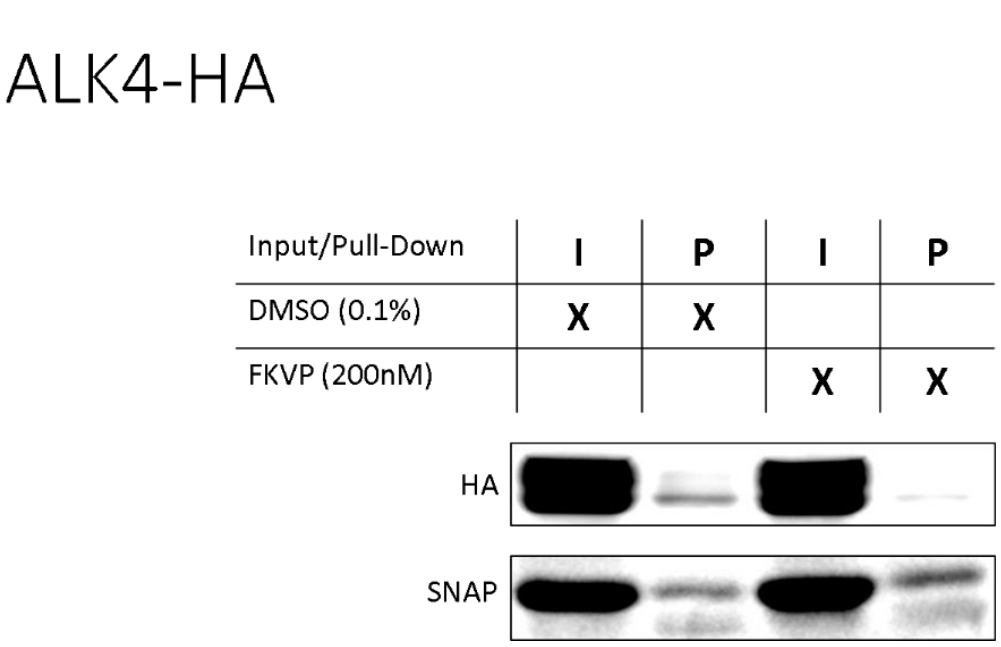

Figure 3.23: Pulldown of ALK4 receptor by FKBP12 is competed by FKVP treatment. HA-tagged ALK4 receptor and FKBP12-SNAP were co-expressed in FKBP12KO Hek293T cells, and SNAP-functionalized beads were used to precipitate associated proteins. Pulldowns were performed in the absence and presence of FKVP.

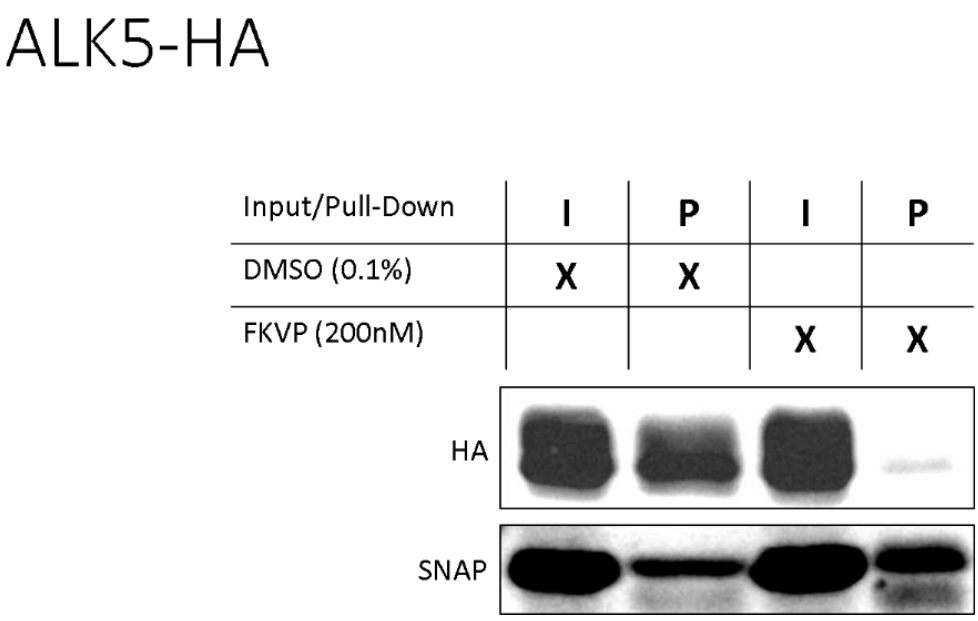

Figure 3.24: Pulldown of ALK5 receptor by FKBP12 is competed by FKVP treatment. HA-tagged ALK5 receptor and FKBP12-SNAP were co-expressed in FKBP12KO Hek293T cells, and SNAP-functionalized beads were used to precipitate associated proteins. Pulldowns were performed in the absence and presence of FKVP.

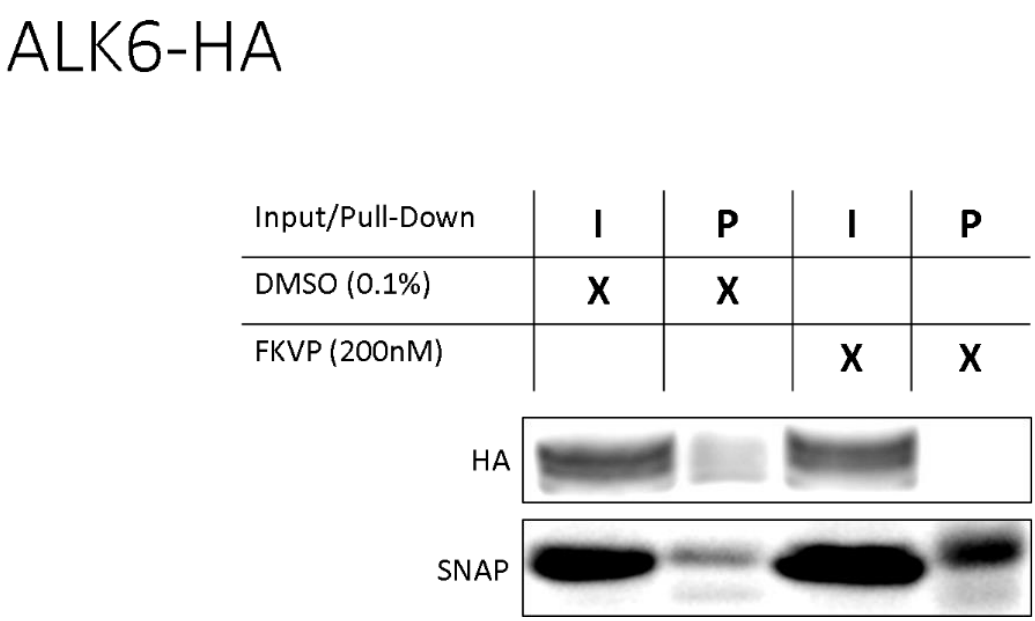

Figure 3.25: Pulldown of ALK6 receptor by FKBP12 is competed by FKVP treatment. HA-tagged ALK6 receptor and FKBP12-SNAP were co-expressed in FKBP12KO Hek293T cells, and SNAP-functionalized beads were used to precipitate associated proteins. Pulldowns were performed in the absence and presence of FKVP.

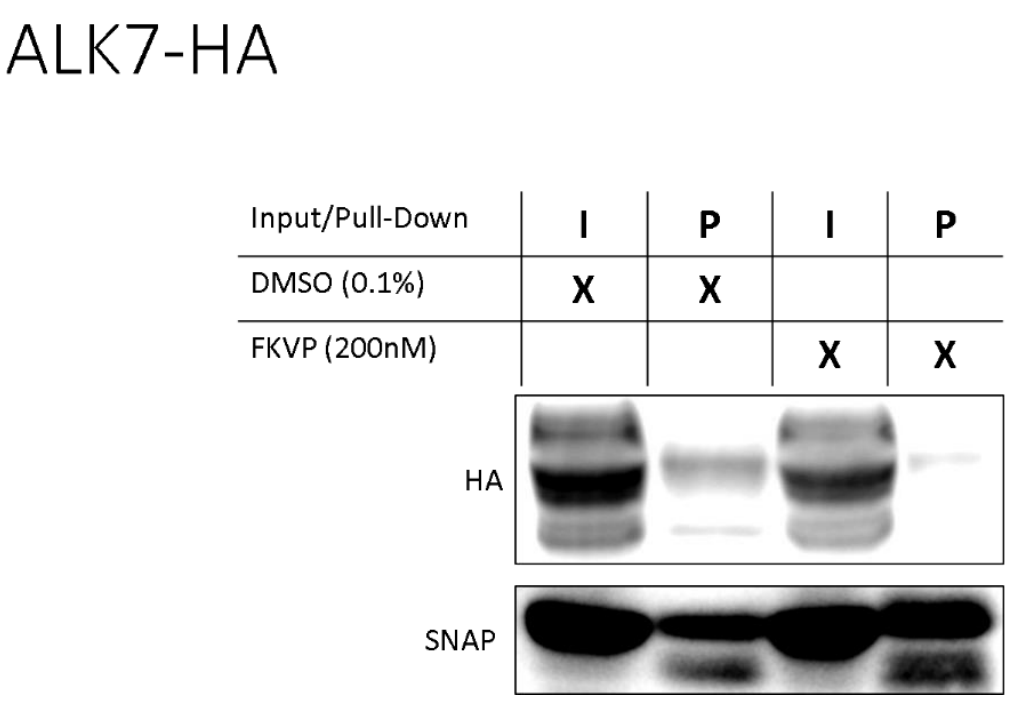

Figure 3.26: Pulldown of ALK7 receptor by FKBP12 is competed by FKVP treatment. HA-tagged ALK7 receptor and FKBP12-SNAP were co-expressed in FKBP12KO Hek293T cells, and SNAP-functionalized beads were used to precipitate associated proteins. Pulldowns were performed in the absence and presence of FKVP.

BMP signaling is required for the effect of AF combination in accelerating wound healing

To determine if BMP activation by FK506 is responsible for accelerated wound healing, a selective BMPR1 kinase inhibitor, LDN-193189 (2mg/kg/day, i.p.) was administered to wounded GK rats treated with saline or AF combination. LDN has been shown effective in vivo (Cuny et al., 2008; Sun et al., 2013), and alone showed no effect on wound healing. Interestingly, LDN abolished the beneficial effect of AF combination therapy and increased the time for complete healing from 21 to 25 days (**Fig. 3.27A and 3.27B**).

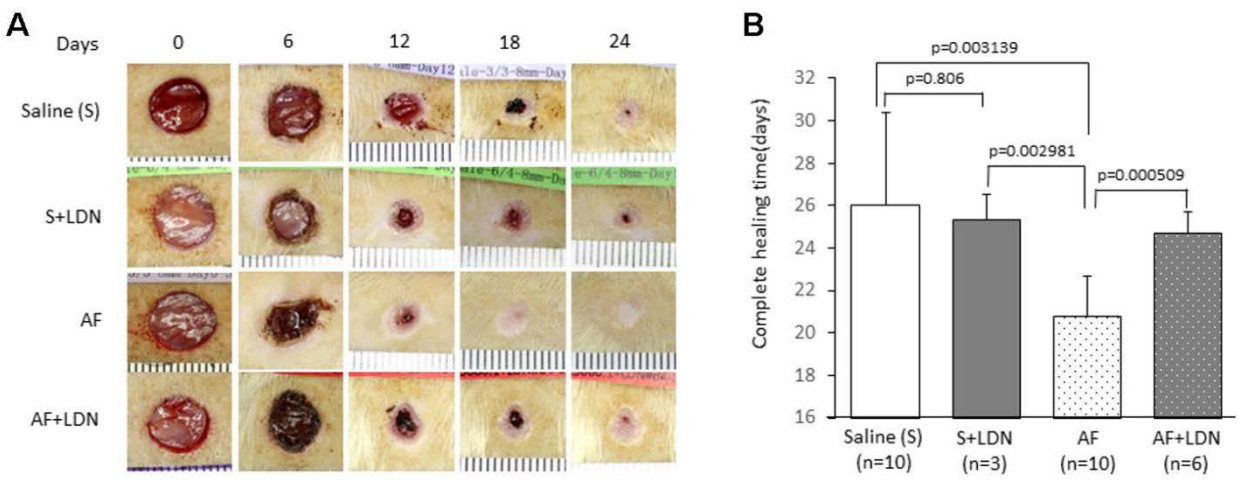

Figure 3.27: Blockade of BMP signaling abrogates the beneficial effect of AF combination therapy in wound healing. (**A**) Representative photographs of wounds in GK rats treated with saline, LDN, AF or AF plus LDN showing difference between AF and AF plus LDN beginning at day 12. (**B**) Quantitative analysis of complete healing time in GK rats. All data represented by mean ± SEM.

We have reported that FK506 plays a key role in recruitment of AMD3100 mobilized CD133 stem cells into wound sites (Lin et al., 2014) or injured organs (Okabayashi et al., 2011; Hu et al., 2016; Cameron et al., 2016; Zhai et al., 2018). To further confirm if blocking BMP signaling inhibits the recruitment of stem cells, we performed immunohistochemistry staining for CD133 in wound tissue sections recovered from animals at day 7 after surgery. A few CD133+ cells were identified in wound tissue sections from animals treated with saline (**Fig. 3.28**). The number of CD133+ cells was significantly increased in newly formed granulation tissues of the wounds in animals receiving AF combination therapy. Strikingly, administration of BMP inhibitor LDN dramatically reduced the number of CD133+ cells in the wounds in animals with AF combination treatment. Taken together, these results suggest that the recruitment of more CD133+ stem cells into the wound sites by AF combination treatment depends on BMP activation by FK506, and that blockade of BMP signaling with LDN eliminates the beneficial effect of AF combination therapy.

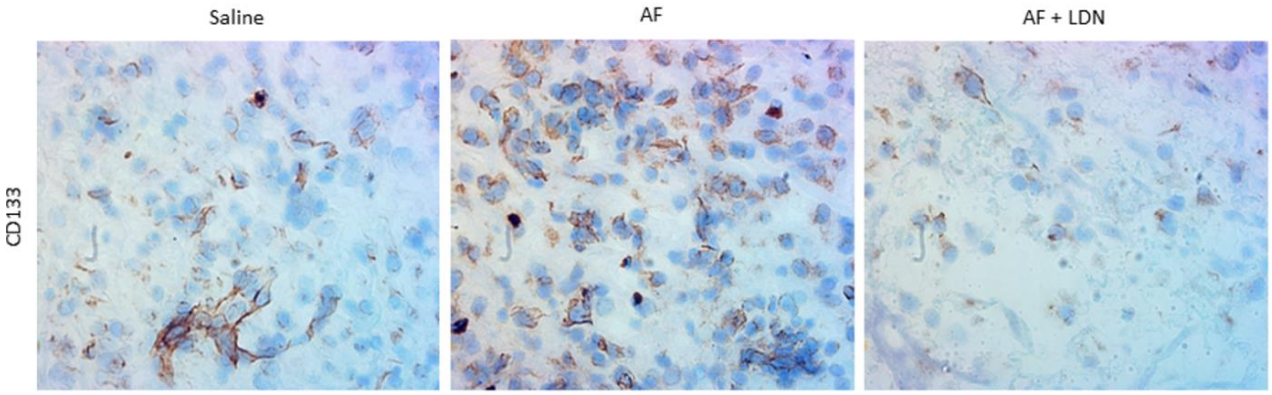

Figure 3.28: Blockade of BMP signaling prevents CD133 recruitment induced by AF combination therapy. Representative immunohistochemical staining for the stem cell marker CD133 in granulation tissues of GK rats at day 7. The rats receiving AF treatment had significantly higher number of CD133 cells (brown) in granulation tissues compared to the saline control group, while LDN treatment dramatically reduced the number of CD133 stem cells in the wound sites.

To detect *in vivo* SMAD1/5 phosphorylation, we employed a PE-conjugated pSMAD1/5 antibody to measure BMP activation by flow cytometry. Preliminary *in vitro* testing in Jurkat cells showed 2 hour FKVP or BMP-4 treatment resulted in increased staining, while DMSO results resembled the unstained control (**Fig. 3.29**).

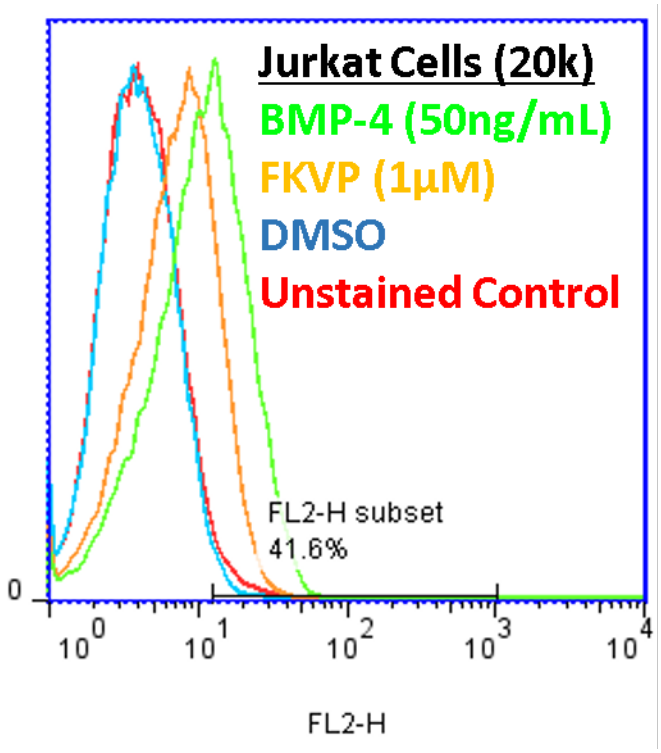

Figure 3.29: Flow cytometry testing of pSMAD1/5-PE antibody in Jurkat cells. Twenty thousand events were collected for each group after 2 hour treatment. Both FKVP and BMP-4 show enhanced PE fluorescence.

To measure in vivo SMAD1/5 phosphorylation in stem cells, we co-stained PBMCs from treated GK rats with antibodies for both pSMAD1/5 and the surface marker CD133. While the results were insignificant due to small sample size, there is a trend of increased $pSMAD^{+}CD133^{+}$ cells after AF treatment that is mildly reduced by LDN co-treatment (**Fig. 3.30**).

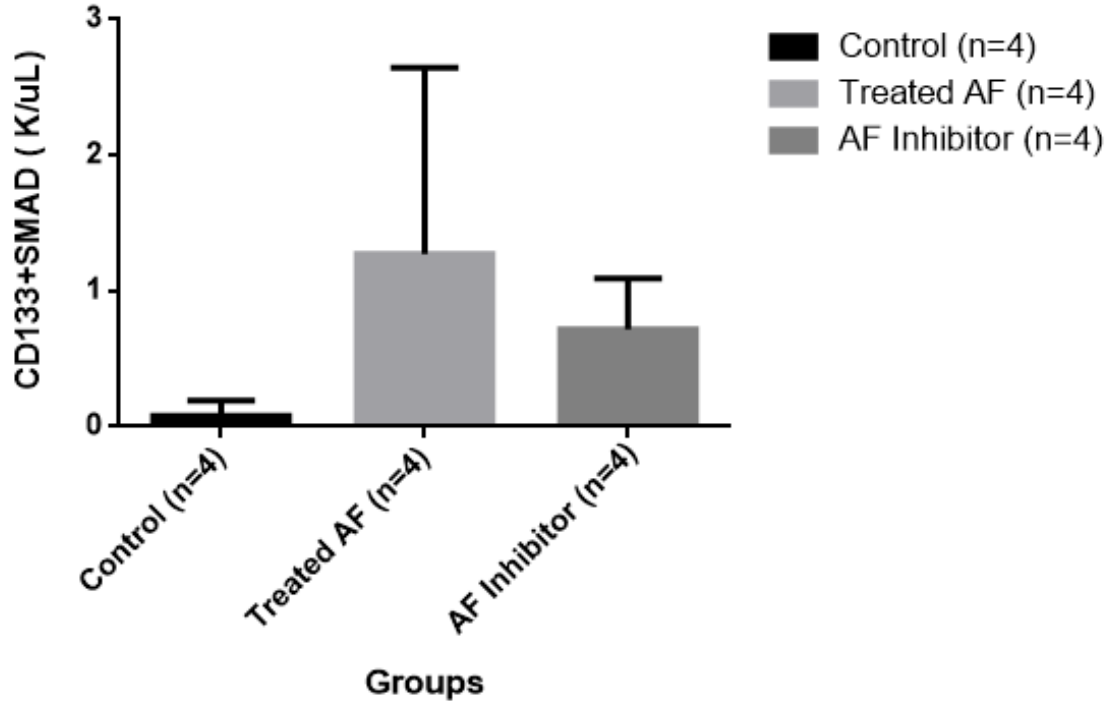

Figure 3.30: BMP inhibitor LDN may reduce AF-induced SMAD1/5 phosphorylation in circulating CD133+ cells of GK rats. GK rats were treated with ether saline, AF therapy, or AF + LDN for 3 hours before PBMC isolation and staining for CD133 and pSMAD1/5. AF therapy appears to increase SMAD1/5 phosphorylation in CD133+ cells, and this increase may be reduced by LDN treatment. Final results were insignificant but could be improved by proper timing of treatment administration and increased sample size.

We questioned whether or not SMAD1/5 phosphorylation could influence endothelial progenitor cell mobilization, aiding in wound healing through increased neovascularization. PBMCs from treated GK rats were stained for both CD133 and CD31, an endothelial cell marker. AF treatment significantly enhanced endothelial progenitor mobilization, an effect rendered insignificant by co-administration of the BMP inhibitor LDN (**Fig. 3.31**).

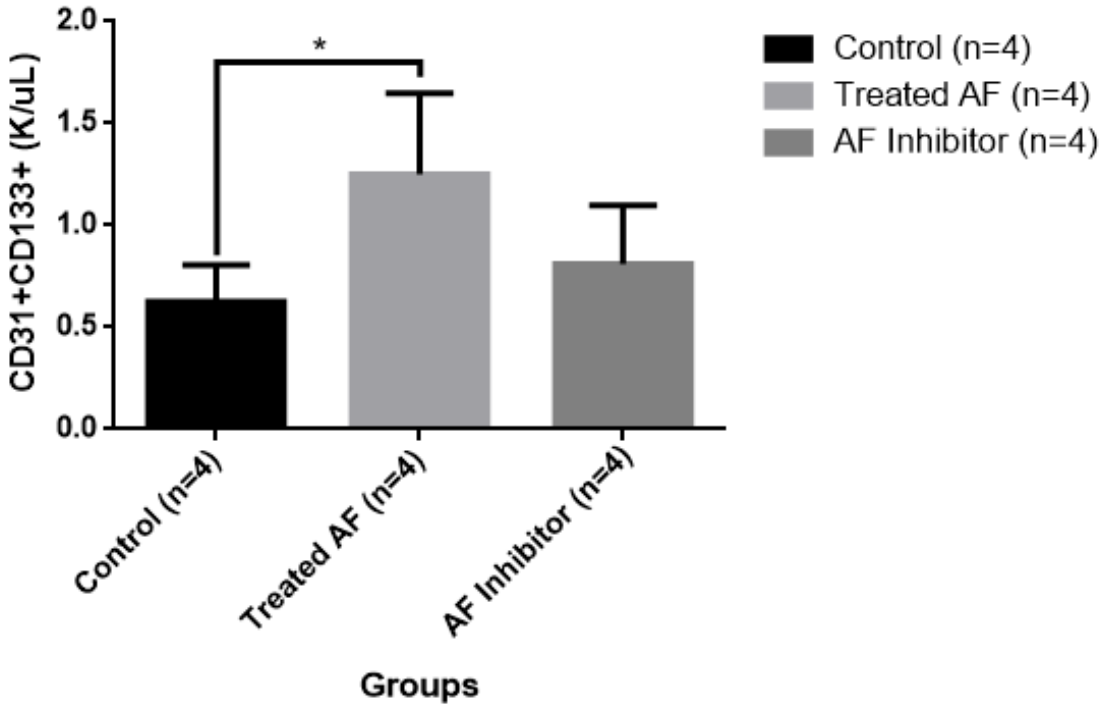

Figure 3.31: BMP inhibitor LDN reduces circulating CD133+ CD31+ cells in GK rats after AF treatment. GK rats were treated with ether saline, AF therapy, or AF + LDN for 3 hours before PBMC isolation and staining for extracellular markers. LDN affectively reduced the number of cells mobilized by AF therapy to the point of insignificance compared to saline.

3.3 METHODS

Reagents and Materials

Reactions were monitored by mass spectrometry provided by Agilent 6120 Quadrupole LC/MS. PLC Silica gel 60 F_{254}, 1mm supplied by EMD Millipore using UV light as visualizing agent.

^{1}H-NMR was recorded on Bruker Avance III 500 MHz NMR spectrometer. TMS was used as internal standard for ^{1}H-NMR (0 ppm). High-resolution mass spectra (HRMS) were recorded on Waters Synapt G2-Si mass spectrometer using ESI (electrospray ionization). FK-506 (Tacrolimus) was purchased from Biotang Inc. Zhan-1b catalyst, palladium acetate and tris(o-tolyl)phosphine were purchased from Aldrich.

Chemicals: Research-grade FK506 (>98%) was purchased from APExBIO. LDN-193189 hydrochloride, 4-vinylpyridine, and solvents were purchased form MilliporeSigma. Zhan-1b Ruthenium catalyst (CAS: 918870-76-5) was purchased from STREM Chemicals.

Cell Culture and Transfections

Jurkat (E6.1, ATCC) cells were cultured in RPMI with 10% FBS and 1.5% PennStrep. Jurkat cells (1 x 10^{6}) were transfected with 10 μg of BRE-Luciferase (kindly provided by Martine Roussel & Peter ten Dijke) or NFAT-Luciferase cDNA (Promega) by electroporation (BioRad, square-wave, 250V, 950μF) in 400 μL serum/antibiotic free RPMI with 0.5% DMSO. Thirty minutes after transfection, cells were transferred to complete RPMI and rested overnight. Before plating, cells were re-suspended in fresh

media and diluted to $0.5x10^6$ cells/mL. HEK293T cells were cultured in DMEM with 10% FBS, 1% PennStrep, and 500 µg/mL G418 (Corning). Cells were transfected using SuperFect reagent and supplied transfection protocols. HUVEC cells were cultured in Lonza Endothelial Cell Growth Medium (EGM-2) and used between passages 3 and 7. All cells were cultured at 37 °C with 5% CO_2.

Cell Viability Assays

Jurkat or HUVEC cells were plated at 1000 cells/well in 180 µL growth media before addition of 20 µL of 10X drug/protein stock. After incubation for 72 h, 22 µL of a resazurin sodium salt solution (0.1 mg/mL stock in water) was added to each well and allowed to incubate at 37°C. The metabolic conversion of resazurin dye was monitored by absorbance at 570 nm after 6 h. After background subtraction (media only + dye), absorbance values were left as arbitrary absorbance units or normalized to those obtained from cells treated with DMSO.

Western Blot

Jurkat T cells were collected by centrifugation (300g, 5 min), washed with PBS, and lysed in RIPA buffer containing protease and phosphatase inhibitors (Cell Signaling) with sonication. Lysates were normalized using DC assay (BioRad) and run on SDS-PAGE gels. Proteins were transferred to nitrocellulose membranes overnight at 100mA. After blocking with 5% milk in TBS-T for 20 min, membranes were incubated overnight at 4°C with primary antibodies (**Table 3.1**). After washing three times with TBS-T,

membranes were incubated with secondary antibody (**Table 3.1**) for 1 hour. After 3 additional washes, blots were visualized using SynGene, either using ECL substrate (Thermo) or laser excitation and filter (647nm).

Table 3.1: Manufacturers' information and recommended concentrations of antibodies for western blotting and IHC.

Target	Conjugate	Recommended Concentration	Manufacturer	Catalog #	Antibody Usage
p-SMAD1/5	None	1:750	Cell Signaling	41D10	WB Primary
SMAD1	None	1:500	Cell Signaling	9473S	WB Primary
p-SMAD2/3	None	1:400	Cell Signaling	8828S	WB Primary
NFATc2	None	1:100	Santa Cruz	SC-7296	WB Primary
p-S6	None	1:1000	Santa Cruz	SC-293144	WB Primary
S6	None	1:1000	Cell Signaling	2217	WB Primary
ID1	HRP	1:100 or 1:500 w/secondary	Santa Cruz	SC-133104-HRP	WB Primary
FKBP12	None	1:750	Abcam	92459	WB Primary
FKBP51	None	1:750	Abcam	Ab126715	WB Primary
FKBP52	None	1:750	Santa Cruz	SC-1803	WB Primary
mTOR	None	1:1000	Cell Signaling	2983S	WB Primary
Pan Calcineurin	None	1:1000	Cell Signaling	2614S	WB Primary
HA-Tag	None	1:1000	Cell Signaling	3724S	WB Primary
V5-Tag	None	1:1000	Thermo	46-0705	WB Primary
HSP90α/β	None	1:1000	Santa Cruz	SC-13119	Loading Control (WB Primary)
GAPDH	None	1:2000	Santa Cruz	SC-20357	Loading Control (WB Primary)
HSP90α/β	None	1:1000	Santa Cruz	SC-7947	Loading Control (WB Primary)
Rabbit 2°Ab	HRP	1:10000	Cell Signaling	7074S	WB Secondary
Rabbit 2°Ab	Alexa 647	1:1000	Thermo	A-31573	WB Secondary
Mouse 2°Ab	HRP	1:8000	GE Healthcare	NA931V	WB Secondary
Goat 2°Ab	HRP	1:10000	Santa Cruz	SC-2354	WB Secondary
CD133	None	1:300	Abcam	ab19898	IHC Primary
Rabbit 2°Ab	Biotin	1:200	Cell Signaling	14708S	IHC Secondary

FKBP12-SNAP Cloning

FKBP12-SNAP was cloned using pSNAPf vector (New England Bio) and PCR-amplified FKBP12 (a gift from Tobias Meyer, Addgene plasmid # 20175) with added EcoRI and BsrGI restriction sites. Gel-purified plasmids were ligated using T4 DNA ligase (Thermo), transformed into DH5α, and plated on LB-agar plus ampicillin for single colony selection, sequencing, and plasmid purification.

FKBP12-SNAP Full Sequence: Deduced from CMV-forward primer sequencing aligned with sequences provided by NEB (6166 bp)

1 GACGGATCGG GAGATCTCCC GATCCCCTAT GGTGCACTCT CAGTACAATC TGCTCTGATG
61 CCGCATAGTT AAGCCAGTAT CTGCTCCCTG CTTGTGTGTT GGAGGTCGCT GAGTAGTGCG
121 CGAGCAAAAT TTAAGCTACA ACAAGGCAAG GCTTGACCGA CAATTGCATG AAGAATCTGC
181 TTAGGGTTAG GCGTTTTGCG CTGCTTCGCG ATGTACGGGC CAGATATACG CGTTGACATT
241 GATTATTGAC TAGTTATTAA TAGTAATCAA TTACGGGGTC ATTAGTTCAT AGCCCATATA
301 TGGAGTTCCG CGTTACATAA CTTACGGTAA ATGGCCCGCC TGGCTGACCG CCCAACGACC
361 CCCGCCCATT GACGTCAATA ATGACGTATG TTCCCATAGT AACGCCAATA GGGACTTTCC
421 ATTGACGTCA ATGGGTGGAG TATTTACGGT AAACTGCCCA CTTGGCAGTA CATCAAGTGT
481 ATCATATGCC AAGTACGCCC CCTATTGACG TCAATGACGG TAAATGGCCC GCCTGGCATT
541 ATGCCCAGTA CATGACCTTA TGGGACTTTC CTACTTGGCA GTACATCTAC GTATTAGTCA
601 TCGCTATTAC CATGGTGATG CGGTTTTGGC AGTACATCAA TGGGCGTGGA TAGCGGTTTG
661 ACTCACGGGG ATTTCCAAGT CTCCACCCCA TTGACGTCAA TGGGAGTTTG TTTTGGCACC
721 AAAATCAACG GGACTTTCCA AAATGTCGTA ACAACTCCGC CCCATTGACG CAAATGGGCG
781 GTAGGCGTGT ACGGTGGGAG GTCTATATAA GCAGAGCTCT CTGGCTAACT AGAGAACCCA
841 CTGCTTACTG GCTTATCGAA ATTAATACGA CTCACTATAG GGAGACCCAA GCTTGGTACC
901 GAGCTCGGAT CGTCGCTAGC GATATCGGCG CGCCAGCATT TAAATCTGTA CAATGGGAGT
961 GCAGGTGGAA ACCATCTCCC CAGGAGACGG GCGCACCTTC CCCAAGCGCG GCCAGACCTG
1021 CGTGGTGCAC TACACCGGGA TGCTTGAAGA TGGAAAGAAA TTTGATTCCT CCCGGGACAG
1081 AAACAAGCCC TTTAAGTTTA TGCTAGGCAA GCAGGAGGTG ATCCGAGGCT GGGAAGAAGG
1141 GGTTGCCCAG ATGAGTGTGG GTCAGAGAGC CAAACTGACT ATATCTCCAG ATTATGCCTA
1201 TGGTGCCACT GGGCACCCAG GCATCATCCC ACCACATGCC ACTCTCGTCT TCGATGTGGA
1261 GCTTCTAAAA CTGGAAGAAT TCACCATGGA CAAAGACTGC GAAATGAAGC GCACCACCCT
1321 GGATAGCCCT CTGGGCAAGC TGGAACTGTC TGGGTGCGAA CAGGGCCTGC ACCGTATCAT
1381 CTTCCTGGGC AAAGGAACAT CTGCCGCCGA CGCCGTGGAA GTGCCTGCCC CAGCCGCCGT
1441 GCTGGGCGGA CCAGAGCCAC TGATGCAGGC CACCGCCTGG CTCAACGCCT ACTTTCACCA
1501 GCCTGAGGCC ATCGAGGAGT TCCCTGTGCC AGCCCTGCAC CACCCAGTGT TCCAGCAGGA
1561 GAGCTTTACC CGCCAGGTGC TGTGGAAACT GCTGAAAGTG GTGAAGTTCG GAGAGGTCAT
1621 CAGCTACAGC CACCTGGCCG CCCTGGCCGG CAATCCCGCC GCCACCGCCG CCGTGAAAAC
1681 CGCCCTGAGC GGAAATCCCG TGCCCATTCT GATCCCCTGC CACCGGGTGG TGCAGGGCGA
1741 CCTGGACGTG GGGGGCTACG AGGGCGGGCT CGCCGTGAAA GAGTGGCTGC TGGCCCACGA
1801 GGGCCACAGA CTGGGCAAGC CTGGGCTGGG TCCTGCAGGC GGATCCGCGT TTAAACTCGA
1861 GGTTAATTAA TGAGCGGCCG CATAGATAAC TGATCCAGTG TGCTGGAATT AATTCGCTGT
1921 CTGCGAGGGC CAGCTGTTGG GGTGAGTACT CCCTCTCAAA AGCGGGCATG ACTTCTGCGC
1981 TAAGATTGTC AGTTTCCAAA AACGAGGAGG ATTTGATATT CACCTGGCCC GCGGTGATGC
2041 CTTTGAGGGT GGCCGCGTCC ATCTGGTCAG AAAAGACAAT CTTTTTGTTG TCAAGCTTGA
2101 GGTGTGGCAG GCTTGAGATC TGGCCATACA CTTGAGTGAC AATGACATCC ACTTTGCCTT
2161 TCTCTCCACA GGTGTCCACT CCCAGGTCCA ACTGCAGGTC GAGCATGCAT CTAGGGCGGC
2221 CAATTCCGCC CCTCTCCCCC CCCCCCTTTT CCCTCCCCCC CCCCTAACGT TACTGGCCGA
2281 AGCCGCTTGG AATAAGGCCG GTGTGCGTTT GTCTATATGT TATTTTCCAC CATATTGCCG
2341 TCTTTTGGCA ATGTGAGGGC CCGGAAACCT GGCCCTGTCT TCTTGACGAG CATTCCTAGG
2401 GGTCTTTCCC CTCTCGCCAA AGGAATGCAA GGTCTGTTGA ATGTCGTGAA GGAAGCAGTT

2461 CCTCTGGAAG CTTCTTGAAG ACAAACAACG TCTGTAGCGA CCCTTTGCAG GCAGCGGAAC
2521 CCCCCACCTG GCGACAGGTG CCTCTGCGGC CAAAAGCCAC GTGTATAAGA TACACCTGCA
2581 AAGGCGGCAC AACCCCAGTG CCACGTTGTG AGTTGGATAG TTGTGGAAAG AGTCAAATGG
2641 CTCTCCTCAA GCGTATTCAA CAAGGGGCTG AAGGATGCCC AGAAGGTACC CCATTGTATG
2701 GGATCTGATC TGGGGCCTCG GTGCACATGC TTTACATGTG TTTAGTCGAG GTTAAAAAAA
2761 CGTCTAGGCC CCCCGAACCA CGGGGACGTG GTTTTCCTTT GAAAAACACG ATGATAAGCT
2821 TGCCACAACC CGGGATAATT CCTGCAGCCA ATATGGGATC GGCCATTGAA CAAGATGGAT
2881 TGCACGCAGG TTCTCCGGCC GCTTGGGTGG AGAGGCTATT CGGCTATGAC TGGGCACAAC
2941 AGACAATCGG CTGCTCTGAT GCCGCCGTGT TCCGGCTGTC AGCGCAGGGG CGCCCGGTTC
3001 TTTTTGTCAA GACCGACCTG TCCGGTGCCC TGAATGAACT GCAGGACGAG GCAGCGCGGC
3061 TATCGTGGCT GGCCACGACG GGCGTTCCTT GCGCAGCTGT GCTCGACGTT GTCACTGAAG
3121 CGGGAAGGGA CTGGCTGCTA TTGGGCGAAG TGCCGGGGCA GGATCTCCTG TCATCTCACC
3181 TTGCTCCTGC CGAGAAAGTA TCCATCATGG CTGATGCAAT GCGGCGGCTG CATACGCTTG
3241 ATCCGGCTAC CTGCCCATTC GACCACCAAG CGAAACATCG CATCGAGCGA GCACGTACTC
3301 GGATGGAAGC CGGTCTTGTC GATCAGGATG ATCTGGACGA AGAGCATCAG GGGCTCGCGC
3361 CAGCCGAACT GTTCGCCAGG CTCAAGGCGC GCATGCCCGA CGGCGATGAT CTCGTCGTGA
3421 CCCATGGCGA TGCCTGCTTG CCGAATATCA TGGTGGAAAA TGGCCGCTTT TCTGGATTCA
3481 TCGACTGTGG CCGGCTGGGT GTGGCGGACC GCTATCAGGA CATAGCGTTG GCTACCCGTG
3541 ATATTGCTGA AGAGCTTGGC GGCGAATGGG CTGACCGCTT CCTCGTGCTT TACGGTATCG
3601 CCGCTCCCGA TTCGCAGCGC ATCGCCTTCT ATCGCCTTCT TGACGAGTTC TTCTGAGGGG
3661 ATCAATTCTC TAGATAACTG ATCATAATCA GCCATACCAC ATTTGTAGAG GTTTTACTTG
3721 CTTTAAAAAA CCTCCCACAC CTCCCCCTGA ACCTGAAACA TAAAATGAAT GCAATTGTTG
3781 TTGTTAACTT GTTTATTGCA GCTTATAATG GTTACAAATA AAGCAATAGC ATCACAAATT
3841 TCACAAATAA AGCATTTTTT TCACTGCATT CTAGTTGTGG TTTGTCCAAA CTCATCAATG
3901 TATCTTAACG CGTCGAGTGC ATTCTAGTTG TGGTTTGTCC AAACTCATCA ATGTATCTTA
3961 TCATGTCTGT ATACCGTCGA CCTCTAGCTA GAGCTTGGCG TAATCATGGT CATAGCTGTT
4021 TCCTGTGTGA AATTGTTATC CGCTCACAAT TCCACACAAC ATACGAGCCG GAAGCATAAA
4081 GTGTAAAGCC TGGGGTGCCT AATGAGTGAG CTAACTCACA TTAATTGCGT TGCGCTCACT
4141 GCCCGCTTTC CAGTCGGGAA ACCTGTCGTG CCAGCTGCAT TAATGAATCG GCCAACGCGC
4201 GGGGAGAGGC GGTTTGCGTA TTGGGCGCTC TTCCGCTTCC TCGCTCACTG ACTCGCTGCG
4261 CTCGGTCGTT CGGCTGCGGC GAGCGGTATC AGCTCACTCA AAGGCGGTAA TACGGTTATC
4321 CACAGAATCA GGGGATAACG CAGGAAAGAA CATGTGAGCA AAAGGCCAGC AAAAGGCCAG
4381 GAACCGTAAA AAGGCCGCGT TGCTGGCGTT TTTCCATAGG CTCCGCCCCC CTGACGAGCA
4441 TCACAAAAAT CGACGCTCAA GTCAGAGGTG GCGAAACCCG ACAGGACTAT AAAGATACCA
4501 GGCGTTTCCC CCTGGAAGCT CCCTCGTGCG CTCTCCTGTT CCGACCCTGC CGCTTACCGG
4561 ATACCTGTCC GCCTTTCTCC CTTCGGGAAG CGTGGCGCTT TCTCATAGCT CACGCTGTAG
4621 GTATCTCAGT TCGGTGTAGG TCGTTCGCTC CAAGCTGGGC TGTGTGCACG AACCCCCCGT
4681 TCAGCCCGAC CGCTGCGCCT TATCCGGTAA CTATCGTCTT GAGTCCAACC CGGTAAGACA
4741 CGACTTATCG CCACTGGCAG CAGCCACTGG TAACAGGATT AGCAGAGCGA GGTATGTAGG
4801 CGGTGCTACA GAGTTCTTGA AGTGGTGGCC TAACTACGGC TACACTAGAA GAACAGTATT
4861 TGGTATCTGC GCTCTGCTGA AGCCAGTTAC CTTCGGAAAA AGAGTTGGTA GCTCTTGATC
4921 CGGCAAACAA ACCACCGCTG GTAGCGGTGG TTTTTTTGTT TGCAAGCAGC AGATTACGCG
4981 CAGAAAAAAA GGATCTCAAG AAGATCCTTT GATCTTTTCT ACGGGGTCTG ACGCTCAGTG
5041 GAACGAAAAC TCACGTTAAG GGATTTTGGT CATGAGATTA TCAAAAAGGA TCTTCACCTA
5101 GATCCTTTTA AATTAAAAAT GAAGTTTTAA ATCAATCTAA AGTATATATG AGTAAACTTG
5161 GTCTGACAGT TACCAATGCT TAATCAGTGA GGCACCTATC TCAGCGATCT GTCTATTTCG
5221 TTCATCCATA GTTGCCTGAC TCCCCGTCGT GTAGATAACT ACGATACGGG AGGGCTTACC
5281 ATCTGGCCCC AGTGCTGCAA TGATACCGCG AGACCCACGC TCACCGGCTC CAGATTTATC
5341 AGCAATAAAC CAGCCAGCCG GAAGGGCCGA GCGCAGAAGT GGTCCTGCAA CTTTATCCGC
5401 CTCCATCCAG TCTATTAATT GTTGCCGGGA AGCTAGAGTA AGTAGTTCGC CAGTTAATAG
5461 TTTGCGCAAC GTTGTTGCCA TTGCTACAGG CATCGTGGTG TCACGCTCGT CGTTTGGTAT
5521 GGCTTCATTC AGCTCCGGTT CCCAACGATC AAGGCGAGTT ACATGATCCC CCATGTTGTG
5581 CAAAAAAGCG GTTAGCTCCT TCGGTCCTCC GATCGTTGTC AGAAGTAAGT TGGCCGCAGT
5641 GTTATCACTC ATGGTTATGG CAGCACTGCA TAATTCTCTT ACTGTCATGC CATCCGTAAG
5701 ATGCTTTTCT GTGACTGGTG AGTACTCAAC CAAGTCATTC TGAGAATAGT GTATGCGGCG
5761 ACCGAGTTGC TCTTGCCCGG CGTCAATACG GGATAATACC GCGCCACATA GCAGAACTTT
5821 AAAAGTGCTC ATCATTGGAA AACGTTCTTC GGGGCGAAAA CTCTCAAGGA TCTTACCGCT
5881 GTTGAGATCC AGTTCGATGT AACCCACTCG TGCACCCAAC TGATCTTCAG CATCTTTTAC
5941 TTTCACCAGC GTTTCTGGGT GAGCAAAAAC AGGAAGGCAA AATGCCGCAA AAAAGGGAAT
6001 AAGGGCGACA CGGAAATGTT GAATACTCAT ACTCTTCCTT TTTCAATATT ATTGAAGCAT
6061 TTATCAGGGT TATTGTCTCA TGAGCGGATA CATATTTGAA TGTATTTAGA AAAATAAACA
6121 AATAGGGGTT CCGCGCACAT TTCCCCGAAA AGTGCCACCT GACGTC

ALK1-V5 Cloning

Alk1-V5 plasmid was generated by gateway cloning of pDONR223-ACVRL1(Alk1) (a gift from William Hahn & David Root, Addgene plasmid # 23873) and pEF-DEST51 (Thermo) vectors using LR Clonase enzyme mix (Thermo). Plasmid was transformed into DH5α and plated on LB-agar plus ampicillin for single colony selection, sequencing, and plasmid purification. HA-tagged Alk2, Alk3 and Alk6 plasmids were a gift from Aristidis Moustakas (Addgene plasmid # 80870, 80873, 80882).

ALK1-V5 Sequencing Data: Sequenced using T7-forward primers (1051 bp)

ORIGIN

```
   1 NNNNNNNNNN NNGCTTGNTN NNCAAGTTTG TANAAAAAAG TTGGCATGAC CTTGGGCTCC
  61 CCCAGGAAAG GCCTTCTGAT GCTGCTGATG GCCTTGGTGA CCCAGGGAGA CCCTGTGAAG
 121 CCGTCTCGGG GCCCGCTGGT GACCTGCACG TGTGAGAGCC CACATTGCAA GGGGCCTACC
 181 TGCCGGGGGG CCTGGTGCAC AGTAGTGCTG GTGCGGGAGG AGGGGAGGCA CCCCCAGGAA
 241 CATCGGGGCT GCGGGAACTT GCACAGGGAG CTCTGCAGGG GGCGCCCCAC CGAGTTCGTC
 301 AACCACTACT GCTGCGACAG CCACCTCTGC AACCACAACG TGTCCCTGGT GCTGGAGGCC
 361 ACCCAACCTC CTTCGGAGCA GCCGGGAACA GATGGCCAGC TGGCCCTGAT CCTGGGCCCC
 421 GTGCTGGCCT TGCTGGCCCT GGTGGCCCTG GGTGTCCTGG GCCTGTGGCA TGTCCGACGG
 481 AGGCAGGAGA AGCAGCGTGG CCTGCACAGC GAGCTGGGAG AGTCCAGTCT CATCCTGAAA
 541 GCATCTGAGC AGGGCGACAG CATGTTGGGG GACCTCCTGG ACAGTGACTG CACCACAGGG
 601 AGTGGCTCAG GGCTCCCCTT CCTGGTGCAG AGGACAGTGG CACGGCAGGT TGCCTTGGTG
 661 GAGTGTGTGG GAAAAGGCCG CTATGGCGAA GTGTGGCGGG GCTTGTGGCA CGGTGAGAGT
 721 GTGGCCGTCA AGATCTTCTC CTCGAGGGAT GAACAGTCCT GGTTCCGGGA GACTGAGATC
 781 TATAACACAG TGTTGCTCAG ACACGACAAC ATCCTAGGCT TCATCGCCTC AGACATGACC
 841 TCCCGCAACT CGAGCACGCA GCTGTGGCTC ATCACGCACT ACCACGAGCA CGGCTCCCTC
 901 TACGACTTTC TGCAGAGACA GACGCTGGAG CCCCATCTGG CTCTGAGGCT AGCTGTGTCC
 961 GCGGCATGCG GCCTGGCGCA CCTGCACGTG GAGATCTTCG GTACACAGGG CAAACCAGCC
1021 ATTGCCCACC GCGACTTCAA GAGCCGCAAT G
```

ALK Receptor Pulldowns using FKBP12-SNAP

FKBP12-SNAP (5 μg) and tagged ALK receptor plasmids (5 μg) were co-transfected into Hek293T cells using SuperFect and supplied protocol. After 48 hours, cells were treated with DMSO (0.1%) or 1 μM FKVP for 30 min. After 1 hour, cells were lysed in vessel with 1mL lysis buffer (150mM NaCl, 50mM Tris-HCl, 0.1% Trition-100, 5% glycerol, protease and phosphatase inhibitors) and plate scraper. Lysate was transferred to 2mL

eppendorf and rotated at 4C for 20min. Lysates were centrifuged at 14000g for 10min, and ~1mL supernatant was transferred to a new tube with 200nM drug or 0.2% DMSO. 20uL input was taken and mixed with 20uL 2x loading buffer before boiling. Each lysate sample was then mixed with 250uL of SNAP buffer (lysis buffer + 5mM DTT) containing 40µL of magnetic SNAP-capture beads (New England Bio) and rotated at 4°C for 1 hour. Beads were washed 3 times with 1mL lysis buffer before boiling in 100µL 2X loading buffer. Boiled lysates were vortexed and centrifuged, lysate (~90µL) was carefully removed from beads and used for western blotting.

The same method was used for calcineurin-FK506 and mTOR-rapamycin pull-downs after transfection of 10ug FKBP12-SNAP cDNA only.

FKBP Knockout Lines

Jurkat T and HEK293T cells were transfected as previously described with all-in-one CRISPR/Cas9 (mCherry tagged) plasmids (Genecopeia) containing guide-RNAs for FKBP12 (HCP267023-CG01-3-B), FKBP51 (HCP257374-CG01-3-B), or FKBP52 (HCP205551-CG01-3-B). After 48 hours, cells were sorted for mCherry fluorescence (650nm laser) into 96-well plates (1 cell/well). After 2 weeks of culture, single clones were validated by western blotting.

BMP and NFAT Pathway Reporters

Jurkat T cells transfected with BRE-Luc were split into a 96-well plate (80 µL/well of $0.5x10^6$ cells/mL)) and treated with previously stated compounds/proteins (20 µL of 5X stock in RPMI, 0.5% DMSO) for 18 h. rBMP-4 and rTGF-β1 (R&D) were used as positive and negative controls, respectively. Plates were centrifuged at 3000 rpm for 10min, then carefully aspirated. Cells were re-suspended in 100 µL lysis buffer (per well) and placed on a plate-shaker for 30 min. An aliquot of 80 µL of lysate was transferred to a white-walled 96-well plate, and luminescence was recorded 2 seconds after automated injection of luciferase substrate. Luminescence values were background subtracted (lysis buffer + substrate) and normalized to DMSO control values.

FKBP12KO Jurkat T cells transfected with FKBP12-SNAP plasmid were selected with 1200 µg/mL G418 for seven days before use in BRE-Luc assays.

FKVP Synthesis and Formulation for Animal Studies

To a solution of FK506 (100 mg, 0.120 mmol) and 40 mol% Zhan1b catalyst $RuCl_2[C_{21}H_{26}N_2][C_{12}H_{17}NO_3S]$, in 3 mL anhydrous DCE was added 4-vinylpyridine (14.2 µL, 0.132 mmol). The mixture was stirred for 30 s before microwave irradiation at 120°C for 20 min. The mixture was then purified using flash chromatography (0-25% MeOH in DCM), preparative-TLC (9:1 DCM:MeOH), and reverse-phase HPLC (45-85% ACN in H_2O). Conversion=25%, Purified Yield=8%. ^{1}H-NMR experiments (**Fig 2.16**) were used to confirm the new compound was >99% pure. Product was characterized

using High-Resolution MS (**Fig. 2.6**) and ^{1}H-NMR (**Fig 2.16**), then dissolved into DMSO or used in formulation for animal experiments.

For animal experiments, FKVP powder was dissolved into 80% EtOH/20% Cremophor RH60 solution at 5mg/mL. This stock was diluted 1:50 into saline before subcutaneous injection.

Declaration of Ethical Animal Care and Use

Goto-Kakizaki (GK) type-2 diabetic rats obtained from Charles River (Boston, MA) were housed in a pathogen-free facility and cared for according to NIH guidelines and a protocol approved by the Johns Hopkins University Animal Care and Use Committee (ACUC). Both male and female GK rats at age of 4-5 months were used in this study.

In vivo Excisional Wound Model

Full-thickness wounds were created in the dorsal skin of rats with a sterile disposable biopsy punch (8 mm in diameter). The animals were injected subcutaneously with saline, AMD3100 (1mg/kg) plus FK506 (0.1mg/kg) or AMD3100 (1mg/kg) plus FKVP (0.1mg/kg) immediately after wounding and every other day until complete healing, defined as complete re-epithelialization of the wound area. For assessing the role of BMP signaling, animals were injected intraperitoneally (i.p.) with LDN-193189 (2mg/kg/day) in addition to standard saline or AF treatment. Wounds were evaluated daily according to the method described previously (Lin et al., 2014).

Immunohistochemistry

Cut sections of 5 μm were prepared from frozen tissue for immunohistochemistry staining. Frozen sections were fixed with acetone at −20 °C for 10 min and dried for 1 h at room temperature. After inactivation of endogenous peroxidase and blocking of nonspecific antibody binding, the specimens were incubated with anti-CD133 (1:300, ab19898; Abcam) at 4 °C overnight. The tissue sections were then subsequently incubated with biotin-conjugated goat anti-rabbit IgG (1:200, #14708S Cell Signaling, Danvers, MA) for 30 minutes at room temperature. The VectaStain Elite ABC kit (HRP) (Vector Laboratories, Burlingame, CA) was used to increase the sensitivity of the staining. Diaminobenzidine tetrahydrochloride (5 min, D4293, Sigma-Aldrich, St. Louis, MO) was used as the chromogen, and Mayer's Hematoxylin (30 s, Dako, S3309) was used for counterstaining.

Statistics

The one-way analysis of variance (ANOVA) was used to determine the statistically difference in wound healing among AF, AF+LDN, Saline and S+LDN groups or between AF, AV and Saline groups when comparing days of wound healing. Bonferroni-Holm post-hoc procedure was used for p value adjustment. $p<0.05$ is considered significantly different.

3.4 DISCUSSION

In this study, we investigated the mechanism by which FK506 accelerated WH when used in combination with AMD3100. Using FKVP, a non-immunosuppressive analog of FK506, we ruled out calcineurin as a mediator of both WH accelleration, raising the possibility that FKBPs are the primary target for both effects. Moreover, we demonstrated that macrocyclic FKBP ligands activate BMP signaling by relieving the inhibition of BMPR1 by endogenous FKBP12. We show that FKBP12 plays an essential role in the BMP signaling pathway, an effect that can be mediated without calcineurin inhibition through the use of non-immunosupressive FK506 analogs. We found that BMP receptor signaling is required for wound healing enhancement by FK506, and that blocking this activation results in fewer numbers of stem cells recruited to the wound area. BMP signalling may maniuplate several cell types in the wound healing mechanism, such as chemotaxis of stem cells or endothelial adhesion of mobilized cells in the wounded tissue (**Fig. 3.32**).

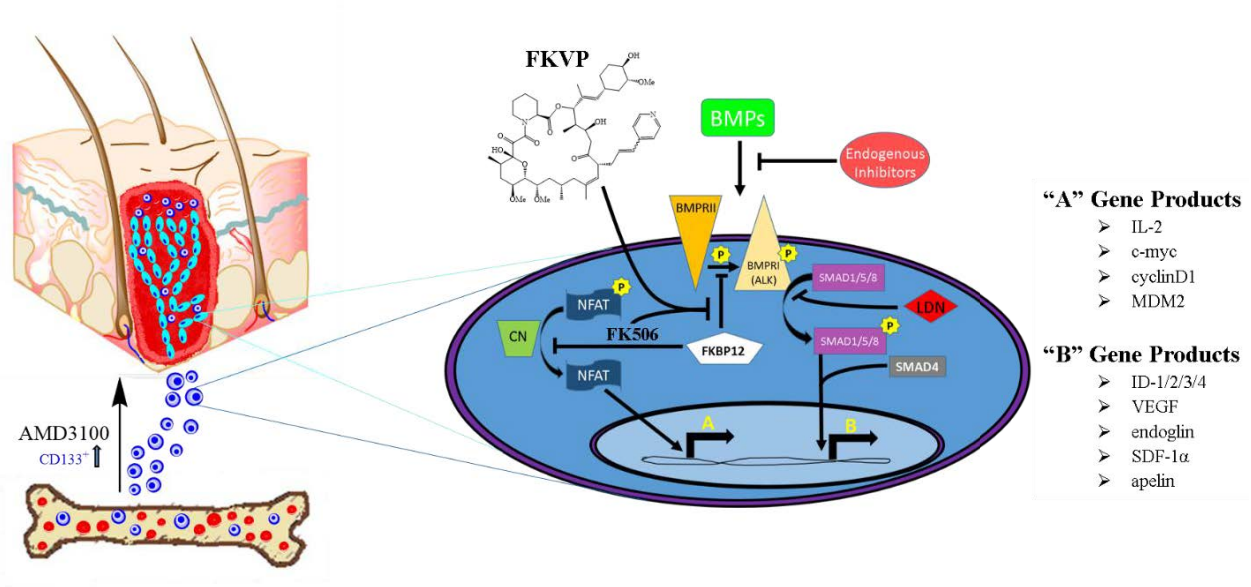

Figure 3.32: Mechanistic overview of enhanced healing by FKVP and AMD3100. AMD3100 releases CD133+ stem cells into circulation, where FKVP-mediated BMP activation influences recruitment to wounded tissues. Systemic inhibition of FKBP12 by FKVP allows for BMP-related gene expression in both mobilized stem/progenitor cells and the endothelium without affecting the necessary immune responses to wounding.

FKBP12, a founding member of the FKBP superfamily, has been shown to possess multiple cellular and physiological functions in addition to its role in mediating inhibition of calcineurin and T cell activation by FK506. The association with, and inhibition by FKBP12 adds another layer of BMPR1 kinase regulation. That relieving FKBP12 inhibition by FK506 or FKVP is sufficient to activate the ID-1luciferase reporter gene suggests that there is a basal level of activity of BMPR that is normally suppressed by FKBP12 and relief of this inhibition leads to significant, albeit moderate,

activation of the signaling pathway in comparison to BMP-4 binding. Thus, BMPR may exist in three distinc activation states, upon release of FKBP12 inhibition, upon BMP binding and both. Our results revealed that the partial activation of BMP pharmacologically with FK506 or FKVP is sufficient to accelerate wound healing in combination with AMD3100. It remains to be seen whether that activation state is also achievable under physiological stimulation, and is involved in regulation of healing in vivo.

Type 2 BMP receptors are reported to constitutively phosphorylate the GS domain of type 1 receptors (ALKs). FKBP12 is believed to inhibit random activation of ALKs by binding to residues in the GS domain (Chaikuad et al., 2012). Our results indicated that this association is competed by FKVP for all BMP-specific ALKs. We showed that loss of FKBP12 results in elevated basal phosphorylation of SMAD1/5, suggesting a partially activated state of ALKs in the absence of its endogenous intracellular inhibitor FKBP12. The additive increase in ID-1 reporter stimulation from concommitant FKVP and rBMP treatment is also consistent the three activation states of BMPR1. Futhermore, addition of the BMP inhibitor noggin did not prevent ID-1 reporter stimulation by FKVP, suggesting that the regulation of BMPR by endogenous FKBP12 is independent of BMP protein-receptor binding.

Several solved crystal structures of both BMP and TGF-β ligands and receptors in complex show key structural differences (Mueller et al., 2015). For example, the TGFβ-TGFBR1-TGFBR2 complex is reported to involve type1-type2 receptor interactions, a feature absent in BMPR-ligand complexes. These specific interactions are believed to be a consequence of ligand binding, as TGFBR1 shifts its orientation to contact the bound

ligand. This added layer of regulation may explain discrepancies in TGF-β reporter activation by FK506 when compared to BMP, as FKBP12 dissociation may be a *second* added layer of protection in the TGF-β pathway.

Inhibition of calcineurin by FK506 has been shown to be responsible for both its potent immunosuppressive activity and a number of its side effects including nephrotoxicity and neurotoxicity (Bechstein et al., 2000, Naesens et al., 2009). By placing a molecular "bump" on the calcineurin-interacting effector domain of FK506, the resultant FKVP lost its immunosuppressive activity as judged by the NFAT reporter gene assay (**Figure 2.6**). In comparision to calcineurin, the loss of function of FKBP12 and other members seems to have much fewer and less drastic impact on both yeast and mammals. Aside from BMP receptors, FKBP12 has been reported to modulate calcium flux in inositol 1,4,5-trisphosphate (IP_3) and ryanodine receptors (Cameron et al., 1995; Jayaraman et al., 1992), suggesting FK506 may affect vascular or cardiac smooth muscle contractility. However, calcineurin inhibition alone has been recognized as a key potentiator of hypertension (Hoorn et al., 2012). As such, non-immunosuppressive FKBP ligands should have fewer side effects, resulting in safer and more selective pharmacological BMP agonists. Moreover, FKBP52 inhibition by FK506 has been shown to augment nerve regeneration (Gold, B.G., 1999; Gold, B.G. et al, 1999), suggesting the effect may synergize with FKBP12–mediated tissue regeneration through BMP signalling. In addition to wound healing, FK506 has also been shown to be effective against pulmonary artirial hypertension and invasiveness in bladder cancer through activation of BMPR signaling (Spiekerkoetter et al., 2013; Shin et al., 2014). It is possible that FKVP and other analogs may find use in treating these conditions.

That FKVP is as effective in the enhancement of WH as FK506 also has important clinical implications due to its lack of immunosuppressive effect. In patients with a greater risk of infection, such as those with diabetes, treatment with FKVP will provide effective treatment without the risks associated with immunosupressants. This is higlighted in our use of Goto-Kakazaki rats for this study; a rat model that spontaneously develops type-2 diabetes after 3-4 months of age and suffers from many of the same physiological manifests that affect humans with the disease, including significantly impaired wound healing. By using such a model for this study, we aim to convey the power of this treatment and its application to clinical use. Our demonstration that FKVP recapitulates the WH efficacy of FK506 in the challenging rat model makes FKVP an attractive lead compound, and it is expected that other non-immunosuppressive ligands devoid of inhibitory activity towards calcineurin similar to FKVP will possess similar beneficial effects. Furthermore, the synergistic activities of AMD3100 and FKVP demonstrate a regenerative therapy that could potentially be applied to several other types of tissue damage. Beyond WH, our lab has shown improved liver regeneration after partial hepatectomy and AF combination treatment (Zhai et al., 2018). Thus, FKVP and other non-immunosuppressive FKBP12 ligands may find use in both wound healing and regenerative therapies.

4. Structure-Activity Relationships Highlight an Alternative Mechanism for Calcineurin Repulsion in Non-Immunosuppressive FK506 Analogs Generated by One-Step Heck Reaction*#

*This work was completed in collaboration with Dr. Yuefan Wang.
#YW synthesized and characterized analogs, BP performed cell-based assays

4.1 INTRODUCTION

In the previous chapter, a novel non-immunosuppressive FK506 analog named FKVP was described that retains FKBP binding and lacks calcineurin inhibition activity (Peiffer et al, 2019). FKVP was found to activate Bone Morphogenic Protein (BMP) signaling in lymphocytes and endothelial cells through inhibition FKBP12-BMPR1 interaction. Moreover, the combination of FKVP and AMD3100 was found to accelerate wound-healing in diabetic rats in a BMP receptor-dependent manner.

To conduct a structure-activity relationship study, we needed to synthesize new analogs of FKVP containing the pyridine core structure. In the past, we and others have relied on ruthenium-catalyzed cross metathesis reaction (CM) to modify the terminal alkene of FK506 (C40) to generate non-immunosuppressive FK506 analogs (Clemons et al, 2002). Unfortunately, coupling of nitrogen-containing heterocycle and aniline routinely suffer from low yield. This is most likely due to the nitrogen lone electron pair that competitively binds to the ruthenium metal center (Compain et al., 2007). Soluble ammonium salts (Woodward et al., 2011) displayed improved yields in CM of analogs with amines (**Chapter 2, Fig 2.2**), but not in the case of our lead compound, FKVP.

Accounting for the issues associated with ruthenium-catalyzed coupling, we evaluated use of the Heck reaction to install aryl-halides at the terminal alkene. Palladium catalysts

used in the Heck reaction are compatible to nitrogen-containing heterocycles such as pyridine (Heck et al, 1972).

We found that palladium complexes can efficiently catalyze reactions between aryl halides (Br or I) and the immunosuppressive drug FK506 at the terminal alkene position. From this novel approach, we increased the synthetic yield of FKVP over eight fold, and the one-step reaction allowed for fast and efficient SAR of the lead. Activity studies of pyridine analogs provided insights into the steric and electrostatic interactions beween the allyl group in the effector domain of FK506 and calcineurin, spurring development of selective FKBP antagonists for pharmacological BMP activation.

4.2 RESULTS

The heck reaction was optimized using FKVP as a model synthesis. Various conditions were tested including different temperatures, base reagents, and additives reported in literature. The highest yield of FKVP resulted from standard conditions with an organic base (**entry 6, Fig. 4.1**).

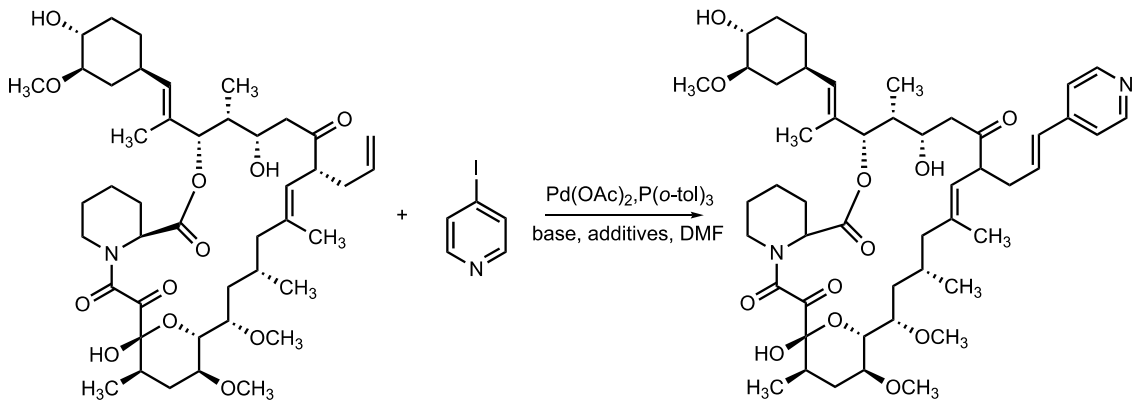

Entry	base	additives	temperature	time / h	Yield (%)[b]
1	$NaHCO_3$	$^nBu_4NBr$	100 °C	24	N. D.
2	$NaHCO_3$	none	100 °C	24	decomposed
3	K_2CO_3	$^nBu_4NBr$, H_2O	50 °C	2	decomposed
4	$NaHCO_3$	$^nBu_4NCl$	100 °C	24	decomposed
5	2,6-lutidine	none	100 °C	24	low conversion
6	Et_3N	none	100 °C	24	66

Figure 4.1 Heck synthesis optimization of FKVP synthesis. Reaction conditions and reagents were varied using different bases and additives. Triethylamine showed the most successful conversion to product (^{n}Bu = n-butyl).

With FKVP as the lead compound, we selected 7 nitrogen-containing heterocyclic halides with a pyridine core and 4 halides with substituted anilines as substrates for the Heck reaction. To our delight, all halide substrates were successfully coupled to FK506 with moderate to good yields (36-78%, **Fig. 4.2**).

Aryl-halide substrates displayed distinct reactivity in the Heck reaction. First, bromides and iodides gave similar yields. Second, electron-withdrawing groups on the pyridines and quinolines appeared to increase the yields (entry **4,6,7**). Third, unprotected anilines gave the lowest yields (entry **9-11**). Importantly, the unreacted FK506 starting material in the reaction mixture was easily separated from the more polar nitrogen-containing products with flash chromatography.

Figure 4.2: Synthesis scheme of FK506 analogs prepared by Heck reaction and table of substrates. Compounds 1-11 were prepared in moderate yields using the presented scheme. (**Figure on next page**)

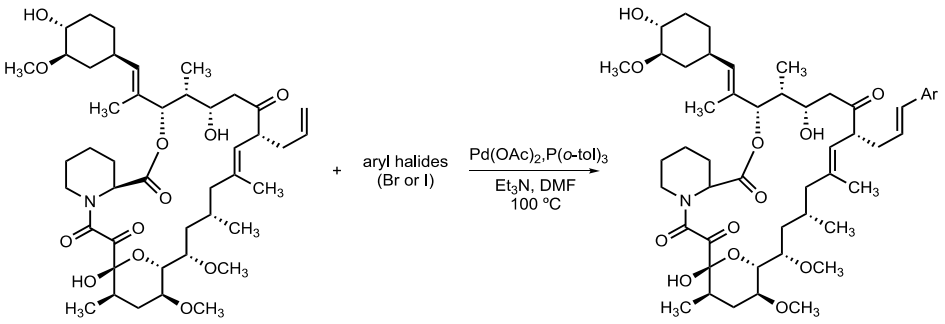

Entry	Aryl Halide	Product (Ar =)	Time / h	Yield (%)[b]
1	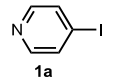 **1a**	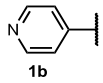 **1b**	24	66
2	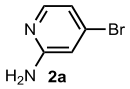 **2a**	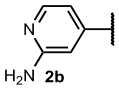 **2b**	24	42 (52)[c]
3	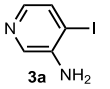 **3a**	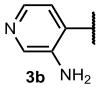 **3b**	24	40 (54)[c]
4	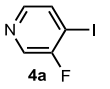 **4a**	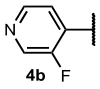 **4b**	24	78
5	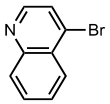 **5a**	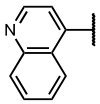 **5b**	18	72
6	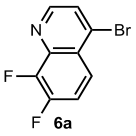 **6a**	 **6b**	18	70
7	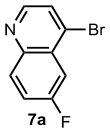 **7a**	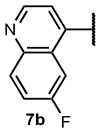 **7b**	18	68
8	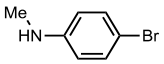 **8a**	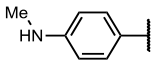 **8b**	20	62
9	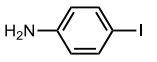 **9a**	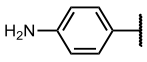 **9b**	12	36
10	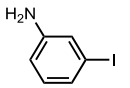 **10a**	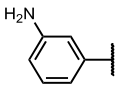 **10b**	12	42
11	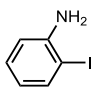 **11a**	 **11b**	12	45

[a] Reaction condition: FK-506 (0.050 mmol), aryl halide (0.10 mmol), $Pd(OAc)_2$ (0.0050 mmol), P(*o*-tol)$_3$ (0.010 mmol) and Et_3N (0.10 mL) in DMF (1.0 mL) at 100 °C under Ar. [b] Isolated yield. [c] Yield in parentheses is based on FK-506 recovery

With FK506 analogs in hand, we assessed their effects on cell viability, BMP activation and NFAT activation at two concentrations. In the HUVEC cell viability assay, we found that quinoline analogs (**5b-7b**) inhibit cell proliferation at 10 μM (**Fig. 4.3**), while other compounds (**1b-4b, 8b-11b**) show comparable cytotoxicity to FK506. Interestingly, all compounds gave cell viability scores similar to others in their class (i.e. pyridine > aniline > quinolone). This suggests that cell viability can be affected by even small molecular changes at the terminal alkene.

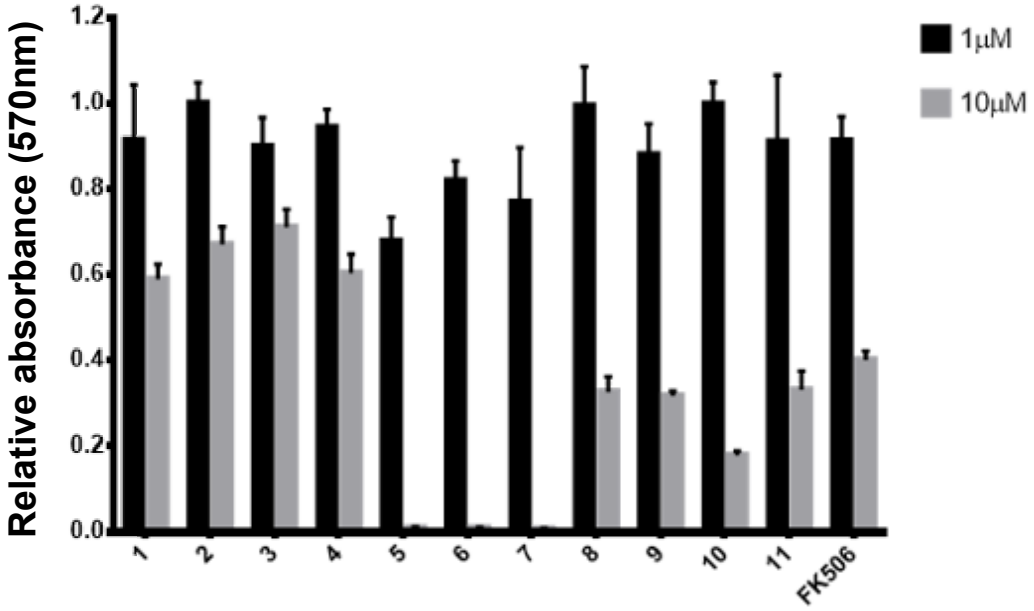

Figure 4.3: FK506 analogs display variable cell-viability. Cell viability after 72-hour analog treatment in HUVEC cells. Error bars represent standard deviation from mean for all measurements (n=3), and absorbance values were normalized to DMSO treated cells.

We used a BMP-response-element (BRE) pathway reporter (luciferase under the control of the ID1 gene promoter) (**Figure 2.7)** (Spiekerkoetter et al, 2013) in Jurkat T-cells to determine whether the new analogs were capable of activating the BMP signaling pathway. Initial screening of the compounds showed that most analogs had similar activity as FK506 or FKVP. This is somewhat expected, as we have previously shown that FKBP12 binding is necessary and sufficient for activation of BMP signaling (**Fig. 4.4**)

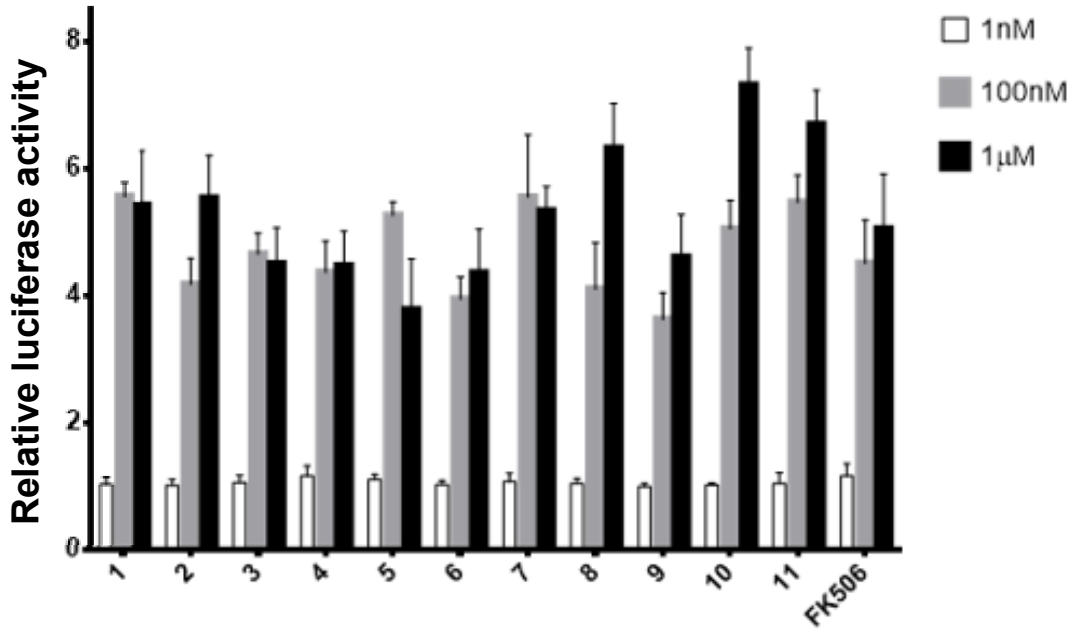

Figure 4.4: FK506 analogs display similar BMP activation potential. All analogs activate a BMP pathway reporter in Jurkat cells with similar potency to FK506. Error bars represent standard deviation from mean for all measurements (n=3), and absorbance/luminescence values were normalized to DMSO treated cells.

To determine the effect of the analogs on calcineurin, we turned to a PMA/ionomycin-activated Nuclear Factor of Activated T-cells (NFAT) reporter system (**Figure 2.5**) in Jurkat T cells (luciferase under the control of the IL-2 promoter) (Clemons et al., 2002) (**Fig. 4.5**). Two analogs (2b, 3b) did not cause significant inhibition of the NFAT-Luciferase reporter at concentrations up to 10 μM, similar to FKVP (1b). Surprisingly, most other analogs showed either partial or nearly complete inhibition of the NFAT reporter at 1 μM (**Fig. 4.5**). It is noteworthy that some of the immunosuppressive analogs, including 5b, 6b and 7b, have bulkier substituents than 2b and 3b due to the presence of a fused aromatic ring. How those bulkier groups are accommodated at the binding site of calcineurin remains to be determined.

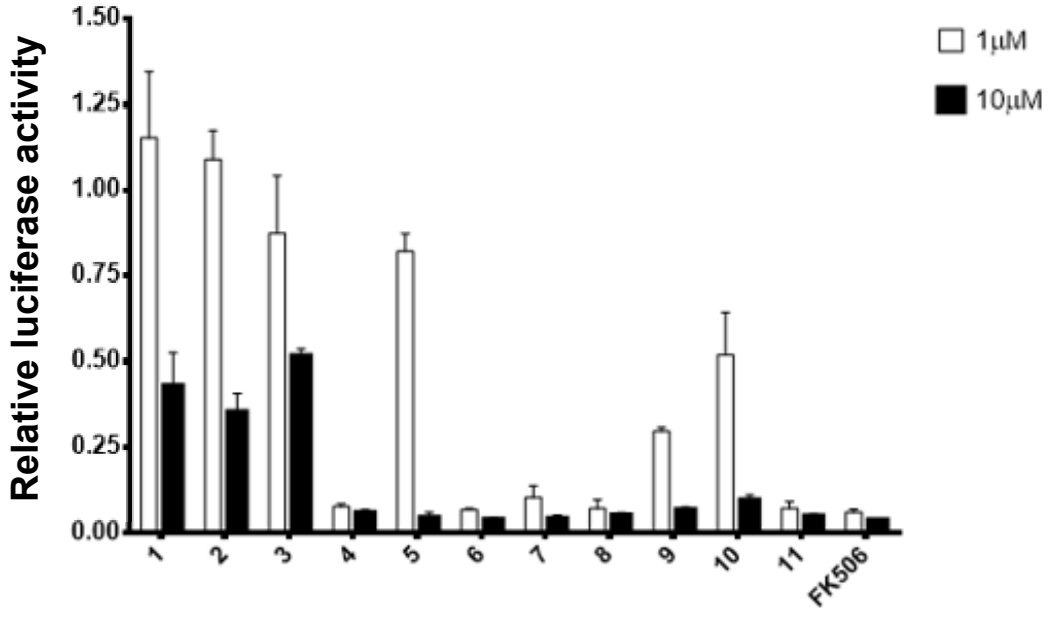

Figure 4.5: FK506 analogs display variable immunosuppressive qualities. Derivatives show structure-dependent effects in NFAT reporter inhibition in Jurkat cells. Error bars

represent standard deviation from mean for all measurements (n=3), and absorbance/luminescence values were normalized to DMSO treated cells.

We determined EC_{50} values of three non-immunosuppressive analogs (1b-3b) in the BMP luciferase assay. All 3 analogs were found to be slightly more potent than FK506 (**Fig. 4.6**), likely attributable to increased solubility due the more polar pyridine substituents. Among the three analogs, FKVP remained the most active among the group with an IC_{50} of 12.4 nM. However, compounds 2 and 3 remained similarly effective (insignificantly different from FKVP ($p>0.05$), suggesting that they could be further tested for in vivo PK enhancement.

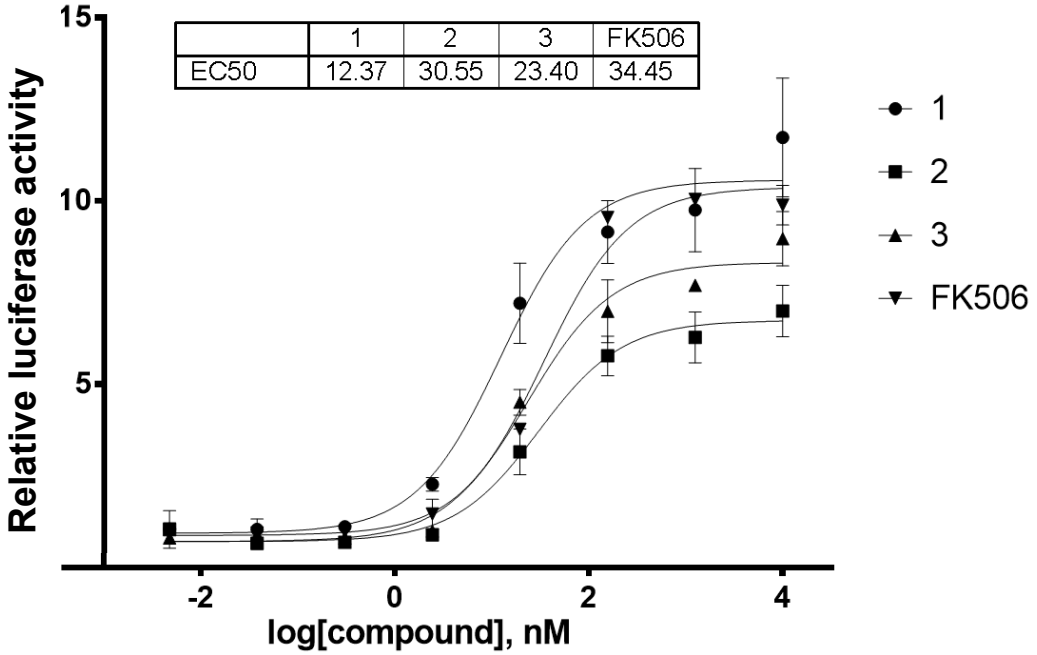

Figure 4.6: Dose-response curves for BMP reporter activation by three non-immunosuppressive analogs (1b, 2b, and 3b) and FK506. FKVP and amine-substituted pyridine analogs show potent BMP activation after dose-response treatments in BRE-luc transfected Jurkat cells.

4.3 MATERIALS AND METHODS

General Information

Normal phase disposable flash columns RediSep®Rf for flash chromatography were purchased from Teledyne Isco, Inc. Solvent was used extra dry over molecular sieve, stabilized, AcroSeal®. Yields refer to chromatographically homogeneous materials. Reactions were monitored by mass spectrometry provided by Agilent 6120 Quadrupole LC/MS. PLC Silica gel 60 F_{254}, 1mm supplied by EMD Millipore using UV light as visualizing agent.

^{1}H-NMR was recorded on Bruker Avance III 500 MHz NMR spectrometer. TMS was used as internal standard for ^{1}H-NMR (0 ppm). High-resolution mass spectra (HRMS) were recorded on Waters Synapt G2-Si mass spectrometer using ESI (electrospray ionization). FK-506 (Tacrolimus) was purchased from Biotang Inc. Zhan-1b catalyst, palladium acetate and tris(o-tolyl)phosphine were purchased from Aldrich.

Cell Culture and Transfections

Jurkat (E6.1, ATCC) cells were cultured in RPMI with 10% FBS and 1.5% PennStrep. Jurkat cells (1 x 10^6) were transfected with 10 μg of BRE-Luciferase (kindly provided by Martine Roussel & Peter ten Dijke) or NFAT-Luciferase cDNA (Promega) by electroporation (BioRad, square-wave, 250V, 950 μF) in 400 μL serum/antibiotic free RPMI with 0.5% DMSO. Thirty minutes after transfection, cells were transferred to complete RPMI and rested overnight. Before plating, cells were re-suspended in fresh media and diluted to 0.5x10^6 cells/mL.

HUVEC cells were cultured in Lonza Endothelial cell Growth Medium (EGM-2) and used between passages 3 and 7. All cells were grown and assayed at 37°C with 5% added CO_2.

Cell Viability Assays

HUVEC cells were plated at 1000 cells/well in 180 μL growth media before addition of 20 μL of 10X drug/protein stock. After 72-hour treatment, 22 μL of a resazurin sodium salt solution (0.1 mg/mL stock in water) was added to each well and allowed to incubate at 37°C. The metabolic conversion of resazurin dye was monitored by absorbance at 570 nm after 6 hours. After background subtraction (media only + dye), absorbance values were left as arbitrary absorbance units or normalized to those obtained by DMSO.

BMP and NFAT Reporters

Jurkat cells used for each experiment were transfected at the same time and cultured together overnight until plating and treatment the following day.

Jurkat T cells transfected with BRE-Luc were split into a 96-well plate (80 μL/well of $0.5x10^6$ cells/mL)) and treated with previously stated compounds (20 μL of 5X stock in RPMI, 0.5% DMSO) for 18 hours. Cells were lysed and measured for luminescence as previously reported (Peiffer et al., 2018). Luminescence values were background subtracted (lysis buffer + substrate) and normalized to DMSO control values.

Jurkat T cells transfected with NFAT-Luc were split into a 96-well plate (80 μL/well of $0.5x10^6$ cells/mL) and treated with indicated compounds (20 μL of 5X stock in RPMI, 0.5% DMSO) 30 min before activation with PMA/Ionomycin (40 nM/1 μM). After 6 hours, wells were lysed and measured for luminescence as previously stated (Peiffer et al., 2019). FK506 served as positive control while DMSO and non-activated wells gave negative and background control values, respectively.

EC_{50} Determinations

Calculations were performed using GraphPad Prism 6. Curves were fit using non-linear, log(agonist) vs. response (three parameters). 95% confidence intervals of EC_{50} values are reported below.

Optimization of Heck reaction conditions:

To a mixture of FK-506 (0.0500 mmol, 40 mg, 1.0 equiv), $Pd(OAc)_2$(0.00500 mmol, 1.1 mg, 0.10 equiv), P(*o*-tol)$_3$(0.0100 mmol, 3.0 mg, 0.20 equiv), base and additives in flame-dried 10 mL-Schlenk tube, dry DMF(1.0 mL) was added under Ar balloon protection, and the mixture was stirred at specific temperature. The reactions were monitored by mass spectrometry.

General procedure for the Heck reaction

To a mixture of FK-506 (0.0500 mmol, 40 mg, 1.0 equiv), aryl halides (2.0 equiv) and $Pd(OAc)_2$(0.00500 mmol, 1.1 mg, 0.10 equiv) and P(*o*-tol)$_3$(0.0100 mmol, 3.0 mg, 0.20 equiv) in flame-dried 10 mL-Schlenk tube, dry DMF(1.0 mL) and Et_3N(0.10 mL) dried over K_2CO_3 was added under an inert atmosphere of Argon, and the mixture was stirred at 100 °C. When the reaction was complete, (determined by mass spectrometry) the crude mixture was cooled to RT and purified by flash chromatography (gradient elution using dichloromethane and methanol) to give the corresponding product. If necessary, preparative TLC was used to separate byproducts from base-epimerization of FK506.

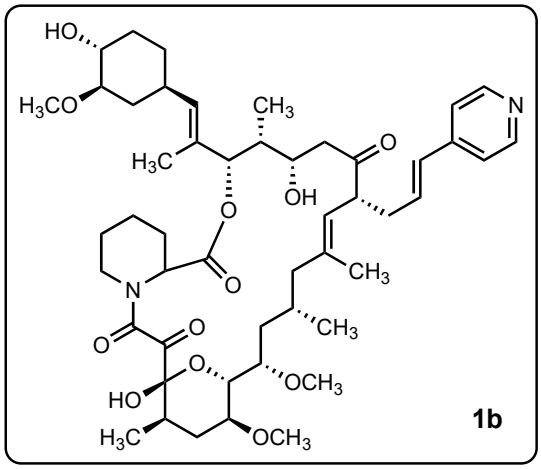

1b: ^{1}H-NMR (500MHz, $CDCl_3$) 8.51 (br s, 2H), 7.18 (br s, 2H), 6.40-6.32 (m, 2H), 5.33 and 5.18 (rotamers, d, *J* = 1.05, 1H), 5.11-5.05 (m, 2H), 4.99 and 4.65 (rotamers, d, *J* = 4.55, 1H), 4.71 and 4.24 (rotamers, s, 1H), 4.43 and 3.72 (rotamers, d, *J* = 12.5, 1H), 3.94-3.84 (m, 1H), 3.72-3.61 (m, 2H), 3.44-3.35 (m, 9H), 3.34-3.29 (m, 3H), 3.06-2.96 (m,2H), 2.84-2.61 (m,3H), 2.33-2.25 (m,2H), 2.21-1.96 (m, 7H), 1.95-1.85 (m, 2H), 1.72-1.44 (m, 18H), 1.03-0.81 (m, 11H); HRMS (ESI): m/z calcd for $C_{49}H_{73}N_2O_{12}$ $[M+H]^+$: 881.5164, found 881.5164.

4.4 DISCUSSION

The structure of the complex of FKBP12-FK506-calcineurin has been previously determined by X-ray crystallography (Griffith et al., 1995, Kissinger et al., 1995). In this complex, the terminal alkene of FK-506 fits into a binding pocket in calcineurin formed by hydrophobic amino acids (**Fig. 4.7a**). When modeled in place of FK506, the pyridine moiety in FKVP (1b) has a steric clash with residue M118 of calcineurin (**Fig. 4.7b**), which explains the elimination of calcineurin binding by analogs 1b-3b. However, how other analogs bearing bulkier substituents than FKVP at the same position remain immunosuppressive cannot be explained by the structure.

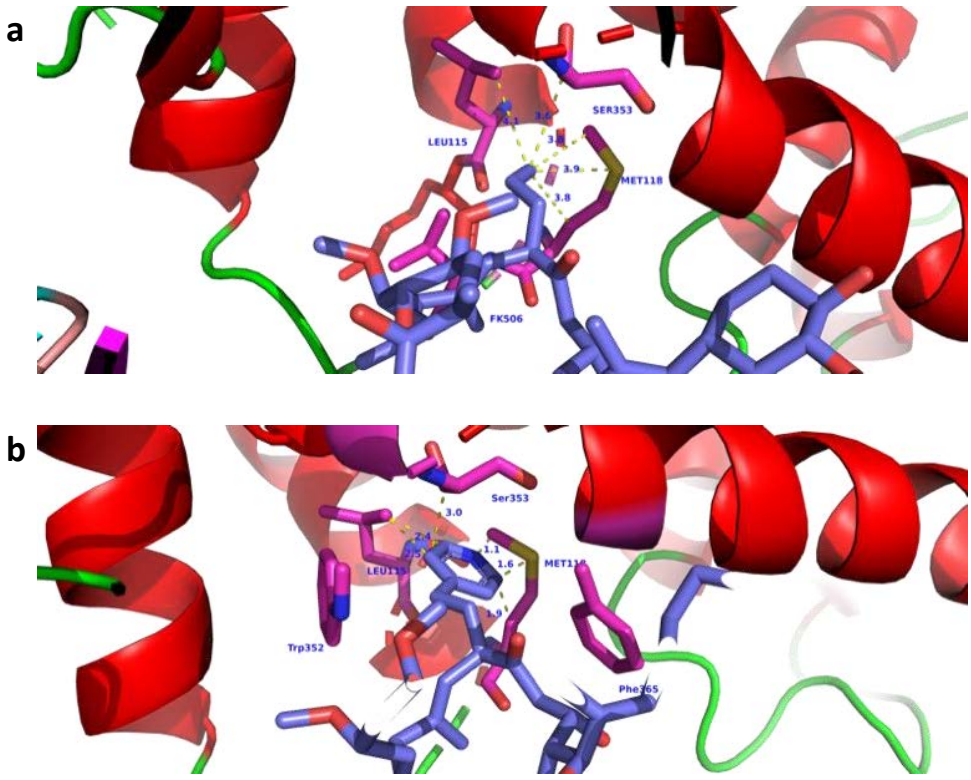

Figure 4.7: Modeling of FKVP at the FK506-binding site of calcineurin. (a) Expanded view of FK-506 terminal olefin with calcineurin. **(b)** Steric effect of FKVP with calcineurin.

After surveying pKa values of the newly-added moeities (SciFinder, **Table 4.1**), we noticed that compounds with higher pKa values (**1b,2b,3b,5b**) showed less calcineurin inhibition. Conversely, those with a lower pKa caused by electron-withdrawing groups were all immunosuppressive at 1 μM (**4b,6b,7b**). The pKa value of aniline (**9b-11b**) is lower than pyridine (**1b**), which may also explain its retention of inhibitory activity for calcineurin.

Table 4.1: pKa values for selected nitrogen-containing substrates.

Substrate	**pKa**
pyridine	5.2
4-vinylpyridine	5.5
3-aminopyridine	6.1
2-aminopyridine	6.9
3-fluoropyridine	3.0
quinoline	4.9
aniline	4.6

These observations suggest that the formation of positively charged pyridinium appendage at the terminal alkene of FK506 plays a more important role in disrupting the interaction between the terminal alkene of FK506 and the hydrophobic pocket in calcineurin. These observations present an alternative and complementary mechanism for

the loss of calcineurin inhibition in non-immunosuppressive FK506 analogs, which in the past has been rationalized by a large molecular "bump" to sterically hinder calcineurin binding (Clemons et al., 2002). It is likely that the same binding pocket in calcineurin has significant conformational flexibility to accommodate non-charged bulky aromatic rings such as those present in **4b**, **6b** and **7b**.

In summary, we have developed a one-step synthesis of FK506 analogs containing nitrogen bases using the Heck reaction. We identified three non-immunosuppressive analogs with higher potency in activating the BMP signaling pathway. We found that a key element in disrupting FK506-calcineurin interaction is through electrostatic rather than steric alteration. Given the role of BMP signaling in wound healing and tissue regeneration, the newly developed synthetic route to FKVP and analogs will facilitate the pharmacokinetic development of non-immunosuppressive analogs of FK506 for regenerative medicine (**Figure 4.8**).

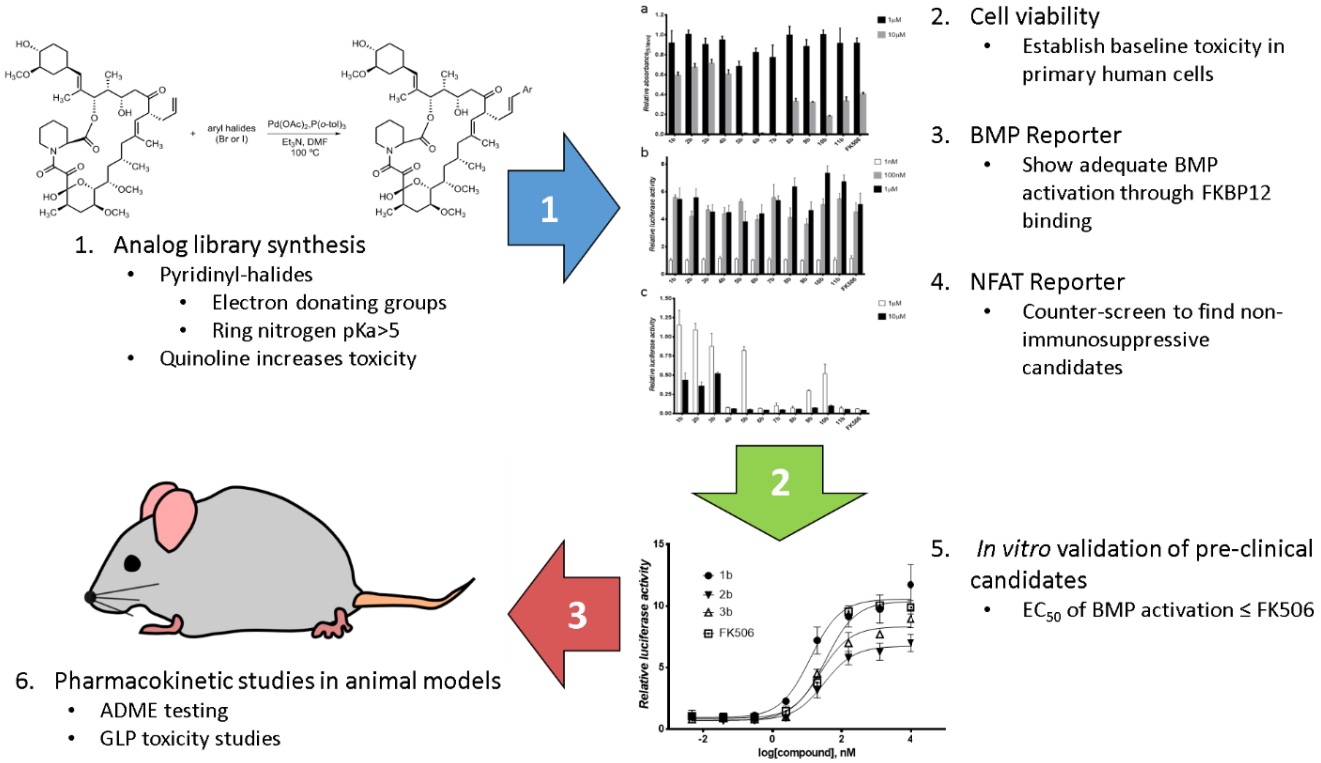

Figure 4.8: Proposed workflow for identification of clinic-ready FK506 analogs for pharmacological BMP activation. (**1**) A rationally designed FK506 analog library is screened using a high-throughput compatible, three-assay system. (**2**) Top performing candidates are then validated *in vitro* through EC50 analysis in the BMP-reporter assay. (**3**) Validated compounds are moved into pre-clinical animal studies to determine inter-analog differences in ADME (absorption, distribution, metabolism, excretion) and *in vivo* toxicity profiles.

5. INTERACTOME STUDIES AND ENHANCED BMP ACTIVATION THROUGH CHEMICALLY-INDUCIBLE FKBP12 DEGRADATION

5.1 INTRODUCTION

The recent resurgence of thalidomide in chemical biology has opened a new field in the small-molecule therapeutic landscape. By conjugating thalidomide to other small molecules, scientists have been able to selectively degrade target proteins for several applications (**Figure 5.1**) (Neklesa et al, 2017).

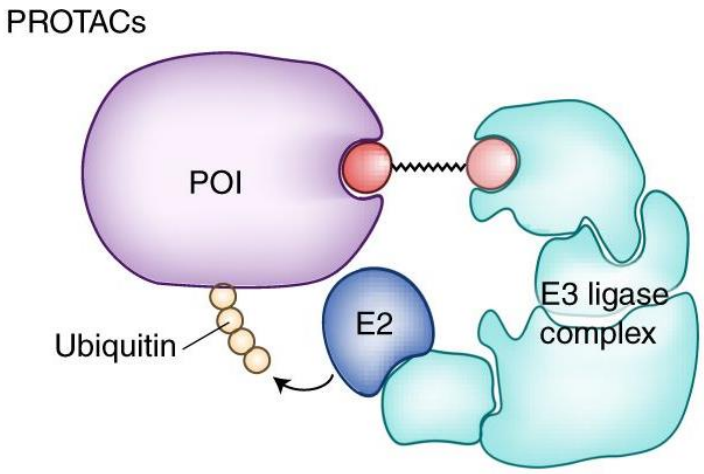

Figure 5.1: Chemically induced proteasomal degradation of proteins of interest (POI). A fusion molecule induces dimerization of both POI and the E3 ligase complex. Subsequent proximity to the E2 ligase promotes ubiquitination of POI, causing proteasomal recognition and degradation (adapted from Yesbolatova and Kanemaki, 2018).

Thalidomide was discovered as a modulator of E3 ligase-mediated ubiquitination of target proteins for degradation. Specifically, thalidomide and its derivatives was shown

to interact with the substrate recognition adaptor protein, cereblon (CRBN). It was first shown that conjugation of thalidomide to the FKBP-binder Shield-1(SLF derivative) caused potent CRBN-dependent degradation of FKBP12 (**Figure 5.2**) (Winter et al., 2015). This occurs through induced association of FKBP12 and CRBN, facilitating FKBP12 ubiquitination by the E3 ligase complex and subsequent proteasomal degradation. Further studies showed that thalidomide conjugation could induce degradation of several proteins, and other E3 ligase modulators showed similar activities when conjugated (Neklesa et al, 2017). These discoveries spurred the creation of proteolysis targeting chimeras (PROTACs) for the degradation of unwanted proteins in biological systems.

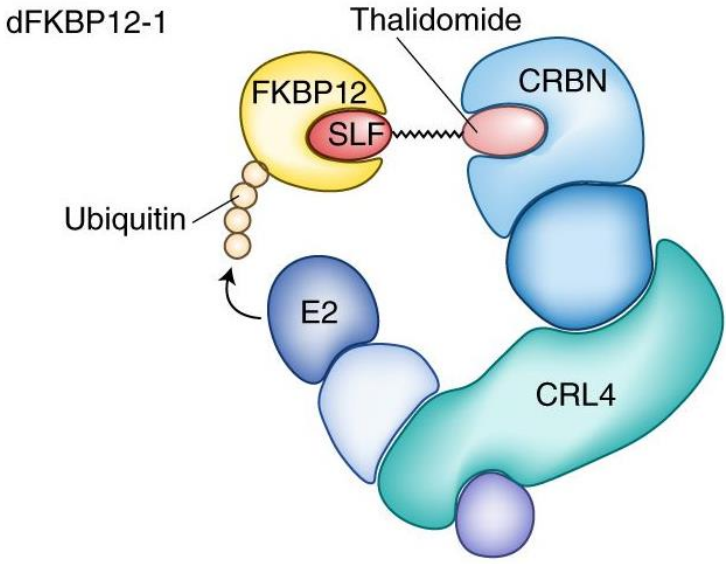

Figure 5.2: Chemically induced proteasomal degradation of FKBP12. A fusion molecule of synthetic ligand of FKBP (SLF) and thalidomide induces dimerization of FKBP12 and cereblon (CRBN). Subsequent proximity to the E2 ligase promotes ubiquitination of FKBP12, causing proteasomal recognition and degradation (adapted from Yesbolatova and Kanemaki, 2018).

That a small-molecule could efficiently degrade FKBP12 is of great interest to our lab. As shown in Chapter 3, FKBP12 deletion caused increased basal SMAD1/5 phosphorylation. We theorized that acute degradation of FKBP12 may result in a more sustained BMP activation, increasing potency of wound healing therapy.

It was hypothesized that any FKBP-binding molecule would act similarly when conjugated to thalidomide, as Shield-1 is not an FKBP12 selective compound. To this end, we decided to again use FK506 as our FKBP-binding scaffold. Macrocyclic structures such as FK506 show increased cell-penetration and binding affinities over linear FKBP12 binding molecules (Marinec et al., 2009), and our recent success with cross-metathesis presented a simple synthetic process for compound development. Testing of our thalidomide-conjugated FK506 analog (FKTM) revealed potent FKBP12 degradation, as well as concurrent degradation of fused fluorescent proteins. This raised the possibility that tightly associating proteins could be targeted through the same degradation mechanism.

In this study, we employed lessons learned from synthesis and testing of FKTM to develop a new strategy for interactome studies in living cells. Using thalidomide conjugation at allosteric sites, we show that protein binding partners are also subject to promiscuous ubiquitination through CRBN. Therefore, relative protein abundance serves as a measure of its association with the thalidomide-tagged target. As a proof of concept, we employ this method to study both inducible (FKBP12-FK506-Calcineruin) and endogenous (FKBP12-ALK1) protein-protein interactions.

5.2 RESULTS

Synthesis of thalidomide-conjugated FK506

Thalidomide-conjugated FK506 (FKTM) was designed using a 6-carbon linker with a terminal alkene for CM and an iodine leaving group (**Fig. 5.3**). Previous work in this area showed that small linkers (4 carbons + 1 peptide) were amenable to FKBP12 association with CRBN (Winter et al, 2015). Synthesis of FKTM proceeded by CM reaction of FK506 and 6-iodohexene, followed by nucleophilic substitution by a phenol-substituted thalidomide. HPLC purification produced a stable product that was characterized by high-resolution mass spectroscopy, performed by the facilities at UCIC (**Fig. 5.4**).

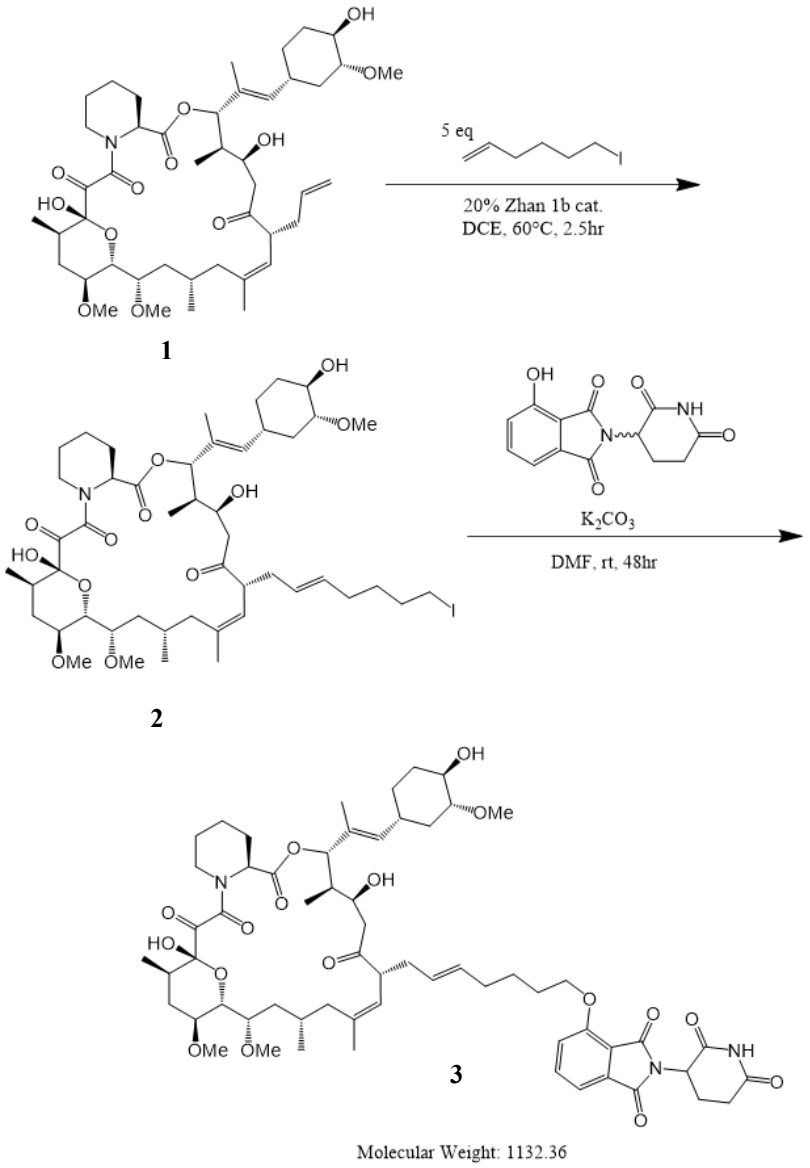

Figure 5.3: Synthesis of thalidomide-conjugated FK506 (FKTM). Two step synthesis using cross metathesis of 6-iodohexene, followed by S_n2 substitution of iodine by phenol-conjugated thalidomide (kindly provided by Dr. Wukun Liu).

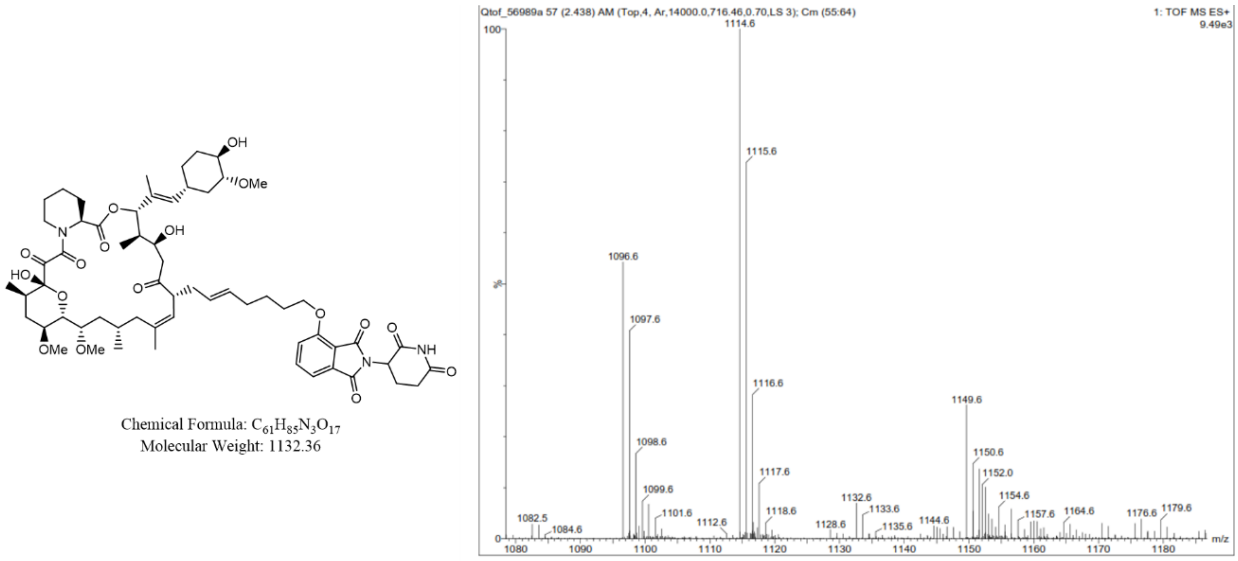

Figure 5.4: Hi-resolution mass-spectrometry profile of FKTM.

Calculated mass = 1132.5959, Found = 1132.5957.

FKTM selectively degrades FKBP12 in wild-type Jurkat cells

We first tested the ability of FKTM to degrade FKBP12 in Jurkat cells. Western blotting showed that 100 nM FKTM degrades FKBP12 to the point of being undetectable after 24 hours, as compared with an FKBP12KO cell line (**Fig. 5.5**).

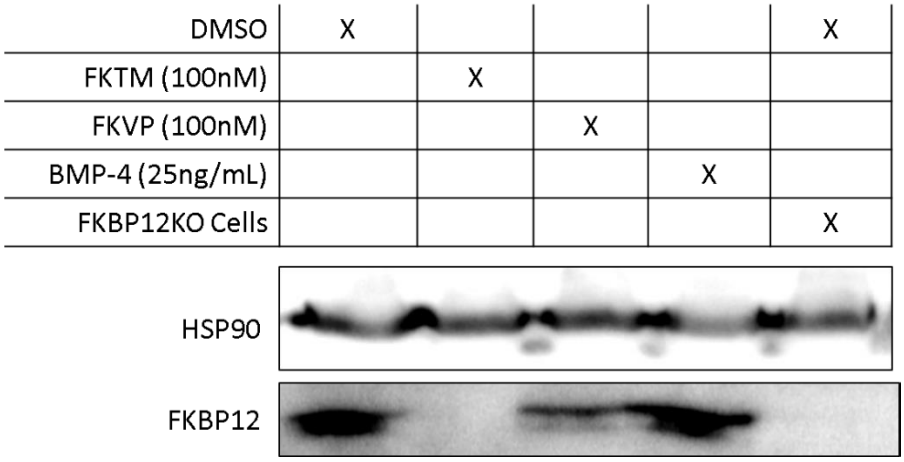

Figure 5.5: FKTM effectively degrades FKBP12 in wild-type Jurkat cells. Western blotting shows FKBP12 is completely degraded in Jurkat cells. FKBP12KO Jurkat cells serve as a positive control while DMSO, FKVP, and BMP-4 serve as negative controls.

Further study by a colleague, Dr. Zufeng Guo, showed that FKBP12 was the only FKBP degraded by FKTM (**Fig. 5.6**). This is surprising, as nearly all FKBP proteins have nanomolar affinity for FK506. This effect may be due to the relatively high expression of FKBP12, or the mechanism of degradation by CRBN modulation. The selectivity of FKTM makes it an attractive candidate for BMP activation in wound healing and regenerative therapies, as we have previously shown isoform FKBP12 dependence in BMP activation (Chapter 3).

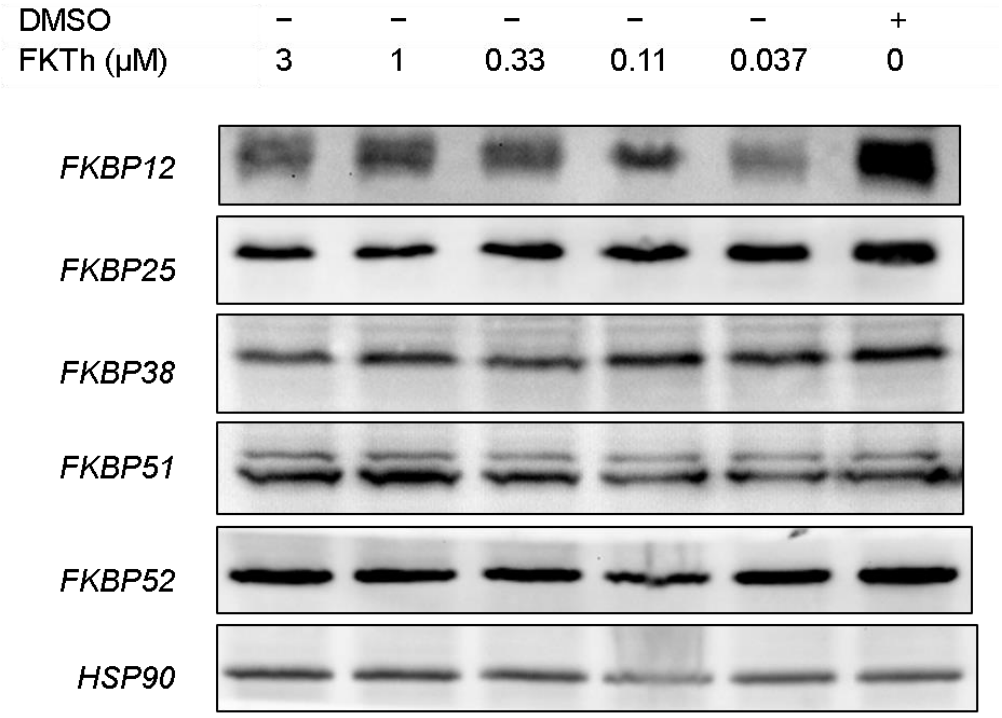

Figure 5.6: FKTM selectively degrades FKBP12 in wild-type Jurkat cells. Western blotting shows only FKBP12 is degraded in Jurkat cells. HSP90 serves as loading control (Courtesy of Dr. Zufeng Guo).

Additionally, Dr. Guo showed that FKTM-induced degradation of FKBP12 was competed by rapamycin and FK506 treatment, confirming that FKTM-FKBP12 binding was necessary for degradation (**Fig. 5.7**). Interestingly, synthetic ligand of FKBP (SLF) was incapable of competing with FKTM for degradation. This may be due to the higher FKBP12 affinities present in macrocyclic FKBP binders.

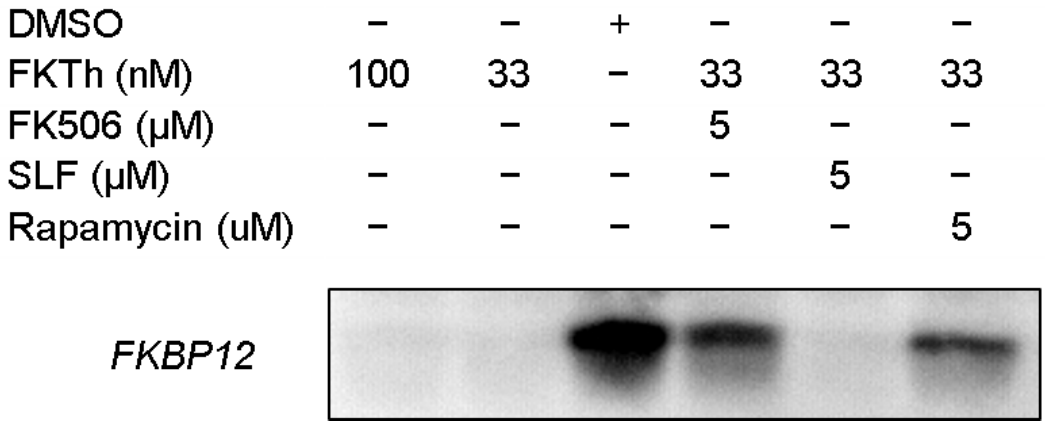

Figure 5.7: FK506 and Rapamycin, but not SLF competes with FKTM for FKBP12 degradation in Jurkat cells. Western blotting shows only the macrocyclic FKBP ligands can compete with FKTM-mediated degradation (Courtesy of Dr. Zufeng Guo).

FKTM potently activates BMP reporter through FKBP12 competition and degradation.

Degradation activity can also be measured by BMP reporter in Jurkat cells, as we have previously reported that FKBP12 knockout causes uncontrolled BMP activation (**Figure 3.17**). In the BMP reporter assay (**Figure 2.7**), FKTM proved to be the most potent BMP activator that we have tested to date, with an EC_{50} below 1 nM (**Fig. 5.8**). This most likely occurs from a combination of FKBP12 dissociation (from BMP receptors) and degradation.

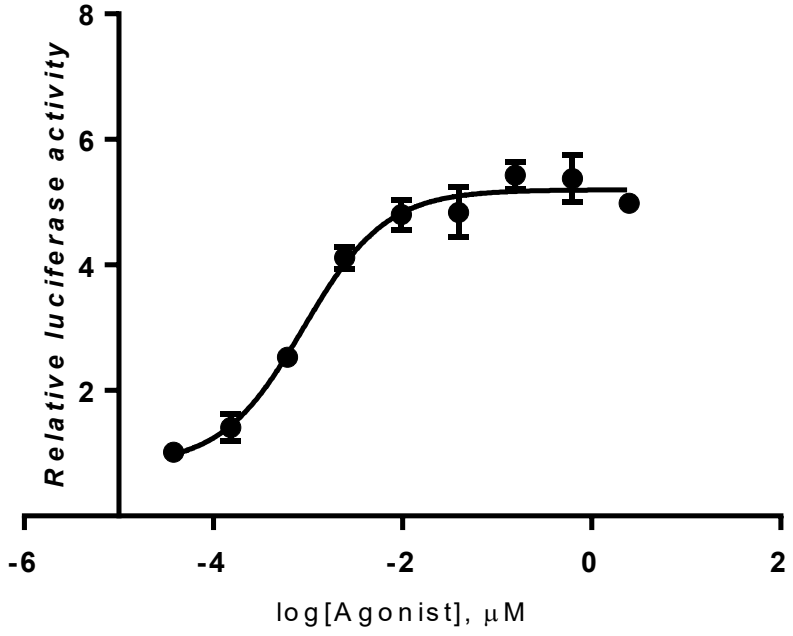

Figure 5.8: FKTM potently activates BMP reporter through FKBP12 competition and degradation. BMP reporter assay in Jurkat cells shows potent activation by FKTM with EC50= 0.90 nM.

FKTM degrades an FKBP12-YFP fusion protein in Hek293T cells.

We then determined the ability of FKTM to degrade an overexpressed FKBP12-YFP fusion protein in HEK293T cells. FKTM significantly reduced YFP fluorescence, which could be competed by FKVP (**Fig. 5.9**). Interestingly, the proteasome inhibitor bortezomib could not block degradation of YFP. This may be due to the low treatment concentration or compound degradation, but a larger dose of bortezomib could not be reliably used due to toxicity problems.

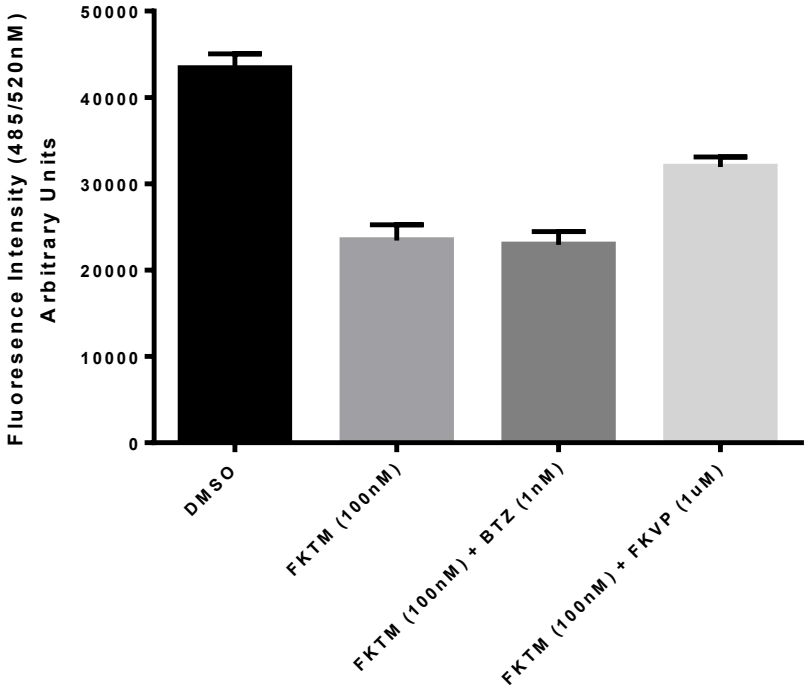

Figure 5.9: FKTM degrades an FKBP12-YFP fusion protein in Hek293T cells. YFP fluorescence was measured in FKBP12-YFP transfected Hek293T cells after 24hr FKTM treatment. This effect was competed by FKVP, but not by bortezomib.

Induced degradation platform proof-of-concept design

The finding that thalidomide conjugation could induce fusion protein degradation raised interesting questions. Specifically, if thalidomide can degrade one protein, could it degrade associated proteins in a complex? To test this possibility, we needed to devise a method for allosterically tagging a protein of interest with thalidomide. This differs from previous reports, as compounds like PROTACs often use the active site for target protein binding (Neklesa et al, 2017). Fortunately, we had designed an FKBP12-SNAP construct for our earlier studies that could be implemented in our novel scheme. SNAP tags allow covalent in-cell attachment of small-molecules to proteins (Keppler et al., 2008), providing an excellent platform for allosteric thalidomide display.

Our plan for this "induced degradation scheme" involves stable expression of a SNAP-tagged protein of interest. When the "induced degradation ligand" is added, the guanine substrate will be displaced by the SNAP tag, displaying a covalently-linked thalidomide molecule for targeted degradation (**Fig. 5.10**). Our hypothesis is that if another protein complexes with the protein of interest, they too may be targeted for degradation by recruitment of promiscuous E3 ligase complexes. As a proof-of-concept, we planned to first use FKBP12 and its known associations.

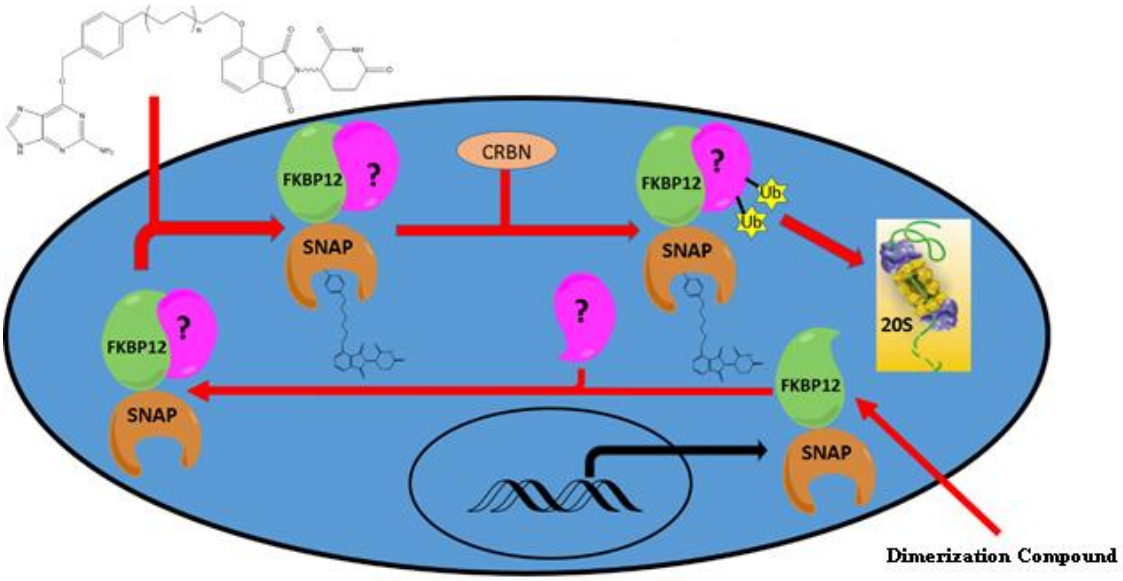

Figure 5.10: Induced degradation platform design. In this scheme, an FKBP12-SNAP fusion protein will be stably expressed in cells. Upon IDL ligand entry to the cell, it covalently binds to the SNAP tag and displays thalidomide, a ligand for the E3 ligase adaptor protein, cereblon (CRBN). The E3 complex then ubiquitinates FKBP12, along with induced (FKBP12:FK506:Calcineurin) and naturally associating (FKBP12:ALK receptor) proteins. This system provides an in-cell assay for interactome studies, and could easily be streamlined by high-throughput mass-spectrometry.

Synthesis scheme of IDL ligand for SNAP-dependent degradation

In our first attempt to synthesize IDL, we used published methods for obtaining o-benzyl protected guanine paired with synthetic methods used for obtaining FKTM (**Fig 5.11**). Synthesis was not optimized, but still produced 2mg of product with modest purity (<75%).

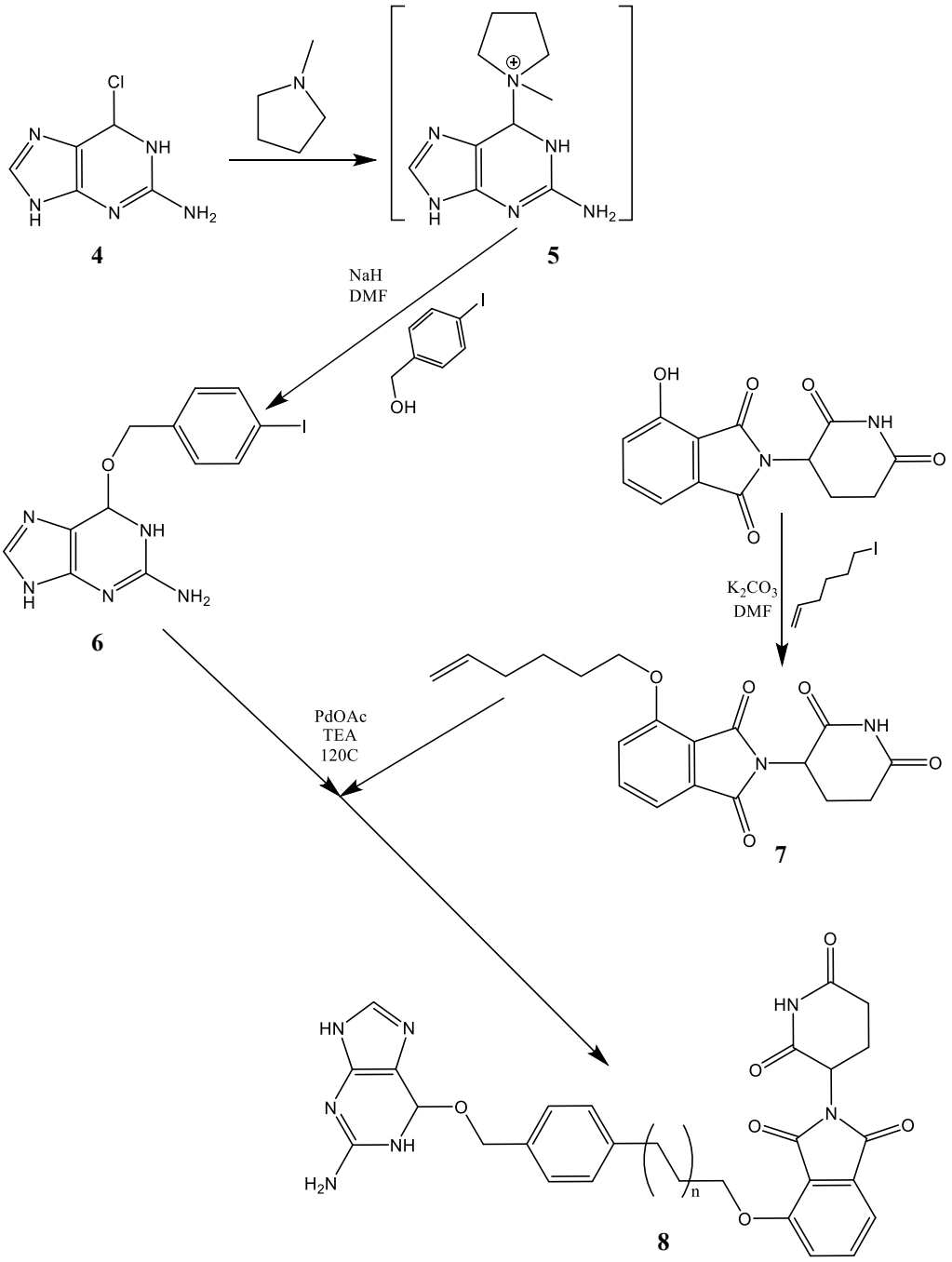

Figure 5.11: Synthesis scheme of IDL ligand. IDL ligand was generated through NMP-activated substitution of 2-amino-6-chloropurine with 4-iodobenzylalcohol, followed by Heck reaction with thalidomide-conjugated hexane (prepared similarly to FKTM).

IDL ligand activates the BMP pathway reporter through FKBP12 degradation.

We had found that the fastest way to test compounds for FKBP12 degradation was to use the BMP pathway reporter. To accomplish this, we compared IDL-induced BMP reporter activation in WT and FKBP12KO Jurkat cells after transfection with FKBP12-SNAP. Results showed that only cells with FKBP12-SNAP were sensitive to IDL treatment (**Fig. 5.12**). This suggests that both the SNAP and thalidomide portions of the molecule performed correctly, causing targeted degradation of FKBP12-SNAP and therefore BMP reporter activation.

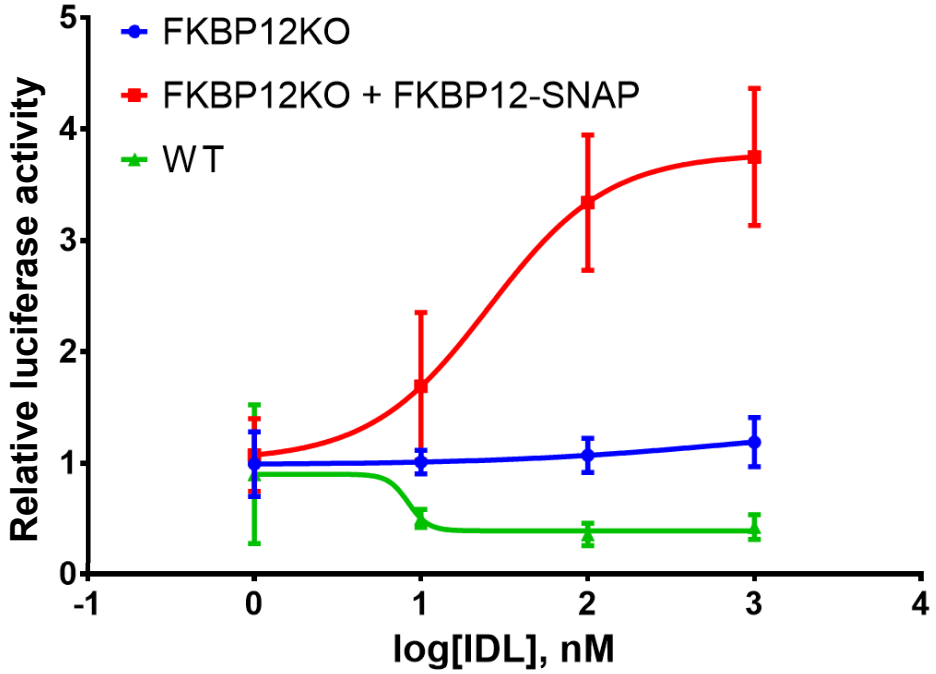

Figure 5.12: IDL ligand activates the BMP pathway reporter through FKBP12 degradation. IDL ligand shows dose-dependent activation of the BMP reporter in FKBP12-SNAP expressing cells only. Error bars represent standard deviation from mean

for all measurements (n=3), and absorbance/luminescence values were normalized to DMSO treated cells.

IDL ligand degrades the FKBP12-interacting protein calcineurin in the presence of FK506

To continue our proof-of-concept study, we explored FKBP12 degradation in the context of the FKBP12-calcineurin complex. Western blotting showed IDL potently degraded the FKBP12-SNAP fusion protein in HEK293T cells (**Fig. 5.13**). Interestingly, there was a clear reduction in calcineurin protein abundance when IDL was combined with FK506. This gives strong evidence that proteins could be targeted for degradation through association with the tagged protein. Conversely, mTOR was not reduced by combined IDL and rapamycin treatment (data not shown). This outcome is rationalized though the large size of mTOR and the alternate degradation pathways it may follow.

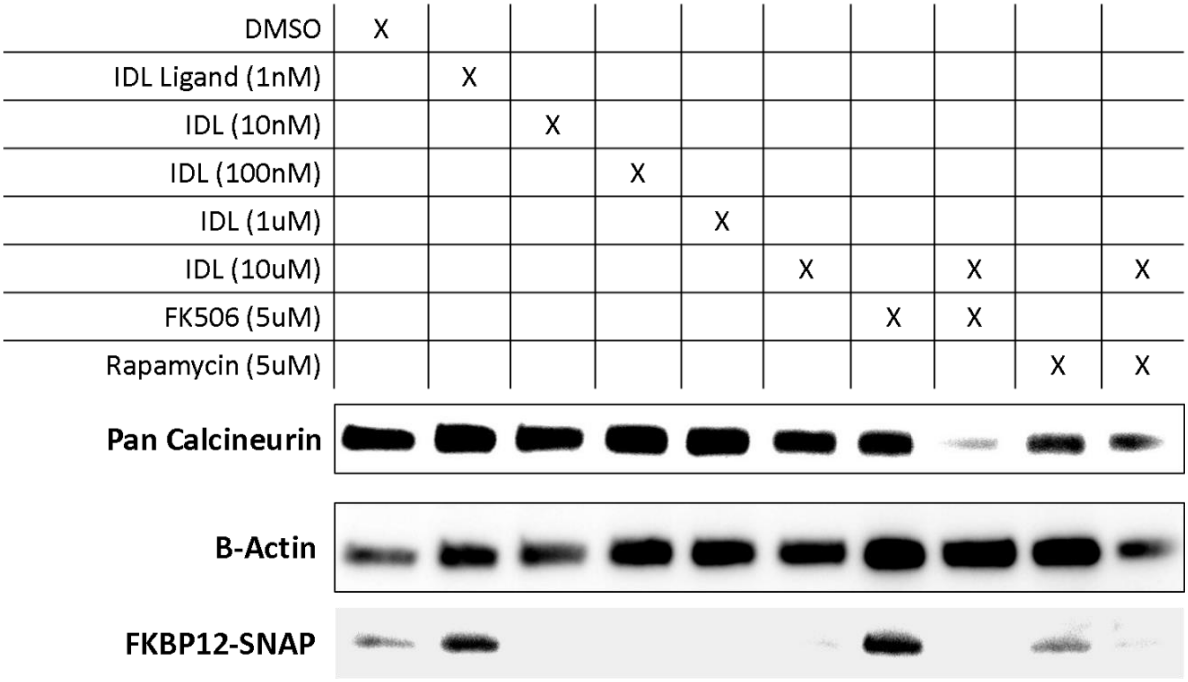

Figure 5.13: IDL ligand degrades the FKBP12-interacting protein calcineurin in the presence of FK506. Western blotting shows IDL ligand degrades calcineurin and FKBP12-SNAP when combined with FK506 in FKBP12KO HEK293T cells.

IDL ligand degrades the natural FKBP12-interacting protein Alk1

To continue our study, we investigated degradation of endogenously associating proteins. In this context, we used FKBP12-ALK1 as a model for proteins that naturally associate (**Figure 3.20**). In Jurkat cells stably transfected with FKBP12-SNAP, we found that ALK1 was degraded in a dose dependent fashion by IDL (**Fig. 5.14**). Although degradation was not competed by FK506 (data not shown), it may help to explain the accompanying lack of complete reversal in fluorescence experiments. This is most likely because ubiquitination of target proteins is non-reversible in this system.

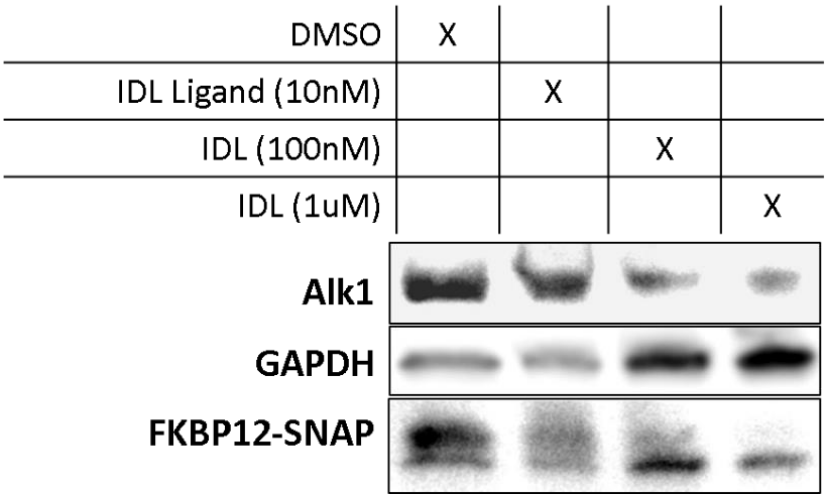

Figure 5.14: IDL ligand degrades the natural FKBP12-interacting protein Alk1. Western blotting shows IDL ligand degrades Alk1 and FKBP12-SNAP in FKBP12KO Jurkat cells.

5.3 MATERIALS AND METHODS

FKBP12KO cells were generated as previously described (**Chapter 3, Fig. 3.15**)

Cell Culture and Transfections

Jurkat (E6.1, ATCC) cells were cultured in RPMI with 10% FBS and 1.5% PennStrep. Jurkat cells (1 x 10^6) were transfected with 10 µg of BRE-Luciferase (kindly provided by Martine Roussel & Peter ten Dijke) or NFAT-Luciferase cDNA (Promega) by electroporation (BioRad, square-wave, 250V, 950 µF) in 400 µL serum/antibiotic free RPMI with 0.5% DMSO. Thirty minutes after transfection, cells were transferred to complete RPMI and rested overnight. Before plating, cells were re-suspended in fresh media and diluted to 0.5x10^6 cells/mL. HEK293T cells were cultured in DMEM with 10% FBS, 1% PennStrep, and 500 µg/mL G418 (Corning). Cells were transfected using SuperFect reagent and supplied transfection protocols. All cells were cultured at 37 °C with 5% CO_2.

Western Blot

Jurkat T cells were collected by centrifugation (300g, 5 min), washed with PBS, and lysed in RIPA buffer containing protease and phosphatase inhibitors (Cell Signaling) with sonication. Lysates were normalized using DC assay (BioRad) and run on SDS-PAGE gels. Proteins were transferred to nitrocellulose membranes overnight at 100mA. After blocking with 5% milk in TBS-T for 20 min, membranes were incubated overnight

at 4°C with primary antibodies (**Table 3.1**). After washing three times with TBS-T, membranes were incubated with secondary antibody (**Table 3.1**) for 1 hour. After 3 additional washes, blots were visualized using SynGene, either using ECL substrate (Thermo) or laser excitation and filter (647 nm).

Fluorescent Protein Degradation

FKBP12KO HEK293T cells were transfected with YFP-FKBP12 as previously described (**Chapter 3**). After 24 hours, cells were split into 96-well plates and treated with FKTM for an additional 24 hours. Afterwards, cells were aspirated and lysed in luciferase lysis buffer before measurement on a plate reader.

IDL Ligand Synthesis

N-Methyl-2-pyrrolidone (NMP)-Protected Guanine (5): Chloro-pyrimidine (**4**) (0.5g) was dissolved in DMF at 50 °C, and cooled to rt before addition of 1.4 mL N-methylpyrrolidine. The final mixture was stirred overnight. Product (440 mg) was obtained after vacuum filtration and washing with ethyl acetate.

4-Iodo-O-benzyl guanine (6): Dry DMF (1mL) was added to 22 mg NaH at 0°C under argon. 4-Iodo-benzyl alcohol was dissolved in 2 mL dry DMF and added dropwise to the NaH solution under argon. After 15 mins, 10 mg DMAP and 100 mg NMP-protected guanine was dissolved in 2 mL dry DMF, and added slowly to the NaH solution. The mixture was stirred and allowed to come to RT and react for 2 hours before quenching

with 2 mL H_2O. Ethyl acetate (3 x 10 mL) was used to extract the compound and dried under vacuum.

Hexene-conjugated thalidomide (7): Phenol-thalidomide (40mg, provided by Dr. Wukun Liu) was dissolved in 2 mL DMF and stirred with 2eq. K_2CO_3 for 20 min at room temperature before addition of 60 µL 6-iodo-1-hexene. The mixture was stirred in the dark and monitored by TLC (10% methanol in dichloromethane). After 4 hours, the reaction was quenched with water (2 mL) and extracted with ethyl acetate (3 x 10 mL). The final product was a light-yellow solid (Mass:357 (H+), 57 mg, 90% crude yield) that was used without further purification.

IDL Ligand (8): 4-iodo-benzyl-guanine and hexane-conjugated thalidomide were mixed 1:1 (0.5 mmol) in 2 mL dry DMF. 5% Palladium acetate and 10% o-tolulyl phosphine was dissolved in 1mL dry DMF and mixed with 100 µL TEA. The mixture was stirred under argon overnight at 100 °C. Product was purified using flash chromatography (gradient elution with dichloromethane and methanol) and HPLC (semi-preparative C18 column).

Synthesis of FKTM (3)

To 40 mg (0.05mmol) of FK506 (**1**) in 3 mL DCE was added 52 mg (0.25mmol) 6-iodo-1-hexene and 7.4 mg (0.01mmol) Dichloro[1,3-bis(2,4,6-trimethylphenyl)-2-imidazolidinylidene][[5-[(dimethylamino)sulfonyl]-2-(1-methylethoxy-O)phenyl]methylene-C]ruthenium(II) (Zhan 1b catalyst). The vial was capped and heated

using microwave at 60 °C for 2.5 hours. Product was flash purified on silica to obtain a mixture of product (**2**) and FK506. Evaporated crude product (20 mg) was then dissolved into 5 mL DMF containing 10 mg (0.075mmol) potassium carbonate and 21 mg (0.075mmol) 4-hydroxythalidomide (Cas. 5054-59-1). The mixture was stirred at room temperature for 48 hours before water quenching (5 mL), ethyl acetate extraction (3 x 10 mL), and HPLC purification (semi-prep C18 column) to obtain FKTM (**3**). Purified yield = 7%.

BMP and NFAT Pathway Reporters

Jurkat T cells transfected with BRE-Luc were split into a 96-well plate (80 µL/well of $0.5x10^6$ cells/mL)) and treated with IDL (20 µL of 5X stock in RPMI, 0.5% DMSO) for 18 h. Plates were centrifuged at 3000rpm for 10min, then carefully aspirated. Cells were re-suspended in 100 µL lysis buffer (per well) and placed on a plate-shaker for 30 min. An aliquot of 80 µL of lysate was transferred to a white-walled 96-well plate, and luminescence was recorded 2 seconds after automated injection of luciferase substrate. Luminescence values were background subtracted (lysis buffer + substrate) and normalized to DMSO control values.

FKBP12KO Jurkat T cells transfected with FKBP12-SNAP plasmid were selected with 1200 µg/mL G418 for seven days before use in BRE-Luc assays.

EC_{50} Determinations

Calculations were performed using GraphPad Prism 6. Curves were fit using non-linear, log(agonist) vs. response (three parameters). 95% confidence intervals of EC_{50} values are reported below.

5.4 DISCUSSION

The selective degradation activity displayed by FKTM has revealed a previously unrecognized method for BMP activation. We have previously shown that genetic deletion of FKBP12 promotes the same BMP signaling activation as FK506 and other FKBP agonists, and we now show that chemical FKBP12 degradation produces similar results. Degradation of FKBP12 by FKTM was found to persist after 24 hours, suggesting compounds like these would serve as long-acting therapeutics. Moreover, our finding that FKBP12 is the only isoform affected by treatment suggests decreased opportunity for off-target effects. FKTM presents a valuable option for pharmacological BMP activation currently under investigation.

This lab has previously reported that FKBP binding molecules synergize with AMD3100 to accelerate wound healing in diabetic GK rats after full-thickness skin excision (Chapter 3), and this effect was found to be BMP-dependent. FKTM represents a new class of compounds that may enhance wound healing through sustained BMP activation. Furthermore, the increased potency of FKTM over previous BMP agonists suggest a lower treatment dose, and the risk of free thalidomide is rendered minimal through use of a stable hydrocarbon linker. Through modification of FKTM's linker region, derivatives could be designed to improve stability, solubility, and degradation activity.

Beyond FKTM, the discovery of degradation-by-association comes as a first in the field of E3 ligase hijacking by small molecules. Till now, the majority of studies involve targeted degradation of one protein of interest. Our findings show that in some cases, protein complexes can be degraded by allosteric tagging of the target protein with an E3 ligase

binder. This data suggests that compounds like PROTACs may non-specifically degrade proteins that associate at allosteric regions of the target protein.

As a proof of concept, we used an FKBP12-SNAP construct and the IDL ligand to show that proteins associating with FKBP12 were degraded in a dose-dependent manner. To highlight its applications, we studied FKBP12 interactions that were both inducible (FKBP12-FK506-Calcineurin) and non-inducible (FKBP12-ALK1). We theorize that this platform can be extended to interactome studies of several other target proteins.

The high-throughput applications of proteomic-mass spectrometry may soon allow us to simultaneously measure all proteins and their abundance in cells stably expressing a SNAP-tagged protein of interest. Interacting proteins could then be identified by relative protein abundance after IDL treatment, creating a comprehensive map of associating proteins in one experiment. This platform has several applications in biology and drug-discovery, and may identify undocumented protein-protein interactions that could be targeted for treatment of complex diseases.

The capabilities of this platform depend largely on the ability of E3 ligases to promiscuously ubiquitinate proteins and their associating partners. However, there are several advancements that can be made to improve this activity. Several other E3 ligases such as MDM2 and XIAP have been shown to degrade proteins displaying specific small molecules (Lai et al., 2017). Creating multiple derivatives of IDL with different E3 ligase modulators will allow us to target more proteins, expanding the scope of the platform. On-chip ubiquitination of immobilized human proteins could be used to determine the promiscuity of these E3 ligases (Cox et al., 2015) and collected data would serve to correlate with in-cell effects. Moreover, by using different tagging methods such as HALO

tags or other covalent modifiers attached at either the C or N termini, we can account for steric clash with proteins that may associate.

In sum, the discovery and development of this platform may allow us to accelerate the discovery of protein-protein interactions, both induced and endogenous. In the near future, this method could be adapted to large scale interactome screening of all human proteins, generating big data on in-cell protein associations that could be mined for new therapy options never considered.

6. REFERENCES

Abraham, R.T., and Wiederrecht, G.J. (1996). Immunopharmacology of rapamycin. Annu. Rev. Immunol. *14*, 483–510.

Albiñana, V., Sanz-Rodríguez, F., Recio-Poveda, L., Bernabéu, C., and Botella, L.M. (2011). Immunosuppressor FK506 increases endoglin and activin receptor-like kinase 1 expression and modulates transforming growth factor-β1 signaling in endothelial cells. Mol. Pharmacol. *79*, 833–843.

Balaji, S., King, A., Crombleholme, T.M., and Keswani, S.G. (2013). The Role of Endothelial Progenitor Cells in Postnatal Vasculogenesis: Implications for Therapeutic Neovascularization and Wound Healing. Adv Wound Care (New Rochelle) *2*, 283–295.

Bechstein, W.O. (2000). Neurotoxicity of calcineurin inhibitors: impact and clinical management. Transpl. Int. *13*, 313–326.

Bennett, J., Cassidy, H., Slattery, C., Ryan, M.P., and McMorrow, T. (2016). Tacrolimus Modulates TGF-β Signaling to Induce Epithelial-Mesenchymal Transition in Human Renal Proximal Tubule Epithelial Cells. Journal of Clinical Medicine *5*, 50.

Bueno, O.F., Brandt, E.B., Rothenberg, M.E., and Molkentin, J.D. (2002). Defective T cell development and function in calcineurin A beta -deficient mice. Proc. Natl. Acad. Sci. U.S.A. *99*, 9398–9403.

Cameron, A.M., Steiner, J.P., Sabatini, D.M., Kaplin, A.I., Walensky, L.D., and Snyder, S.H. (1995). Immunophilin FK506 binding protein associated with inositol 1,4,5-trisphosphate receptor modulates calcium flux. PNAS *92*, 1784–1788.

Cameron, A.M., Wesson, R.N., Ahmadi, A.R., Singer, A.L., Hu, X., Okabayashi, T., Wang, Y., Shigoka, M., Fu, Y., Gao, W., et al. (2016). Chimeric Allografts Induced by Short-Term Treatment With Stem Cell Mobilizing Agents Result in Long-Term Kidney Transplant Survival Without Immunosuppression: II, Study in Miniature Swine. Am. J. Transplant. *16*, 2066–2076.

Chaikuad, A., Alfano, I., Kerr, G., Sanvitale, C.E., Boergermann, J.H., Triffitt, J.T., Delft, F. von, Knapp, S., Knaus, P., and Bullock, A.N. (2012). Structure of the Bone Morphogenetic Protein Receptor ALK2 and Implications for Fibrodysplasia Ossificans Progressiva. J. Biol. Chem. *287*, 36990–36998.

Chen, Y.G., Liu, F., and Massague, J. (1997). Mechanism of TGFbeta receptor inhibition by FKBP12. EMBO J *16*, 3866–3876.

Clemons, P.A., Gladstone, B.G., Seth, A., Chao, E.D., Foley, M.A., and Schreiber, S.L. (2002). Synthesis of calcineurin-resistant derivatives of FK506 and selection of compensatory receptors. Chem. Biol. *9*, 49–61.

Compain, P. (2007). Olefin Metathesis of Amine-Containing Systems: Beyond the Current Consensus. Advanced Synthesis & Catalysis *349*, 1829–1846.

Cox, E., Uzoma, I., Guzzo, C., Jeong, J.S., Matunis, M., Blackshaw, S., and Zhu, H. (2015). Identification of SUMO E3 ligase-specific substrates using the HuProt human proteome microarray. Methods Mol. Biol. *1295*, 455–463.

Csiszar, A., Ahmad, M., Smith, K.E., Labinskyy, N., Gao, Q., Kaley, G., Edwards, J.G., Wolin, M.S., and Ungvari, Z. (2006). Bone Morphogenetic Protein-2 Induces Proinflammatory Endothelial Phenotype. Am J Pathol *168*, 629–638.

Cuny, G.D., Yu, P.B., Laha, J.K., Xing, X., Liu, J.-F., Lai, C.S., Deng, D.Y., Sachidanandan, C., Bloch, K.D., and Peterson, R.T. (2008). Structure-activity relationship study of bone morphogenetic protein (BMP) signaling inhibitors. Bioorg Med Chem Lett *18*, 4388–4392.

Fife, C.E., and Carter, M.J. (2012). Wound Care Outcomes and Associated Cost Among Patients Treated in US Outpatient Wound Centers: Data From the US Wound Registry. Wounds *24*, 10–17.

Fung, J.J. (2004). Tacrolimus and transplantation: a decade in review. Transplantation *77*, S41-43.

Giordano, A., Romano, S., Mallardo, M., D'Angelillo, A., Calì, G., Corcione, N., Ferraro, P., and Romano, M.F. (2008). FK506 can activate transforming growth factor-beta signaling in vascular smooth muscle cells and promote proliferation. Cardiovasc. Res. *79*, 519–526.

Gold, B.G. (1999). FK506 and the role of the immunophilin FKBP-52 in nerve regeneration. Drug Metab. Rev. *31*, 649–663.

Gold, B.G., Densmore, V., Shou, W., Matzuk, M.M., and Gordon, H.S. (1999). Immunophilin FK506-binding protein 52 (not FK506-binding protein 12) mediates the neurotrophic action of FK506. J. Pharmacol. Exp. Ther. *289*, 1202–1210.

Griffith, J.P., Kim, J.L., Kim, E.E., Sintchak, M.D., Thomson, J.A., Fitzgibbon, M.J., Fleming, M.A., Caron, P.R., Hsiao, K., and Navia, M.A. (1995). X-ray structure of calcineurin inhibited by the immunophilin-immunosuppressant FKBP12-FK506 complex. Cell *82*, 507–522.

Hatse, S., Princen, K., Bridger, G., De Clercq, E., and Schols, D. (2002). Chemokine receptor inhibition by AMD3100 is strictly confined to CXCR4. FEBS Lett. *527*, 255–262.

Heck, R.F., and Nolley, J.P. (1972). Palladium-catalyzed vinylic hydrogen substitution reactions with aryl, benzyl, and styryl halides. J. Org. Chem. *37*, 2320–2322.

Hoorn, E.J., Walsh, S.B., McCormick, J.A., Zietse, R., Unwin, R.J., and Ellison, D.H. (2012). Pathogenesis of calcineurin inhibitor-induced hypertension. J. Nephrol. *25*, 269–275.

Houghton, S.R., Melton, J., Fortunak, J., Brown Ripin, D.H., and Boddy, C.N. (2010). Rapid, mild method for phosphonate diester hydrolysis: development of a one-pot synthesis of tenofovir disoproxil fumarate from tenofovir diethyl ester. Tetrahedron *66*, 8137–8144.

Hu, X., Okabayashi, T., Cameron, A.M., Wang, Y., Hisada, M., Li, J., Raccusen, L.C., Zheng, Q., Montgomery, R.A., Williams, G.M., et al. (2016). Chimeric Allografts Induced by Short-Term Treatment With Stem Cell-Mobilizing Agents Result in Long-Term Kidney Transplant Survival Without Immunosuppression: A Study in Rats. Am. J. Transplant. *16*, 2055–2065.

Jayaraman, T., Brillantes, A.M., Timerman, A.P., Fleischer, S., Erdjument-Bromage, H., Tempst, P., and Marks, A.R. (1992). FK506 binding protein associated with the calcium release channel (ryanodine receptor). J. Biol. Chem. *267*, 9474–9477.

Jujo, K., Hamada, H., Iwakura, A., Thorne, T., Sekiguchi, H., Clarke, T., Ito, A., Misener, S., Tanaka, T., Klyachko, E., et al. (2010). CXCR4 blockade augments bone marrow progenitor cell recruitment to the neovasculature and reduces mortality after myocardial infarction. Proc. Natl. Acad. Sci. U.S.A. *107*, 11008–11013.

Keppler, A., Gendreizig, S., Gronemeyer, T., Pick, H., Vogel, H., and Johnsson, K. (2003). A general method for the covalent labeling of fusion proteins with small molecules *in vivo*. Nature Biotechnology *21*, 86–89.

Kissinger, C.R., Parge, H.E., Knighton, D.R., Lewis, C.T., Pelletier, L.A., Tempczyk, A., Kalish, V.J., Tucker, K.D., Showalter, R.E., and Moomaw, E.W. (1995). Crystal structures of human calcineurin and the human FKBP12-FK506-calcineurin complex. Nature *378*, 641–644.

Kozany, C., März, A., Kress, C., and Hausch, F. (2009). Fluorescent probes to characterise FK506-binding proteins. Chembiochem *10*, 1402–1410.

Lai, A.C., and Crews, C.M. (2017). Induced protein degradation: an emerging drug discovery paradigm. Nature Reviews Drug Discovery *16*, 101–114.

Lewis, C.J., Mardaryev, A.N., Poterlowicz, K., Sharova, T.Y., Aziz, A., Sharpe, D.T., Botchkareva, N.V., and Sharov, A.A. (2014). Bone morphogenetic protein signaling suppresses wound-induced skin repair by inhibiting keratinocyte proliferation and migration. J. Invest. Dermatol. *134*, 827–837.

Liles, W.C., Broxmeyer, H.E., Rodger, E., Wood, B., Hübel, K., Cooper, S., Hangoc, G., Bridger, G.J., Henson, G.W., Calandra, G., et al. (2003). Mobilization of hematopoietic progenitor cells in healthy volunteers by AMD3100, a CXCR4 antagonist. Blood *102*, 2728–2730.

Lin, Q., Wesson, R.N., Maeda, H., Wang, Y., Cui, Z., Liu, J.O., Cameron, A.M., Gao, B., Montgomery, R.A., Williams, G.M., et al. (2014). Pharmacological mobilization of endogenous stem cells significantly promotes skin regeneration after full-thickness excision: the synergistic activity of AMD3100 and tacrolimus. J. Invest. Dermatol. *134*, 2458–2468.

Liu, J., Farmer, J.D., Lane, W.S., Friedman, J., Weissman, I., and Schreiber, S.L. (1991). Calcineurin is a common target of cyclophilin-cyclosporin A and FKBP-FK506 complexes. Cell *66*, 807–815.

Marinec, P.S., Evans, C.G., Gibbons, G.S., Tarnowski, M.A., Overbeek, D.L., and Gestwicki, J.E. (2009). Synthesis of Orthogonally Reactive FK506 Derivatives via Olefin Cross Metathesis. Bioorg Med Chem *17*, 5763–5768.

Mueller, T.D. (2015). Mechanisms of BMP-Receptor Interaction and Activation. Vitam. Horm. *99*, 1–61.

Naesens, M., Kuypers, D.R.J., and Sarwal, M. (2009). Calcineurin Inhibitor Nephrotoxicity. CJASN *4*, 481–508.

Neklesa, T.K., Winkler, J.D., and Crews, C.M. (2017). Targeted protein degradation by PROTACs. Pharmacol. Ther. *174*, 138–144.

Okabayashi, T., Cameron, A.M., Hisada, M., Montgomery, R.A., Williams, G.M., and Sun, Z. (2011). Mobilization of host stem cells enables long-term liver transplant acceptance in a strongly rejecting rat strain combination. Am. J. Transplant. *11*, 2046–2056.

Plikus, M.V., Guerrero-Juarez, C.F., Ito, M., Li, Y.R., Dedhia, P.H., Zheng, Y., Shao, M., Gay, D.L., Ramos, R., Hsi, T.-C., et al. (2017). Regeneration of fat cells from myofibroblasts during wound healing. Science *355*, 748–752.

Rao, A., Luo, C., and Hogan, P.G. (1997). Transcription factors of the NFAT family: regulation and function. Annu. Rev. Immunol. *15*, 707–747.

Schäffer, M.R., Fuchs, N., Proksch, B., Bongartz, M., Beiter, T., and Becker, H.D. (1998). Tacrolimus impairs wound healing: a possible role of decreased nitric oxide synthesis. Transplantation *65*, 813–818.

Shin, K., Lim, A., Zhao, C., Sahoo, D., Pan, Y., Spiekerkoetter, E., Liao, J.C., and Beachy, P.A. (2014). Hedgehog Signaling Restrains Bladder Cancer Progression by Eliciting Stromal Production of Urothelial Differentiation Factors. Cancer Cell *26*, 521–533.

Spiekerkoetter, E., Tian, X., Cai, J., Hopper, R.K., Sudheendra, D., Li, C.G., El-Bizri, N., Sawada, H., Haghighat, R., Chan, R., et al. (2013). FK506 activates BMPR2, rescues endothelial dysfunction, and reverses pulmonary hypertension. J. Clin. Invest. *123*, 3600–3613.

Spiekerkoetter, E., Sung, Y.K., Sudheendra, D., Scott, V., Rosario, P.D., Bill, M., Haddad, F., Long-Boyle, J., Hedlin, H., and Zamanian, R.T. (2017). Randomised placebo-controlled safety and tolerability trial of FK506 (tacrolimus) for pulmonary arterial hypertension. European Respiratory Journal *50*, 1602449.

Sun, C.C., Vaja, V., Chen, S., Theurl, I., Stepanek, A., Brown, D.E., Cappellini, M.D., Weiss, G., Hong, C.C., Lin, H.Y., et al. (2013). A hepcidin lowering agent mobilizes iron for incorporation into red blood cells in an adenine-induced kidney disease model of anemia in rats. Nephrol Dial Transplant *28*, 1733–1743.

Tanaka, H., Kuroda, A., Marusawa, H., Hatanaka, H., Kino, T., Goto, T., Hashimoto, M., and Taga, T. (1987). Structure of FK506, a novel immunosuppressant isolated from Streptomyces. J. Am. Chem. Soc. *109*, 5031–5033.

Tateishi, K., Higuchi, C., Ando, W., Nakata, K., Hashimoto, J., Hart, D.A., Yoshikawa, H., and Nakamura, N. (2007). The immunosuppressant FK506 promotes development of the chondrogenic phenotype in human synovial stromal cells via modulation of the Smad signaling pathway. Osteoarthritis and Cartilage *15*, 709–718.

Wang, T., Li, B.Y., Danielson, P.D., Shah, P.C., Rockwell, S., Lechleider, R.J., Martin, J., Manganaro, T., and Donahoe, P.K. (1996). The immunophilin FKBP12 functions as a common inhibitor of the TGF beta family type I receptors. Cell *86*, 435–444.

Winter, G.E., Buckley, D.L., Paulk, J., Roberts, J.M., Souza, A., Dhe-Paganon, S., and Bradner, J.E. (2015). DRUG DEVELOPMENT. Phthalimide conjugation as a strategy for in vivo target protein degradation. Science *348*, 1376–1381.

Woodward, C.P., Spiccia, N.D., Jackson, W.R., and Robinson, A.J. (2011). A simple amine protection strategy for olefin metathesis reactions. Chem. Commun. (Camb.) *47*, 779–781.

Yesbolatova, A., and Kanemaki, M.T. (2018). TAGing for destruction. Nature Chemical Biology *14*, 414.

Young, K., Conley, B., Romero, D., Tweedie, E., O'Neill, C., Pinz, I., Brogan, L., Lindner, V., Liaw, L., and Vary, C.P.H. (2012). BMP9 regulates endoglin-dependent chemokine responses in endothelial cells. Blood *120*, 4263–4273.

Zhai, R., Wang, Y., Qi, L., Williams, G.M., Gao, B., Song, G., Burdick, J.F., and Sun, Z. (2018). Pharmacological Mobilization of Endogenous Bone Marrow Stem Cells Promotes Liver Regeneration after Extensive Liver Resection in Rats. Scientific Reports *8*, 3587.

7. CURRICULUM VITAE

PROFESSIONAL SUMMARY

- Diverse expertise in molecular biology, immunology, and medicinal chemistry.
- Collaborative researcher with contributions to multidisciplinary projects in stem cell biology, transplantation, and tissue regeneration.
- In process of obtaining patent for a novel, research-related invention for chronic-wound healing.
- One first author publication in press, and another under submission.
- Expertise in growth factors, cytokines, and chemokines that regulate immune system response and wound healing.

EDUCATION

Johns Hopkins University, KSAS // Baltimore, MD 2014 – Feb, 2019

Ph.D., Chemical Biology

Johns Hopkins University, KSAS // Baltimore, MD 2014 – 2016

M.S., Chemical Biology

Millersville University // Millersville, PA 2010 – 2014

B.S., Biochemistry, Departmental Honors

RESEARCH EXPERIENCE

Doctoral Research // Johns Hopkins University 2015 – Present

PI: Jun O. Liu, Ph.D., Pharmacology, Johns Hopkins University School of Medicine

- Lead investigator in a collaborative effort focused on understanding the mechanism of a synergistic drug combination for accelerated wound healing in diabetic animal models.
- Clinical development of a 2nd generation therapeutic in accelerated-healing of chronic wounds.
- Chemically-modified an FDA-approved immunosuppressant to study beneficial off-target effects.
- Worked closely with surgical team in collecting primary tissue samples for analysis.
- Innovated new drug-screening technique using targeted and inducible degradation of a novel fusion-protein.
- Established a unique screening platform for inhibitors of PD-1/PD-L1 immune checkpoints.
- Prepared several gene knockout clones for target validation using CRISPR/Cas9 systems.
- Trained rotation students with customized projects designed to enhance experimental techniques in their desired field.
- Experience with patent filing process, invention disclosures, material-transfer agreements (MTA), and intellectual property policies.

Undergraduate Research // Millersville University 2012 – 2014

PI: Steven Bonser, Ph.D., Department of Chemistry

- Progressed study of a novel diaziridine-opening reaction in the synthesis of 2,4-benzodiazipines.
- Presented work at 247th annual American Chemical Society (ACS) meeting Dallas, TX.

PUBLICATIONS

1. Wang, Y.*, Peiffer, B.*, Su, Q., Liu, J. "One-Step Heck Reaction Generates Non-Immunosuppressive FK506 Analogs for Pharmacological BMP Activation." Chemical Communications (Under Submission).

2. Peiffer, B.*, Qi, L.*, Ahmadi, A., Wang, Y., Sun, Z., Liu, J. O. "Non-Immunosuppressive FKBP12 Ligands Activate BMP Signaling to Accelerate Chronic-Wound Healing in Diabetic Rats." Cell Chemical Biology (In Press).

3. Guo, Z., Hong, S.Y., Wang, J., Rehan, S., Liu, W., Peng, H., Das, M., Li, W., Bhat, S., Peiffer, B., et al. Rapamycin-inspired macrocycles with new target specificity. Nature Chemistry 1 (2018).

4. John G. Kosowicz, Jaeyeun Lee, Brandon Peiffer, Zufeng Guo, Jianmeng Chen, Gangling Liao, S. Diane Hayward, Jun O. Liu, and Richard F. Ambinder. "Drug Modulators of B Cell Signaling Pathways and Epstein-Barr Virus Lytic Activation." Journal of Virology, May 31, 2017, JVI.00747-17. doi:10.1128/JVI.00747-17.

PRESENTATIONS

Poster Presentation at 247th National ACS Meeting and Exposition, Dallas TX 2014

OTHER EXPERIENCE AND PROFESSIONAL MEMBERSHIPS

Chemistry-Biology Interface Forum and Journal Club, JHU 2014-Present

American Chemical Society Student Chapter, Millersville University 2012-2014

HONORS AND AWARDS

Best Poster Award, 2018 Chemistry-Biology Interface Program Retreat 2018

ACS Travel Award 2014

Departmental Honors – Millersville University of PA 2014

National ACS Certification 2014